

POLITECNICO DI TORINO

MASTER OF SCIENCE IN MECHANICAL ENGINEERING



Master thesis

Analytical and Numerical Methods for Assessing the Fatigue Life of Threaded Bores

Supervisor

Prof. Cristiana Delprete

Tutor

Ing. Daniele Lomario

Candidate

Luigi Gianpio Di Maggio

July 2019

Index

1	Fatigue crack mechanism.....	15
1.1	Fracture classification.....	15
1.2	Brittle Fracture.....	18
1.3	Ductile Fracture.....	19
1.4	Fatigue fracture	20
1.5	Parameters for failure prediction: overview	22
1.6	Short cracks.....	30
2	Theory of Critical Distances	33
2.1	Introduction to TCD	34
2.2	TCD Methods	35
2.3	TCD: general aspects and capabilities	38
2.4	TCD and size effect.....	39
2.5	Critical distance.....	41
2.6	Effect of the error on critical distance	46
2.7	TCD: some applications	47
3	Multiaxial Fatigue: design and endurance criteria	54
3.1	Proportionality of loads	57
3.2	Equivalence and critical plane criteria.....	59
3.3	Fatigue life criteria	62
3.4	Dang Van Criterion	64
3.5	Durability analysis in commercial fatigue post-processors.....	67
3.6	Fatigue damage in threaded joints	79

4	Application to a case study: a fatigue assessment in Diesel Engine threaded bores....	85
4.1	Analysis Procedure	86
4.2	Results discussion	88
4.3	Critical distance: sensitivity analysis.....	90
4.4	Dang Van criterion applied to threaded bores	91
5	Numerical-Experimental correlation: Durability Analyses in aluminium notched plate.....	94
5.1	FEM modelling	95
5.2	Fatigue assessment.....	96
5.3	Fatigue Model insensitivity	104
6	Conclusions.....	107
7	Appendix.....	109
7.1	Torsion Bar – Input File.....	116
7.2	U-Notched Plate: input file (load by rigid elements).....	122
7.3	U-Notched Plate: input file (uniformly loaded on border nodes)	125
7.4	Engine and Threaded Bore FEM model.....	128
	References	129

Table of figure

Figure 1 - Fracture process and plastic deformation (1)	16
Figure 2 - Fracture micromechanisms (From top left to bottom right) – Cleavage, Decohesion, Plastic Flow, Ductile Shear, Void Coalescence (1)	17
Figure 3 - Cracking process (1)	18
Figure 4 - Wood's Mechanism (1)	21
Figure 5 - Mode I, Mode II, Mode III (2)	22
Figure 6 - Stress state one point (2)	22
Figure 7 - Mohr's Circles - Simple tension on top, simple torsion on bottom (2)	23
Figure 8 - (a) Plane Stress Yield surfaces. (b) von Mises yield surface in tension-torsion (2)	25
Figure 9 - Isotropic Hardening - Tension-Torsion (2)	26
Figure 10 - Kinematic Hardening – Tension-Torsion (2)	27
Figure 11 - Crack Tip Stress Field (4)	28
Figure 12 - J Integral path (4)	29
Figure 13 - Crack Growth Rate (4)	30
Figure 14 - Kitagawa-Takahashi diagram (4)	31
Figure 15 - Crack initiation in notches (4)	32
Figure 16 - (a) Line Method. (b) Point Method (11)	36
Figure 17 - Crack growth in bone for constant applied stress on the left. (9) FFM assumptions on the right. (10)	37
Figure 18 - Process Zone models (9)	38
Figure 19 - Stress-distance curves for different notch size (9)	39
Figure 20 - Strength prediction in beam for different TCD approaches	40
Figure 21 - Characteristic dimensions in threaded joints	41
Figure 22 - Fracture toughness - Experimental correlation (9)	42
Figure 23 - Critical Distance Estimation (17)	43
Figure 24 - Critical Distance Estimation for sharp and blunt notches (8)	44
Figure 25 - Error on FRF (left) and curve slope (right)	47
Figure 26 - MWCM and TCD (24)	50
Figure 27 - MWCM and TCD - VA loads (24)	52
Figure 28 - Elasto-plastic TCD (26)	53
Figure 29 - Fatigue classification	54
Figure 30 – Sinusoidal stress history (on the left). Different random stress histories (on the right)	55
Figure 31 - Stress history after Rainflow application	56

Figure 32 - Normal Stress and Shear Stress vectors (38)	57
Figure 33 - Body subjected to external forces (a). Shear stress vector path (b) (31)	58
Figure 34 - Load Proportionality. Proportional loads on the left. Non-Proportional loads on the right. (2)	59
Figure 35 - From system of forces (a) to resolved shear stress (c) (31)	60
Figure 36 - Maximum Variance Method (31)	61
Figure 37 - Elastic Shakedown	65
Figure 38 - Dang Van Plot	66
Figure 39 - Goodman and Gerber MSC (14)	68
Figure 40 - FRF calculation (14)	69
Figure 41 - Examples of critical plane algorithms	70
Figure 42 - Critical Plane observations	71
Figure 43 - Material Curve AA 2014-T6	72
Figure 44 - VA Stress History	72
Figure 45 - Normal Stress Algorithm	73
Figure 46 - Normal Stress Projection	73
Figure 47 - Fatigue lives on different planes	74
Figure 48 - Multiaxial non-proportional load history	75
Figure 49 - Normal Stress projection - Non-proportional loads	75
Figure 50 - Fatigue lives non-proportional loadings	75
Figure 51 - Fatigue lives comparison non-proportional loads	76
Figure 52 - Brown-Miller Algorithm	76
Figure 53 - Fatigue lives Normal Stress and Brown-Miller	77
Figure 54 - Fatigue lives comparison	77
Figure 55 - Critical Plane research comparison	78
Figure 56 - FEM model and submodel (55)	79
Figure 57 - Internal thread in cylinder head and Safety Factor evaluation	80
Figure 58 - Mean stress and stress amplitude along threads (56)	81
Figure 59 - Haigh Diagram (56)	82
Figure 60 - Cylinder Block - (a) cut thread (b) rolled thread (60)	83
Figure 61 - Residual stress evaluation	83
Figure 62 - Durability Analysis set-up	86
Figure 63 - FRF Threaded Bore	88
Figure 64 - Sensitivity analysis	90
Figure 65 - Model of Safety Factor sensitivity	91
Figure 66 - Fixed σ_f/τ_f - SF variability	92
Figure 67 - Fixed fatigue limit - SF variability	92
Figure 68 - non-TCD Safety Factor HCF evaluation - Dang Van on the left. Normal Stress/Goodman on the right	93
Figure 69 - Notched Specimens	94
Figure 70 - Notched plate - Geometry and formulas	94
Figure 71 - Input File scheme - Notched Plate	95

Figure 72 - FEM model, loads and constraints	96
Figure 73 - Fatigue algorithms and MSC's	96
Figure 74 - FEA results for different load cases	97
Figure 75 - FOS-LIFE diagram	97
Figure 76 - Normal Stress - FOSLife diagram	98
Figure 77 - FOS - Normal Stress with different MSC's	99
Figure 78 - Normal Stress Algorithm - life-to-life diagram	100
Figure 79 - Brown-Miller and Von Mises - FOSLife diagram	100
Figure 80 - LOGLIFE - Normal Stress with different MSC's	101
Figure 81 - Stress-based Brown-Miller life-to-life diagram	102
Figure 82 - Algorithm comparison life-to-life diagram	102
Figure 83 - LOGLIFE calculated with no MSC on top. FOS calculated with no MSC on bottom	103
Figure 84 - Error types	104
Figure 85 - Stress-distance curve from the notch tip	104
Figure 86 - Positive error zone	105
Figure 87 - Fatigue lives - Models Comparison	106
Figure 88 - Clamped Beam - closed form solution	109
Figure 89 - Selected node	110
Figure 90 - Abaqus input file - clamped beam	110
Figure 91 - FEM error	111
Figure 92 - Fatigue lives	111
Figure 93 - Stress Field along section	112
Figure 94 - Error on section	113
Figure 95 - Mesh refinement	114
Figure 96 - Stress gradients	114
Figure 97 - Effect of torsion and central elements	115

List of acronyms

Constant Amplitude	CA
Dang Van Criterion	DVC
Equivalent Strain Energy Density	ESED
Extended Finite Element Method	XFEM
Finite Element Analysis	FEA
Finite Element Method	FEM
Finite Fracture Mechanics	FFM
High Cycle Fatigue	HCF
Imaginary Crack Method	ICM
Internal Combustion Engine	ICE
Line Method	LM
Linear Elastic Fracture Mechanics	LEFM
Low Cycle Fatigue	LCF
Modified Wöhler Curve Method	MWCM
Partial Differential Equation	PDE
Point Method	PM
Safety Factor	SF
Stress Intensity Factor	SIF
Theory of Critical Distances	TCD
Thermomechanical Fatigue	TMF
Ultimate Tensile Strength	UTS
Variable Amplitude	VA

Abstract

Fatigue damage in Internal Combustion Engines (ICE) is affected by most of the physical phenomena characterizing the study of mechanical components. Mechanical energy transformation by means of deformable bodies inevitably leads to stress and strain fields. Thermal energy involvement makes the role of temperature primary since thermal expansion and thermal diffusivity effects are not negligible, especially if transient states, which cover a significant part of ICE's life, are taken into account. Moreover, thermal cycling for certain temperature regimes may lead to creep phenomena that contribute to fatigue damage and Thermomechanical Fatigue (TMF). Additionally, the contribution of inertia in the dynamic equilibrium of the system combines with elastic forces and external loads, paving the way to the world of resonances and vibrations. Consequent deformations, especially in Compression Ignition ICE, are related to a wide spectrum of exciting harmonics. Furthermore, manufacturing processes introduce residual stresses whose reliable estimation in the engine block is one of the challenges of modern automotive engineering. Finally, predicting loads requires simplifying hypotheses, given the wide working range of ICE.

In this complex scenario, assessing the fatigue life of ICE threaded bores is not a simple task, even by neglecting many of the above-mentioned factors. The engineering approach of dividing a manifold problem into smaller ones is therefore adopted in this work.

Firstly, fatigue damage in presence of stress concentration features and its relationship with fracture mechanism is studied. Among the analysed methods, Theory of Critical Distances (TCD) is examined in depth within non-local approaches. Although critical distance arguments are already detectable in Neuber's and Peterson's works, only researches carried out in last decades showed TCD ability to predict failures in notched structures. TCD stands out as a general fracture theory in which microscale seems to be taken into account

by introducing a new material constant. TCD is considered a generalization of Linear Elastic Fracture Mechanics (LEFM) with a connective role between continuum mechanics, LEFM and microstructure. TCD is found to be relatable to process zone and statistical models, Finite Fracture Mechanics (FFM), microstructure, short cracks and crack closure phenomena.

High Cycle Fatigue (HCF) and models for fatigue crack initiation are explored. Even though designed for uniaxial loadings, threaded joints exhibit multiaxial stress state due to notch effect. Multiaxial fatigue is analysed in the most general case of non-proportional loadings. In this sense, Critical Plane criteria are discussed by comparing the approach of commercial fatigue post-processors, inspired by the research of the lowest Safety Factor (SF), with methods based on actual fracture process. Modified Wöhler Curve Method (MWCM), Dang Van Criterion (DVC) and Maximum Variance Method (MVM) are analysed both from a local and TCD standpoint.

These concepts are applied in a critical review of one of the possible methodologies for fatigue life assessment in ICE threaded bores. Engine FEM models are used to extract boundaries conditions for thermo-structural analyses of the bore sub-model. Conservative hypotheses on the engine working range are advanced and the resulting stress history is post-processed for fatigue assessment. A benchmark analysis is carried out by comparing numerical/analytical predictions with experimental evidence in aluminium specimens. On the basis of this study, strength and weaknesses of different methods are underlined proposing new TCD and non-TCD approaches. The versatility of DVC stands out since no cycle-counting method is needed. However, mesoscopic stress tensors should be computed.

Finally, models for Safety Factor computation are compared with fatigue life approaches that, unlike the former, definitely allows error estimation.

Introduction

The most general point of view from which machines can be seen is the one referring to them as energy converters. Whatever it is the field of application, the statement is always pertinent: machines receive input in the form of energy (thermal, mechanical, electromagnetic, etc.) and return an output either with the same energy form or with another. When mechanical energy is involved in this process, forces and moments are key factors for the energy transfer, together with their direct consequences: displacements and rotations. These originate from the combination of generalized forces, geometry and material behaviour. If forces operate for the global structure equilibrium, stress field arises from continuum mechanics, to make internal equilibrium satisfied in a deformable body.

Generally speaking, stress fields may vary in space and time depending on the complexity of loads, geometry and material response. Variability in space is the most complicated to solve, since this requires a Partial Differential Equation (PDE) system for which a closed solution can be found only in the simplest cases. However, uniqueness and existence of the solution for the elastic problem has been proved almost two centuries ago and extracting stress fields is nowadays relatively simple thanks to several numerical techniques. The great advantage of these methods is not so much the reduction in the complexity of the problem, as the transformation of a continuum PDE problem into a discrete system of matrices, that is the language of computers. Finite Element Method (FEM) is the most used numerical technique in structural analysis.

Although space variability puts its roots in a non-trivial mathematical formulation, once the problem is solved (analytically or numerically) there are few sources of error that

can make results significantly different from experimental evidence. For this reason, static failure is relatively simple to assess.

On the contrary, when loads time variability is taken into account, new elements come into play since material characterization is strongly affected by experimental and statistical variability. The phenomenon for which materials exhibit lower strength when they undergo cyclic deformations along time is called “Fatigue”.

Fatigue failure occurs with modalities completely different from static failure; in the former semi-empirical models are adopted by accepting the presence of high uncertainties in fatigue damage assessment. If the actual fracture process is not modelled, mathematical models are quite easy to deal with but they include wide data scattering. The degree of complexity of fatigue models is definitely lower than that of FEM models: by this reason, the computational time of fatigue post-processors is not comparable with that of Finite Element Analyses (FEA). On the other side, it is also very difficult to correlate fatigue simulations results with experimental data. Surely, these features must be taken into account when simple specimens are analysed and the whole set of parameters acting on them is fully controlled (e.g. loads, temperature, geometry). In such a case, being able to predict fatigue life within a 20% error range is already a great result.

Among practical applications, Internal Combustion Engines (ICE) have an elevated degree of complexity, firstly in terms of geometry and secondly in terms of loads prediction. In terms of geometry, a complex case are the threaded bores, as the presence of multiple notches strongly weakens materials.

As far as loads are concerned, ICE’s have a wide working range and the actual speed and torque profile which will affect components’ loads in their life will be ever unknown. Moreover, part of the deformations experienced by Diesel ICE are due to vibrations much more than spark ignition ICE, as explained in the following. The compression ignition combustion process, even if controlled by multiple injections, results in a sharp pressure profile that, in the frequency domain corresponds to a wide range of exciting harmonics joining the fundamental one. The more the pressure signal resemble Dirac’s Delta

distribution, the higher is the number of frequencies and corresponding structural modes needed to correctly describe the dynamic response. In fact, resonant modes may produce appreciable deformations even if the amplitude of the correspondent harmonic seems to be not significative. This is the game of dynamics, where energetic contribution given by inertia forces, not taken into account in static analyses, may counterbalance the elastic energy part leaving external forces free to deform. In this case, only damping can act as energy absorber. However, when dealing with rotating parts, the co-presence of rotating and non-rotating damping may also affect the stability of the system, leading to self-excited vibrations. Lubrication and its elasto-hydrodynamic interactions, then, can play an important role, but this argument falls outside from work.

Finally, the role of temperature has not to be neglected. Some components may be exposed to such high temperatures and thermal cycling that creep phenomena and Thermomechanical Fatigue (TMF) must be considered. However, threaded bores in the engine block regions interfacing main bearings and engine head do not fall in these cases, as they experience relatively low and quite constant temperatures. In any case, non-uniform temperature distributions cause non-uniform material properties. Especially in the studied case of aluminium-steel contacts, thermal deformations are induced, resulting in stresses linked to different thermal expansion coefficients. Furthermore, if transient states are considered too, thermal diffusivity effects become an essential element to model.

All these factors strongly affect fatigue behaviour of ICE Threaded Bores. The intrinsically stochastic nature of fatigue explains why we certainly can attempt to predict components fatigue life, but very little meaning can be assigned to this prevision if a statistic analysis is not made. Nevertheless, often a non-statistical analysis is the best we can do.

Then, temperature effect may produce bolt relaxation, while the forming process introduces residual stresses (usually compressive and healthy for fatigue life) whose assessment is not simple at all. Only a simulation of the manufacturing process could really assess residual stress distributions. These analyses are non-linear and time-consuming and

this could not always match industrial needs which usually correspond to a trade-off between cost and accuracy.

On the contrary, thermal expansion and diffusivity can be taken into account through FEA by including heat equations beyond continuum mechanics. The complete problem of fatigue assessment procedure has not been solved yet, even by considering fatigue endurance independently from all the other phenomena occurring in engine operation.

Aim of this work is to assess the most common methods to estimate the fatigue life and crack initiation, pointing out their strengths and weaknesses when applied to some case studies. As a starting point, fatigue crack mechanism and fatigue models are introduced and discussed.

1 Fatigue crack mechanism

It is unavoidable to introduce a description of the physical phenomena we want to model, as each of the models adopted is strictly related to a cracking mechanism regardless of the component studied. “Fracture” can be defined as “*the process of separation or fragmentation of a solid body under the action of loads or stresses, thus creating new surfaces, which are referred to as the fractured surfaces*” (1). Fracture is a process resulting from operating stresses and is influenced by microstructure and environment. Fractures may be classified in relation to their: **fracture type, fracture mechanism, fracture micromechanism.**

1.1 Fracture classification

The **Fracture type** (Figure 1) is related to the plastic deformation experienced:

- Brittle fracture exhibits very low plastic deformation.
- Ductile fracture is associated with an appreciable amount of plastic deformation.

The **Fracture mechanism** is linked to the macroscopic phenomenon acting for fracture process:

- *Overload* is the condition in which materials cannot support the applied load since in some regions limit stresses are reached. This is the static failure.
- *Fatigue* is the term used referring to cyclic loadings that, after a certain number of cycles provoke crack initiation and growth.
- *Stress corrosion cracking (SCC)* occurs when the stress effect is combined with a high level of corrosion.
- *Creep* is the phenomenon for which a constant stress, extended in time and in a high temperature regime, results in a deformation process.

- Hydrogen-induced cracking is due to hydrogen inclusion, which in particular conditions may strongly modify internal microstructure leading to cracking.
- Radiation cracking may occur also without and external stress supplier, since radiations alter material at the molecular levels.

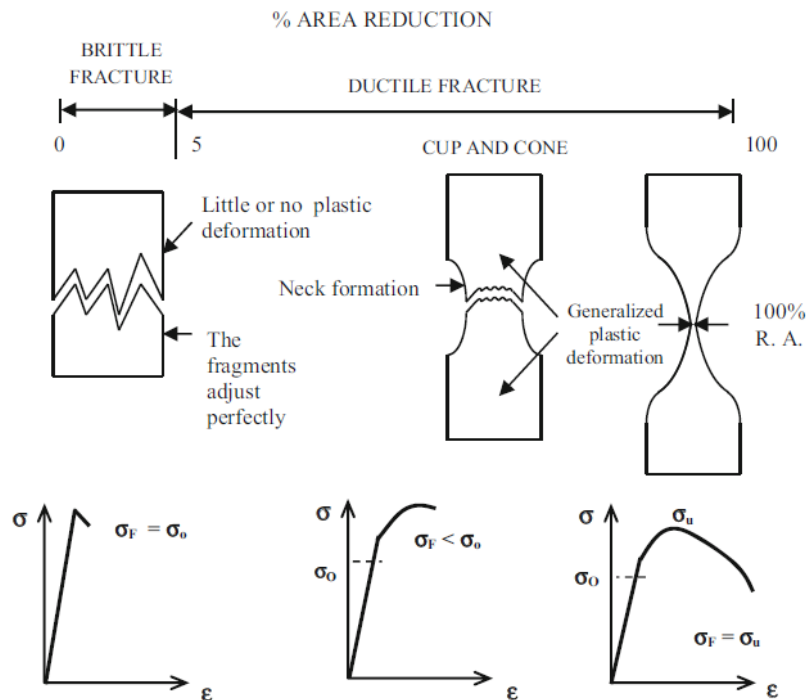


Figure 1 - Fracture process and plastic deformation (1)

The crack path may be:

- *Intergranular*, when the crack path develops along grain boundaries.
- *Transgranular*, if the fracture line follows crystalline planes or, in amorphous materials, non-crystalline planes.

It is indicated as “process zone” the material portion surrounding the crack tip. With this term we refer not only to the zone involved in the plasticization process, but also to the whole area bounding the phenomena acting in the fracture micromechanism.

Fracture micromechanisms are classified as (Figure 2):

- Cleavage is the fracture micromechanism related to the breakage of atomic bonds along precise crystallographic planes. Since no plastic deformation is involved, this is a brittle and transgranular fracture.
- The plastic Flow is linked to the crack propagation due to plastic deformation at crack tips which makes cracks advance. This is a ductile and transgranular fracture.
- The decohesion process does not concern specific crystalline planes, but often occurs at grain boundaries. These zones, being energetically unstable, are prone to the accumulation of defects and inclusions and normal stress may exceed cohesive stress, leading to surfaces separation. No plastic deformation is involved and this mechanism can be addressed to as brittle and intergranular.
- The ductile shear mechanism occurs on maximum shear stress planes when shear strength is surpassed.
- Void Coalescence. When micro-voids form in the material process zone, they may grow due to the stress and coalesce, forming macroscopic cracks.

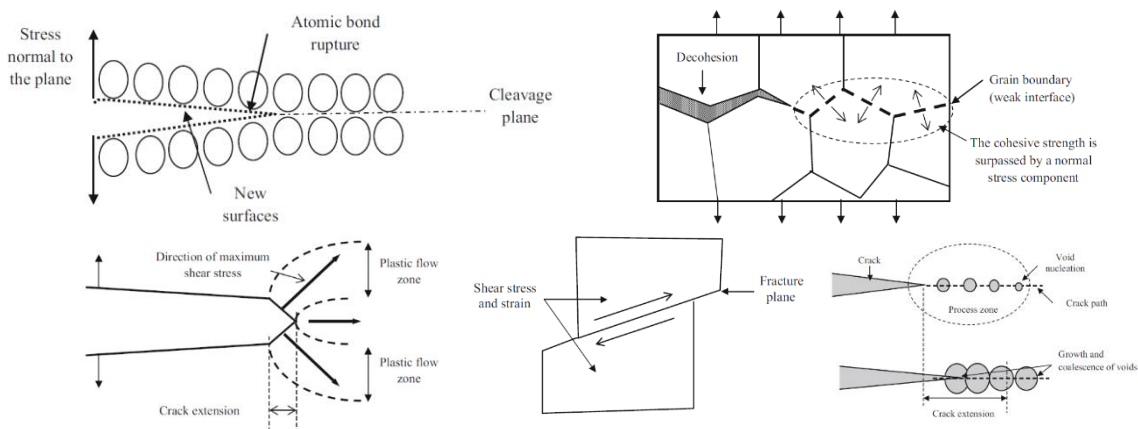


Figure 2 - Fracture micromechanisms (From top left to bottom right) – Cleavage, Decohesion, Plastic Flow, Ductile Shear, Void Coalescence (1)

Generally speaking, the fracture process originates close to stress concentration features, corresponding to geometry discontinuities. Crack nucleation occurs in the **Stage I**. At this stage, the process zone is characterized by particular stress distributions which affect the resulting fracture surfaces. **Stage II** is the crack propagation phase and **Stage III** is when the final failure occurs. In the latter, strong modifications in geometry, stress and strain state have taken place yet. Consequently, fracture surfaces originating from Stage III show direction changes and crack branches.

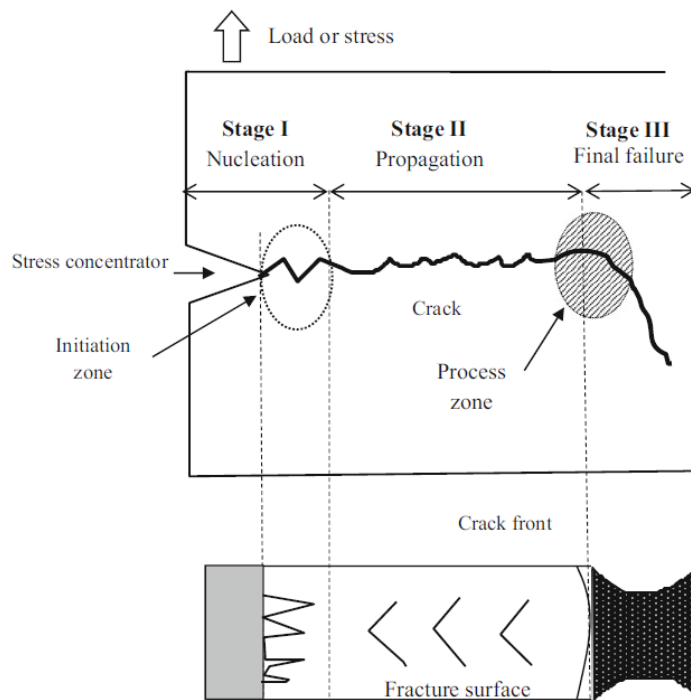


Figure 3 - Cracking process (1)

1.2 Brittle Fracture

The most common mechanism acting in brittle fracture is cleavage, which is caused by normal stresses perpendicular to cleavage planes. The simplest model of cleavage is based on atomic interactions and their equilibrium positions. External loads try to modify the equilibrium condition of the system that responds with attractive forces. When the maximum

attractive force is reached, the stored energy is transformed into surface energy and plane separation occurs. Energy equilibrium in the mathematical form is here reported:

$$\sigma_{TEO} = \sqrt{\frac{E\gamma_s}{a_0}} \quad (1)$$

E is the elastic modulus, γ_s the surface energy and a_0 the lattice parameter. This model actually predicts materials strength σ_{TEO} much higher than the experimental ones, because no real-world material is without defects, which cause stress intensifications and consequently a degradation of the material properties. Brittle fracture can be also intergranular when decohesion occurs at grain boundaries.

1.3 Ductile Fracture

Differently from the brittle fracture, the ductile fracture is associated with a stress localization. Even in tensed specimens without stress concentrations features, when the material can no more support a uniform deformation, a localized deformation occurs and a narrower zone called ‘neck’ forms. In this portion, stress intensifications takes place.

Typically, at this point a triaxial stress state settles and voids nucleate. Then, voids grow because of plastic deformation until they coalesce. The shear stress acting in the remaining section brings components to failure. Inclusions and second phase particles behave as trigger points for voids nucleation. If voids originate from the separation between matrix and particles, **inter-phase decohesion** is the leading nucleation mechanism. On the contrary, if matrix cohesion forces are strong, voids nucleate by particles cleavage (**fracture of brittle particles**). Finally, **dislocation pile-up** occurs when the shear stress acts for dislocation shift. Dislocations move until a critical pile-up, close to particles, is reached creating small voids.

Ductile fracture, because of its mechanism, differs from brittle fracture since it requires more energy and it is shear stress governed. Then, remarkable differences that lie outside this discussion are detectable from a fractographic point of view.

1.4 Fatigue fracture

The fatigue failure is both a brittle and ductile fracture. Components are usually designed to work in the linear elastic regime and no plastic deformation is macroscopically expected to occur in them. However, cycling stresses may generate cracks that behave as stress concentrators in such a way that plasticity in the process zone is inevitably involved. Some materials (e.g. steel) present the so called *fatigue limit* that is a level of cyclic stress below which no fatigue crack develops and fatigue life is infinite.

If plasticity is localized near the crack tip, strains are globally elastic and the number of cycles to failure is very high. This is the **High Cycle Fatigue (HCF)**, 10^6 - 10^7 cycles). When the crack grows in an already plasticized zone, strains in some regions are elastoplastic and **Low Cycle Fatigue (LCF)**, 10^3 - 10^4 cycles) occurs. If cyclic strains are globally plastic, few cycles are sufficient for the component to fail and this is the case of **very low cycle fatigue**.

Fatigue fracture, as anticipated, takes place essentially in three stages:

- **Stage I:** crack initiation and slow crack growth.
- **Stage II:** cyclic deformation makes crack grow. It is clear that, in this stage, stress state is not fully able to describe the fracture process, since crack size and surface energy are quantities not related to the macroscopic stress. As a result, continuum mechanics models leave space to **Linear Elastic Fracture Mechanics (LEFM)**, wherein energetic quantities such as Stress Intensity Factor (SIF) K are employed. In this phase, there is stable crack growth with a defined growth rate.
- **Stage III:** Crack growth becomes unstable. After crack has propagated at the speed of sound, static failure occurs.

Fatigue cracks typically originate on surfaces. **Wood's** model explains crack nucleation by the intrusion-extrusion mechanism. According to this model, dislocation slip is the cause of crack initiation, as when dislocations reach free surfaces metal extrusions form. Consequently, the material close to the extrusion is hollowed by an intrusion that will turn into a crack.

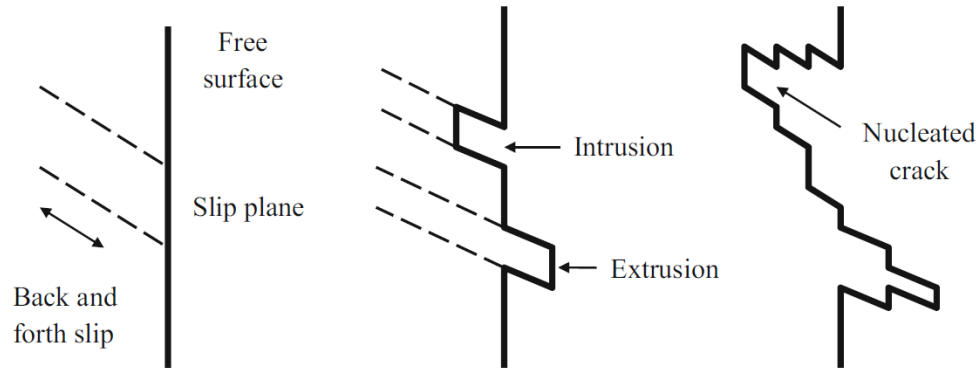


Figure 4 - Wood's Mechanism (1)

Fatigue crack nucleation is a surface phenomenon that originates from dislocation movement occurring on slip planes, defined by crystalline structure. Being the dislocation movement associated with shear stress, it is clear that cycling resolved shear stress plays a primary role in the crack initiation process. In polycrystalline metals, grains are random oriented and the critical resolved shear stress is reached, in each grain, for different values of the external loads. From a microscopic point of view, when the applied stress is low, a few grains are favourable oriented.

Generally speaking, the fracture process does not always involve fatigue and may be controlled by tension stress in materials that exhibit higher resistance in shear than in tension such as brittle materials, or by shear stress in ductile materials that have higher resistance in tension. These behaviours affect the plane on which the fracture process takes place and, consequently, the damage parameter to account for. This explains why static failure criteria for ductile metals search for the maximum shear stress plane, whereas the maximum principal stress is employed for static analyses in brittle materials.

After the crack has nucleated, it can be loaded in different manners called **Mode I**, **Mode II** and **Mode III** (Figure 5). Mode I refers to opening loads such as tension, Mode II is related to the in-plane shear whereas Mode III is linked to the out-of-plane shear. Mode II

controls the Stage I as this phase shear stress dominated, Mode I controls Stage II as tensile stress acts for crack growth.

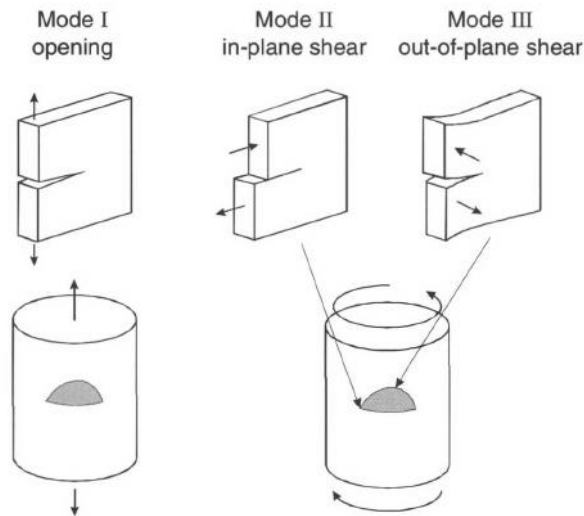


Figure 5 - Mode I, Mode II, Mode III (2)

1.5 Parameters for failure prediction: overview

Continuum mechanics looks at materials to such a scale that no discontinuities due to empty spaces are encountered. Atomic, molecular or grain scales are not contemplated in this theory. This simplification, surely acceptable when macroscale is analysed, allows us to introduce stress and strain as continuous space functions.

The six components symmetric stress tensor is introduced for the definition of the stress state in one point.

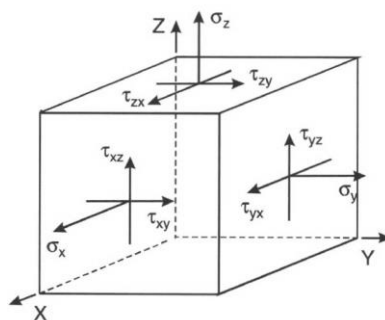


Figure 6 - Stress state one point (2)

$$\sigma = \begin{pmatrix} \sigma_x & \tau_{xy} & \tau_{xz} \\ \tau_{yx} & \sigma_y & \tau_{yz} \\ \tau_{zx} & \tau_{zy} & \sigma_z \end{pmatrix} \quad (2)$$

The stress tensor can be rotated by defining the director cosines of specific planes. In particular, the solution of the eigenvalue problem:

$$\det(\sigma - \lambda I) = 0 \quad (3)$$

gives as result the director cosines (eigenvectors) and the **Principal Stresses** (eigenvalues) defining the stress state in the particular plane for which:

$$\sigma = \begin{pmatrix} \sigma_1 & 0 & 0 \\ 0 & \sigma_2 & 0 \\ 0 & 0 & \sigma_3 \end{pmatrix} \quad (4)$$

the coefficients of the third grade equation coming from Eq. (3) are called **Stress Invariants** I_1, I_2, I_3 , as they do not depend on the original reference system. Mohr's circles graphically represent Principal Stresses and stress state for a specific plane.

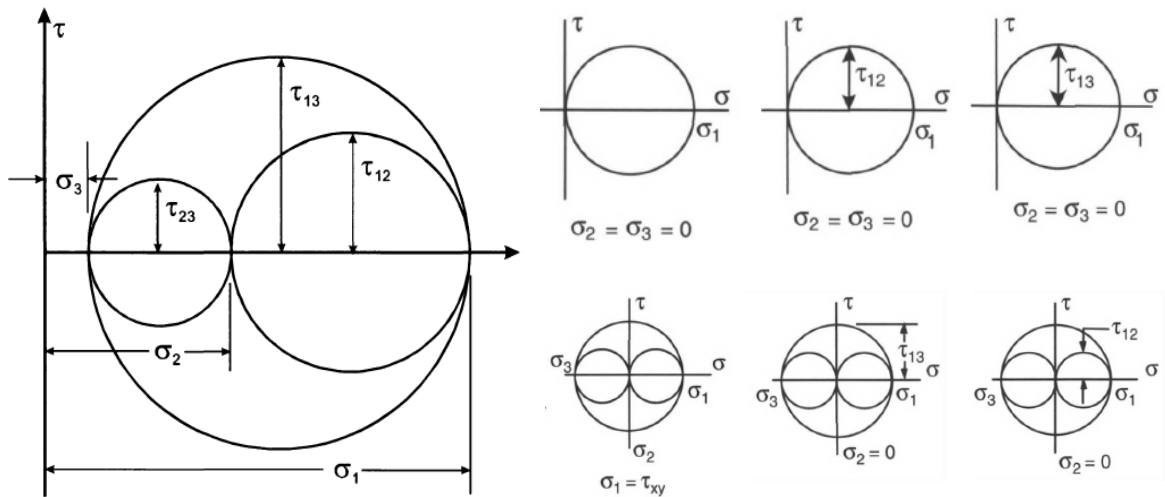


Figure 7 - Mohr's Circles - Simple tension on top, simple torsion on bottom (2)

A PDE problem must be solved to calculate stresses from specific loads acting on the given geometry. In the simplest cases (e.g. beams, plates) there are closed form solutions to the problem, namely ready-to-use formula. In general, a discretization technique such as FEM is needed to solve the elastic problem. Strictly speaking, FEM method does not work directly

with stresses. In fact, it assumes some arbitrary defined shape functions that describe displacements in a discretized domain. Clearly, the more the spatial discretization (Mesh) is dense, the more the reconstructed displacements (obtained as union of pieces of shape functions) retraces the actual deformed shape. Then, strains are derived from displacements and eventually stresses are extracted through the stress-strain relationship. Errors coming from discretization and numerical integration directly affect results, but the study of this subject, although of primary importance, goes beyond the purposes of this works.

Looking at the stress tensor, two particular cases are identifiable. When the analysed point is located on a free surface, for instance, there are no stresses acting on the free surface resulting from the equilibrium. This is the **Plane Stress** ($\sigma_z = \tau_{xz} = \tau_{yz} = 0$). On the contrary, if the point is placed inside the specimen, the elastic surrounding material prevents deformation by acting as a constraint ($\epsilon_z = \gamma_{xz} = \gamma_{yz} = 0$). This is the **Plane Strain**.

Stress/strain parameters used in failure analyses are: **octahedral shear stress**, **hydrostatic pressure** and **deviatoric stress**.

Octahedral shear stress comes from the composition of the shear stresses acting on a plane that intersects principal axes at equal distances (2).

$$\tau_{oct} = \frac{1}{3} \sqrt{(\sigma_x - \sigma_y)^2 + (\sigma_y - \sigma_z)^2 + (\sigma_x - \sigma_z)^2 + 6(\tau_{xy}^2 + \tau_{yz}^2 + \tau_{xz}^2)} \quad (5)$$

The effective octahedral σ_{eff} stress is related to the Von Mises energetic yielding criterion for ductile metals:

$$\sigma_{eff} = \frac{1}{\sqrt{2}} \sqrt{(\sigma_x - \sigma_y)^2 + (\sigma_y - \sigma_z)^2 + (\sigma_x - \sigma_z)^2 + 6(\tau_{xy}^2 + \tau_{yz}^2 + \tau_{xz}^2)} \quad (6)$$

hydrostatic pressure is defined as:

$$p = \frac{(\sigma_x + \sigma_y + \sigma_z)}{3} = \frac{I_1}{3} \quad (7)$$

whereas deviatoric stress tensor is:

$$s_{ij} = \sigma_{ij} - \frac{I_1}{3} \delta_{ij} \quad (8)$$

The invariants of the deviatoric stress tensor $J_{1,2,3}$ may be related to the stress tensor invariants $I_{1,2,3}$. Moreover:

$$J_2 = \frac{3}{2} \tau_{oct}^2 \quad (9)$$

In elastic conditions, no yielding occurs and the stress-strain relationship, in its most general form, is reported below.

$$\begin{bmatrix} \sigma_x \\ \sigma_y \\ \sigma_z \\ \tau_{xy} \\ \tau_{yz} \\ \tau_{xz} \end{bmatrix} = \frac{E}{(1+\nu)(1-2\nu)} \begin{bmatrix} 1-\nu & \nu & \nu & 0 & 0 & 0 \\ \nu & 1-\nu & \nu & 0 & 0 & 0 \\ \nu & \nu & 1-\nu & 0 & 0 & 0 \\ 0 & 0 & 0 & \frac{1-2\nu}{2} & 0 & 0 \\ 0 & 0 & 0 & 0 & \frac{1-2\nu}{2} & 0 \\ 0 & 0 & 0 & 0 & 0 & \frac{1-2\nu}{2} \end{bmatrix} \begin{bmatrix} \epsilon_x \\ \epsilon_y \\ \epsilon_z \\ \gamma_{xy} \\ \gamma_{yz} \\ \gamma_{xz} \end{bmatrix} \quad (10)$$

When plastic stresses and strains are involved, the concept of **Yield Surfaces** (3) becomes relevant, especially if cycling loads are applied.

In the space defined by normal stresses, the Yield Surface is the locus of points for which yielding takes place. Clearly, the shape of the surface depends on the yielding criterion.

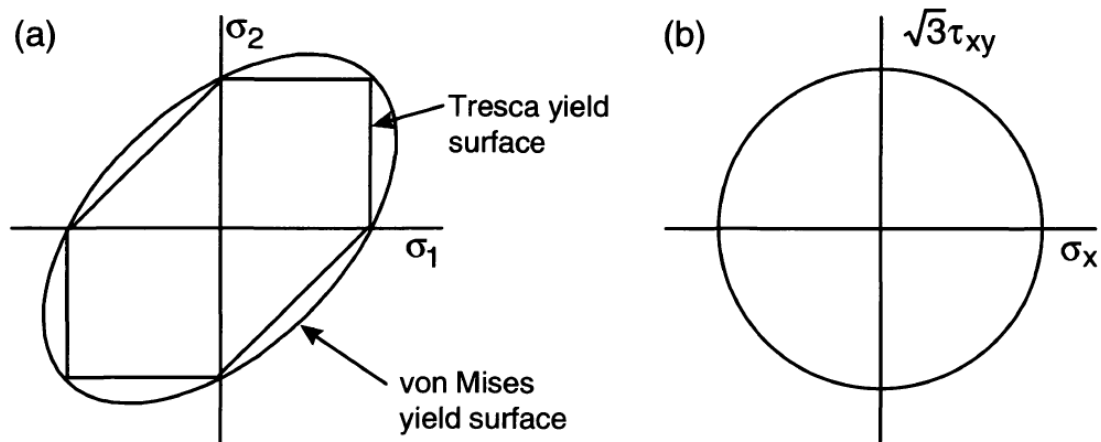


Figure 8 - (a) Plane Stress Yield surfaces. (b) von Mises yield surface in tension-torsion (2)

When cycling loading occurs, yield surfaces may move and deform and this is what define *material hardening*.

Isotropic hardening describes the increment in material strength due to plastic strain (2). If σ_Y is the Yield strength; the von Mises yield surface is (in a tension-torsion case):

$$\sigma^2 + 3\tau^2 - \sigma_Y = 0 \quad (11)$$

isotropic hardening models the so-called material memory effect. Materials that are plastically deformed and unloaded completely “remember” their prior loading and yield with a new stress value. Yield surface expands but does not translate (Figure 9).

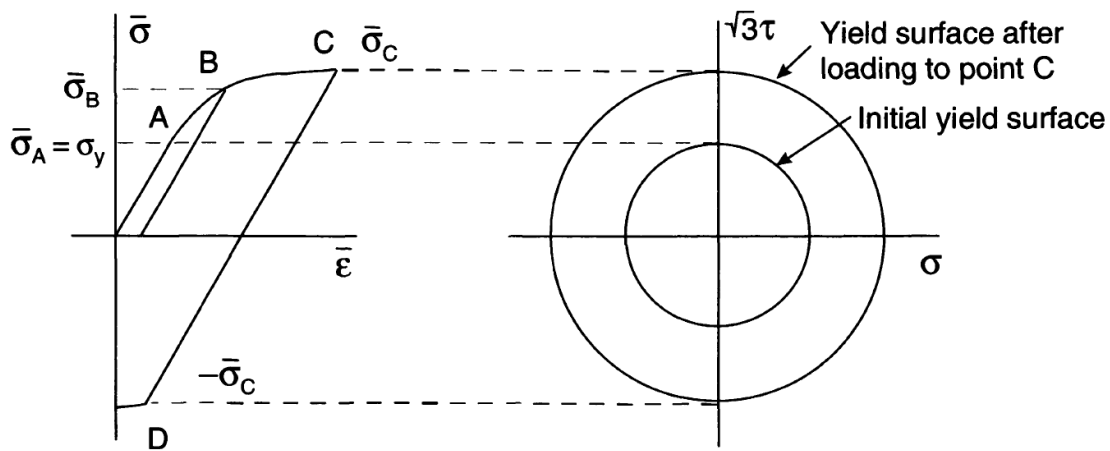


Figure 9 - Isotropic Hardening - Tension-Torsion (2)

Kinematic hardening models Bauschinger effect through the displacement of yielding surfaces. After that tension is applied up to the load $\bar{\sigma}_B$, reverse yielding occurs when the load point $\bar{\sigma}_B - 2\sigma_Y$ is reached (Figure 10). Real materials show a hardening behaviour intermediate between the isotropic and the kinematic ones.

Macroscopic cracks represent discontinuities and mathematical singularities in the continuum mechanics formulation. **LEFM** treats these discontinuities by associating fracture processes to energetic arguments. When available energy equals the energy needed for new surfaces formation, unstable propagation occurs. In its most simplified synthesis: Stress Intensity Factor (SIF) equals fracture toughness K_{IC} . SIF is defined as:

$$K = Y\sigma\sqrt{\pi a} \quad (12)$$

Y is the geometric factor, a is the crack size and σ is the applied stress. According to Eq. (12), the fracture stress σ_f is:

$$\sigma_f = \frac{K_{IC}}{Y\sqrt{\pi a}} \quad (13)$$

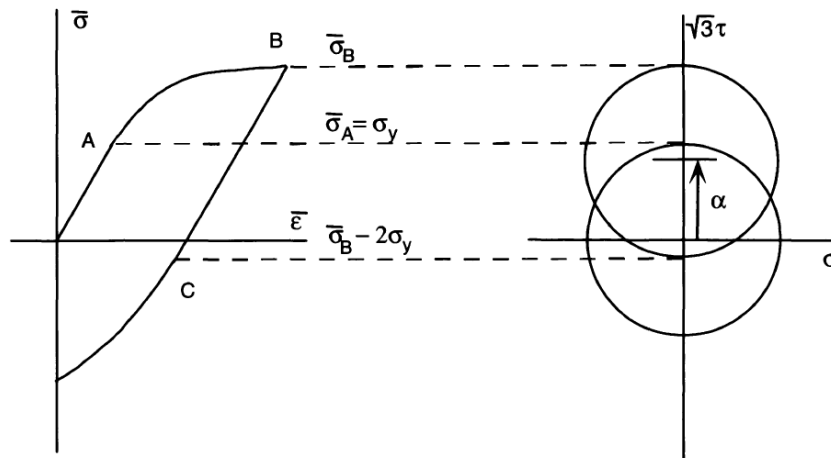


Figure 10 - Kinematic Hardening - Tension-Torsion (2)

It is worth noticing that for null crack lengths, LEFM predicts infinite fracture stresses. This point is not discussed here since it will be later investigated.

SIF is influenced by the crack mode and it stems from the equations describing the elastic stress field close to crack tip. Polar coordinates (ϕ, r) describe the space in the vicinity of crack tip; the stress field in tensor notation is expressed by:

$$\sigma_{ij} = \frac{1}{\sqrt{2\pi r}} (K_I f_{ij}^I(\phi) + K_{II} f_{ij}^{II}(\phi) + K_{III} f_{ij}^{III}(\phi)) \quad (14)$$

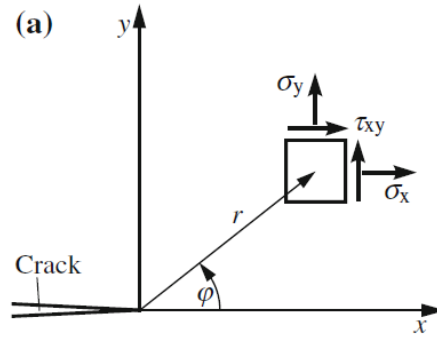


Figure 11 - Crack Tip Stress Field (4)

Clearly, for $r \rightarrow 0$ stress does not really goes to infinite but a certain zone close to the crack tip plasticize. Depending on the size of this zone, LEFM can either correctly approximate crack behaviour or be insufficient for this task. In this case, **Elastic-Plastic Fracture Mechanics** is required.

Energy Release Rate $G_{I,II,III}$ expresses the elastic energy dU released during a crack elongation da (4):

$$G_{I,II,III} = -\frac{dU}{da} \quad (15)$$

for Mode I and plain strain:

$$G_I = \frac{1 - \nu^2}{E} K_I^2 \quad (16)$$

LEFM is based on the assumption that unstable crack propagation occurs when a critical value is reached $G_I = G_{IC}$, when the released energy is sufficient for new surfaces creation.

When the size of the plastic zone is not small as compared to crack length, SIF is no longer able to describe the crack behaviour. Rice (5) introduced the concept of **J integral**. It is a line integral:

$$J = \int (\bar{U} dy - \vec{\sigma} \frac{\partial \vec{u}}{\partial x} ds) \quad (17)$$

where the energy per unit volume \bar{U} is expressed through stress and strain tensors:

$$\bar{U} = \int_0^{\epsilon_{ij}} \sigma_{ij} d\epsilon_{ij} \quad (18)$$

The Rice's integral is independent from the integration path, and for small plastic zones it equals the Energy Release Rate. The following J integral-based fracture criterion emerges as a natural consequence.

$$J = J_{IC} \quad (19)$$

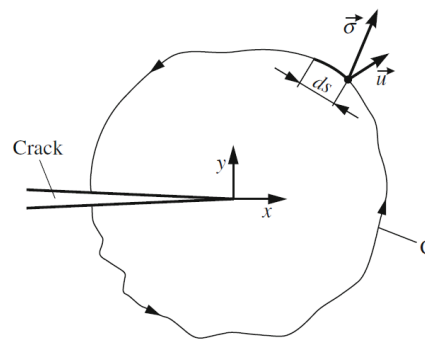


Figure 12 - J Integral path (4)

1.6 Short cracks

Microstructurally short cracks have characteristic dimensions comparable to the microstructure; this limits the applicability of continuum mechanics. Mechanically short cracks mark the limit of LEFM, since the crack size becomes comparable with the dimension of the plastic zone. Physically short cracks, finally, are not detectable with non-destructive methods but LEFM is still applicable.

Generally speaking, short cracks behaviour is different from long cracks one. Short cracks grow faster and **Paris' Law** of Eq. (20) for Stage II growth is not valid.

$$\frac{da}{dN} = C(\Delta K)^n \quad (20)$$

The threshold Cyclic Stress Intensity Factor ΔK_{th} limits the zone beneath which no stable growth occurs.

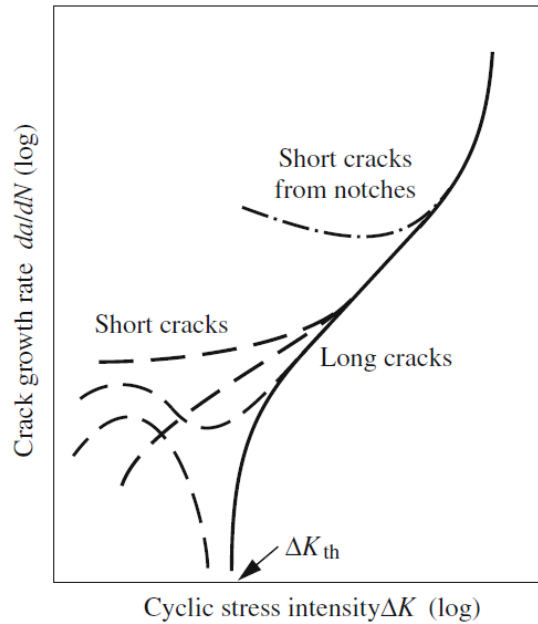


Figure 13 - Crack Growth Rate (4)

As it emerged from Eq. (13), LEFM alone does not give us information on the actual fracture stress when crack size becomes very small. This issue can be solved considering that beyond a certain value a_0 , the crack propagation is avoided for a constant stress value, whereas,

when $a > a_0$, failure limits are defined by a constant K curve. If cyclic loads are applied, the same concepts remain valid for fatigue crack propagation. The Kitagawa-Takahashi diagram expresses these ideas (Figure 14).

When the crack length is almost null, or crack nucleation has not occurred yet, stress-based criteria are able to describe material strength (constant stress failure). Energetic approaches, such as LEFM, can model failures for $a > a_0$ (constant SIF failure).

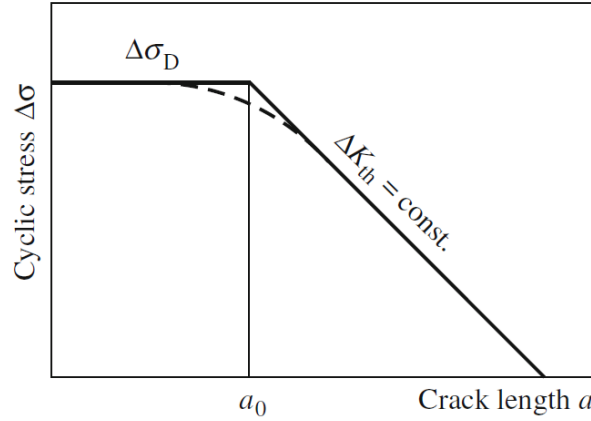


Figure 14 - Kitagawa-Takahashi diagram (4)

The value of a_0 can be obtained from the threshold ΔK_{th} and fatigue strength $\Delta\sigma_D$:

$$a_0 = \frac{1}{\pi} \left(\frac{\Delta K_{th}}{\Delta\sigma_D} \right)^2 \quad (21)$$

At this point, it starts to be clear that a general theory to account for failure prediction should contain both branches of Figure 14. El Haddad (6) described the whole curve as:

$$\Delta\sigma_{th} = \frac{\Delta K_{th}}{\sqrt{\pi(a + a_0)}} \quad (22)$$

Among fracture theories, Theory of Critical Distances (TCD), which will be later described, showed to be able to work in the whole crack length regime. For this reason, TCD candidates itself as a link between LEFM and continuum mechanics, even if the modalities and the causes for this connection, closely related to a_0 , are still open issues.

Actually, divergences between continuum mechanics and LEFM permeate engineering models for failure prediction. Notches exhibit a similar behaviour. The stress concentration factor α_k characterizes notches sharpness: for blunt notches $\alpha_k < \alpha_k^*$ crack initiation is stress governed, whereas sharp notches behave as cracks of equal length and ΔK_{th} is the key factor for crack initiation. The zone in which stress based models and LEFM diverge defines the domain of non-propagating cracks that nucleate but do not develop (Figure 15).

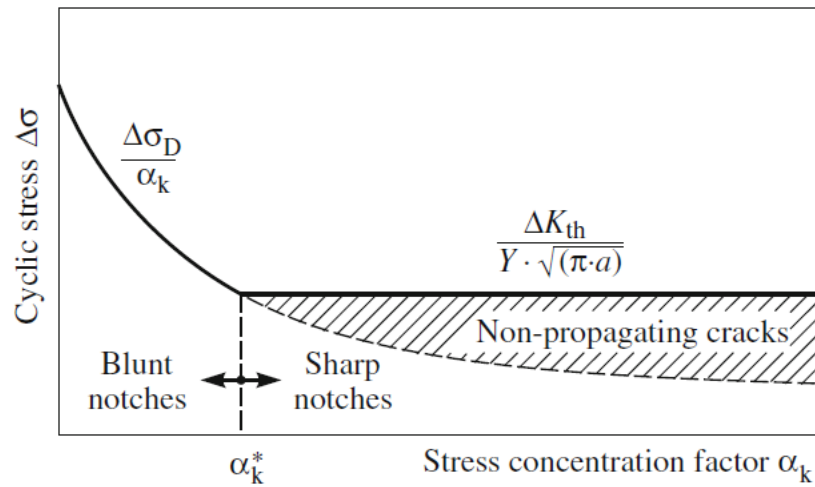


Figure 15 - Crack initiation in notches (4)

2 Theory of Critical Distances

The Theory of Critical Distances (TCD) is intentionally introduced at this point since no fatigue model has been presented yet. Indeed, an extensive research on the applications of the TCD in the industrial world has shown this theory to be often confused with a fatigue criterion itself. Simultaneously, an equally extended research through academic resources has revealed the deeper meaning of this theory that, as anticipated, may act as a link between fracture models.

As the TCD can be referred to as an effort of generalizing fracture theories. It would have no meaning to focus its capability only on fatigue. Literature is full of examples in which the TCD is applied to the study of brittle fracture, ductile materials, strength in concrete (7; 8; 9) as well as in fatigue failure assessment. While Goodman, Sines, Findley, to name a few, gave their names to fatigue criteria whose meaning is bounded by fatigue failures, the TCD is a point of view from which any fracture criteria can be seen. Goodman criterion, for instance, can be used in a TCD sense but it cannot be employed in predicting static failure in bones. On the contrary, the TCD may serve this task. Another aspect is understanding why the TCD can do this and many others tasks since, in its most barren and misleading simplification, the TCD is nothing but looking stress far from hot-spots. Why should this work?

The answer to this question is the starting point for many theoretical discussions that may arise. These dissertations, again, may represent superfluous constraints when the TCD is applied in a varied and complex context such as fatigue assessment in ICE. In fact, heavy simplifications are already made when a procedure is designed to obtain reliable, unambiguous and quick results. **However, the knowledge of the simplifications made in each step is one of the few advantages that engineers, trying to predict components behaviour, have against the doubtless chaotic, non-linear and stochastic attitude of physical and natural phenomena.**

2.1 Introduction to TCD

Taylor and Susmel (9; 10; 11) devoted many research activities to the field of the TCD. The name Theory of Critical Distances, given by Taylor (10), refers to a group of theories adopted for the study of stress concentration features. However, Neuber (12) and Peterson (13) already proposed the idea that notched components could be studied by using non-local approaches. According to the first, strength assessment should be performed by averaging the elastic stress field over a material characteristic dimension, whereas the second considered a reference stress located at a certain distance from the hot-spot. Neuber strongly believed that this approach could be suitable in presence of high stress gradients. Nowadays many engineering companies still take advantage on analytical formula to make fast evaluation on components design; one of the most used relates the notch stress concentration factor K_t to the fatigue notch stress concentration factor K_f .

$$q = \frac{K_f - 1}{K_t - 1} \quad (23)$$

with q notch sensitivity factor. Neuber expressed this relation as:

$$K_f = 1 + \frac{K_t - 1}{1 + \sqrt{\frac{A}{r}}} \quad (24)$$

with r notch radius and A a material characteristic length: this is one of the first attempts at using critical distance concepts (9; 14) and it is still used. The material property L is introduced both in static (Eq. (25)) and fatigue (Eq.(26)) conditions:

$$L = \frac{1}{\pi} \left(\frac{K_{IC}}{\sigma_0} \right)^2 \quad (25)$$

$$L = \frac{1}{\pi} \left(\frac{\Delta K_{th}}{\Delta \sigma_0} \right)^2 \quad (26)$$

σ_0 and $\Delta \sigma_0$ can be considered, at the moment, respectively as the Ultimate Tensile Strength (UTS) σ_u and the fatigue limit of the material, even if in these quantities lies one of the most tricky issue of TCD.

2.2 TCD Methods

By using the scale length introduced by Eq. (25) and Eq. (26), four methods are applicable according to a TCD perspective (9; 10; 11). σ_0 is considered the UTS (failure of plain specimen) but its meaning will be later explained. σ_f is the stress for which the cracked component fails. (Eq. (13))

- Point Method (PM). This method is based on the assumption that the reference stress is placed at a distance from the notch tip equal to $D_{PM} = \frac{L}{2}$. If a sharp notch is considered, it may be approximated by a crack of equal length a whose stress-distance curve is:

$$\sigma(r) = \sigma \sqrt{\frac{a}{2r}} \quad (27)$$

Fracture condition is expressed by Eq. (13). According to TCD assumption, incipient failure occurs when the stress-distance curve $\sigma(r)$ reaches the value of σ_0 . Therefore, in failure conditions:

$$\frac{\sigma_0}{\sigma_f} = \sqrt{\frac{a}{2r}} \quad (28)$$

By using Eq. (13) and Eq. (25) in Eq. (28), it results $r = \frac{L}{2}$. This is one of the examples in which the link between LEFM and TCD can be highlighted.

- Line Method (LM). This approach is similar to PM since it is based on stresses. Stress is averaged over a distance $D_{LM} = 2L$. A link with LEFM may be found as for PM.

$$\sigma_{LM} = \frac{1}{2L} \int_0^{2L} \sigma(r) dr \quad (29)$$

LM can also be considered an extension of PM for what concerns the integral dimensions. Area Method (AM) and Volume Method (VM) are the successive extensions in area and volume integrals. LM and PM are adoptable looking only at stresses coming, for instance, from a FEM model. However, it is not completely true that they work as stress-based methods, since the information on the material

toughness (that is an energetic feature of LEFM) is actually contained in L . This information is not usually contained in the FEM model, as FEM itself is based on continuum mechanics apart from the cases in which singular shape functions are employed and cracks behaviour is modelled through XFEM (Extended Finite Element Method). The peculiar intermediate approach in failure modelling is one of the main features of TCD that, as anticipated, makes this theory suitable both for when cracks are not considered and when long cracks are present; the last case is particularly

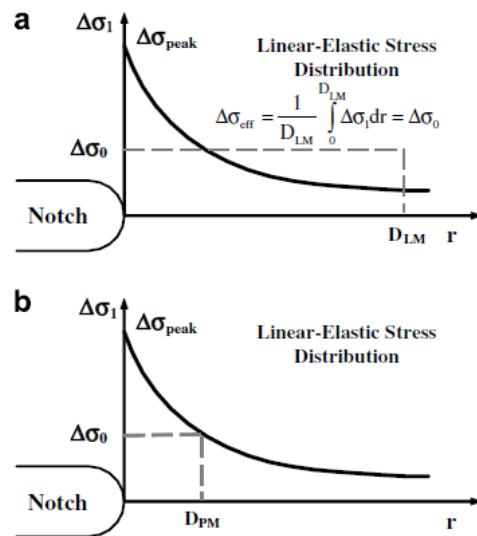


Figure 16 - (a) Line Method. (b) Point Method (11)

noteworthy since apparently stress-based approaches seem to work where only LEFM could.

- Imaginary Crack Method (ICM). In this method, as in FFM, energetic features of TCD are directly appreciable. ICM models an imaginary crack at the notch tip and failure is reached when $K = K_{IC}$. Analogous considerations are possible in fatigue.
- Finite Fracture Mechanics (FFM). FFM (15) is a modification of LEFM in which the integrations necessary to express energies involved in the fracture process are performed in finite steps. The use of a discrete integration space defined by Δa steps rather than da steps brings significant consequences. The strain energy change ΔW for a crack elongation consequently becomes:

$$\Delta W = \int_a^{a+\Delta a} \frac{\sigma^2 \pi}{E} a da \quad (30)$$

Fracture stress now is:

$$\sigma_f = \frac{K_C}{\sqrt{\pi \left(a + \frac{\Delta a}{2} \right)}} \quad (31)$$

it is worth noticing that, for a null crack size, fracture stress is no more infinite as in classic LEFM (Eq. (13)). Furthermore, the model of Eq. (31) is able to retrace the diagram of Figure 14. For $a \gg \frac{\Delta a}{2}$, Eq. (31) follows LEFM, whereas for decreasing a , constant stress failure is predicted:

$$\sigma_f = \frac{K_C}{\sqrt{\frac{\pi \Delta a}{2}}} \quad (32)$$

if $a \cong 0$, it can be supposed that $\sigma_f = \sigma_0$ and the following relation comes out:

$$\frac{\Delta a}{2} = \frac{1}{\pi} \left(\frac{K_C}{\sigma_0} \right)^2 = L \quad (33)$$

From this discussion, it emerges that a relation between critical distance and discrete quanta of crack growth Δa are detectable. According to Taylor (9), the most important aspects of the TCD capability in structural analysis lie in FFM. Experimental evidence shows that the crack growth is a discontinuous process (Figure 17).

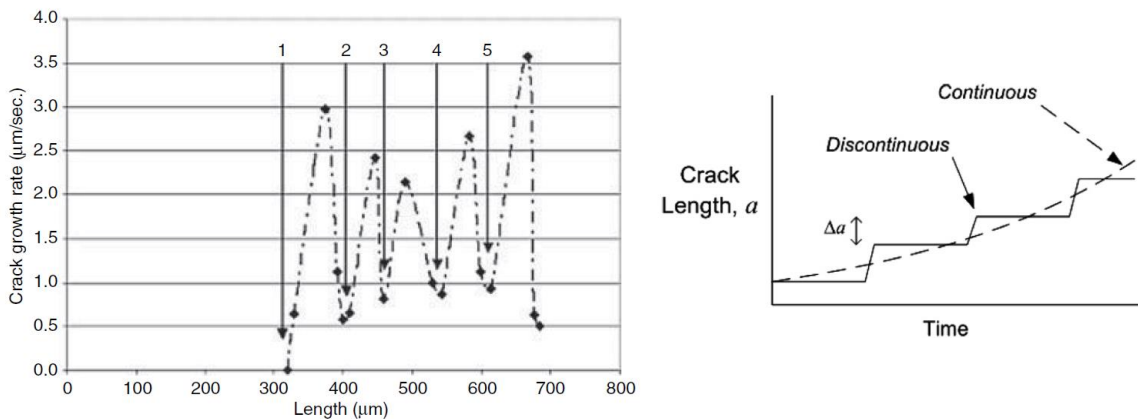


Figure 17 - Crack growth in bone for constant applied stress on the left. (9) FFM assumptions on the right. (10)

2.3 TCD: general aspects and capabilities

Non-local approaches, differently from local approaches, consider the stress distribution in a region that is supposed to affect the behaviour of a single point. These approaches usually work very well when there are high stress gradients. TCD is one of these methods but its ability in predicting strength in stress concentration features may actually have deeper roots.

Surely, a complete model of the fracture process would require the fracture model to contain information about the physical mechanism occurring in microstructure. These mechanistic models are hardly applicable, as the number of degrees of freedom to assess and control definitely increases: continuum mechanics models simplify this kind of complexities but, of course, lose in descriptive power. TCD could lie between the two approaches because of the introduction of the scale length L . If it is reasonable to link critical distance to microstructure, indeed, TCD could act as a reinterpretation of LEFM in which microstructural phenomena are taken into account. This occurs by considering the presence of a scale parameter.

TCD may be related to several fracture theories. Links between TCD and LEFM were already emphasized in 2.2. Process zone models assign particular material properties in the plastic zone where damage occurs. In this zone, stress-strain curves control the process zone size. According to these models, when this dimension becomes critical, fracture takes place.

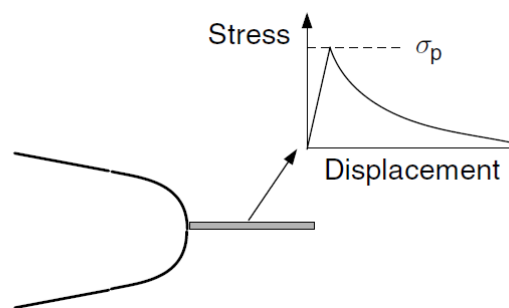


Figure 18 - Process Zone models (9)

Equations behind these models lead to the definition of the process zone size λ as:

$$\lambda = \frac{\pi}{8} \left(\frac{K_C}{\sigma_u} \right)^2 \quad (34)$$

the similarity of this quantity with critical distance is evident.

Statistical models, then, may be related to TCD. Weibull models for failure put in relation the probability density function of failure P_f to the ratio between σ (load) and σ^* (strength).

$$P_f = 1 - e^{-\left(\frac{\sigma}{\sigma^*}\right)^b} \quad (35)$$

When the constant b has a high value, the probability density function essentially predicts failure for a deterministic value of stress. On the contrary, when b has lower values, significant probability of failure far from hot-spot is detectable. This sounds very similar to the critical distance argument when non-local approach is adopted. Namely, a wider portion of material is involved in fracture assessment. Therefore, b may be related to L .

2.4 TCD and size effect

Conventional fracture theories consider material strength independently from component size. However, it is well known that larger components exhibit lower strength than smaller ones, due to statistical effect. Several models for static and fatigue failure can include the **size effect** in elastic problems. As emphasized in 2.3, an existing relation between non-local approaches and statistical models can be found. Among non-local methods, TCD shows its capability in predicting the size effect.

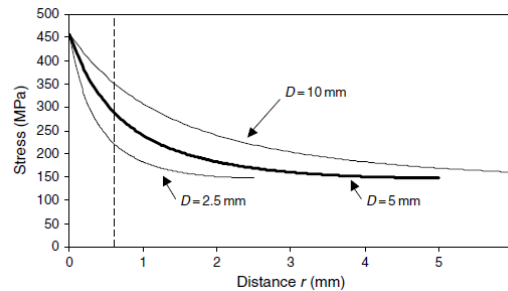


Figure 19 - Stress-distance curves for different notch size (9)

Three stress-distance curves for different notch sizes are reported in Figure 19. The specimens are shaped in such a way that stresses and notch geometries remain the same even though the size changes. By using the PM, it is clear that the reference stress to account for is higher in the biggest notch that, consequently, exhibits lower strength. The stress concentration factor K_t does not give this kind of information, since it is doubtless sensitive to the geometry, but not to the scale of the problem. This is evident when looking at the maximum stresses at the notches tips ($r = 0$) for the three different specimens: both the stress and K_t are the same for all notch sizes.

It is worth noticing that in the case of threaded joints, this represents an important element. It can occur that different threads design have different sizes but keep the same geometry. In this case the use of K_t for size effect evaluation is meaningless.

Moreover, component dimensions are one of the limits of TCD applicability. An explicatory example is reported in the bending beam of Figure 20.

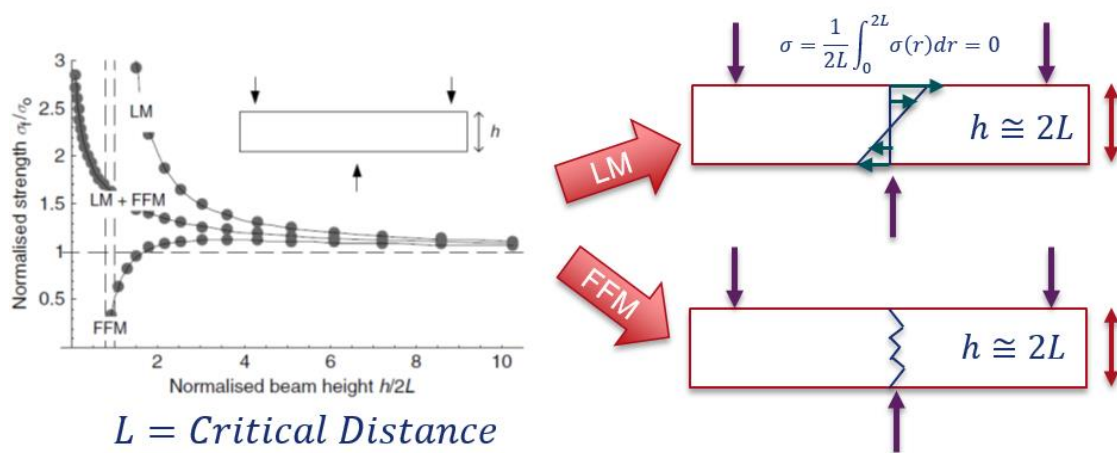


Figure 20 - Strength prediction in beam for different TCD approaches

When the height of the beam h is very high with respect to critical distance $2L$, the fracture stress σ_f corresponds to σ_0 since the crack is negligible. When h becomes very close to $2L$, LM is averaging a bending stress field over the entire beam height. Being this averaged stress null, the beam will be infinitely able to support the stress and σ_f will go to infinite. On the contrary, FFM is modelling a crack whose length completely covers the beam height. In this

case, the material will be infinitely unable to support the stress and σ_f will diverge from the LM prediction. As shown, two different TCD methods are not able to describe the presented situation and they even diverge; this introduces an important requirement for the correct application of the TCD: the component characteristic dimensions must be much greater than critical distance. When this hypothesis is not satisfied, only combined approaches can be used (LM+FFM) (10; 15). These criteria take advantage of a variable L , but their mathematics is quite complex for even the simplest problems and does not make them available for applications in the ICE field.

For threaded joints, a characteristic dimension playing the role of h in the beam could be found. In the TCD analyses carried out in this work all dimensions fulfil the mentioned hypothesis apart from the notch root radius (element 2 in Figure 21).

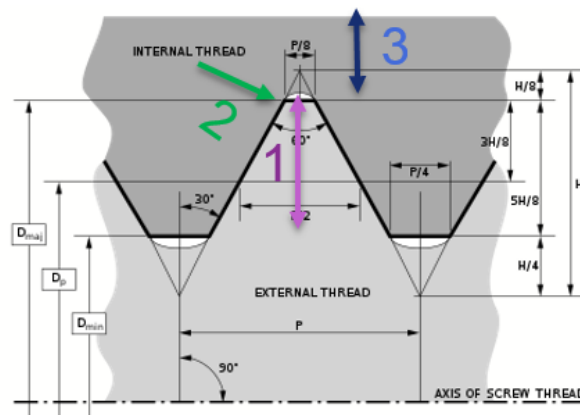


Figure 21 - Characteristic dimensions in threaded joints

2.5 Critical distance

Up to this point, the critical distance has been presented as a material constant depending on fracture toughness properties (K_{IC} , ΔK_{th}) and stress limits (σ_0 , $\Delta\sigma_0$). Actually, it is no easy task to understand why we should be able to predict components failure by considering stress far from hot-spots. Certainly, an important role is played by the critical distance, as it is not simply an arbitrary length on which the stress is averaged. It was already emphasized the TCD ability to play a role of connection between fracture theories, being the TCD a

generalized extension of these. This is confirmed by the fact that the classical fracture theories (LEFM) require some corrections in order to be able to model some phenomena as crack closure, whereas the TCD shows this capability even when these phenomena are not explicitly modelled. Furthermore, the non-local nature of the TCD methods make them suitable for size effect evaluation and strength assessment in stress concentration features. The critical distance was related to discrete quanta of crack propagation, statistical models, process zone models and LEFM. However, it can be also linked to microstructure and grain size. This would be the point in which LEFM is extended by considering mesoscale phenomena. Also non-propagating cracks length showed a link with critical distance (16). Given these evidences, how do we measure the critical distance?

From Eq. (25) and Eq. (26) it seems that the knowledge of two material constants is satisfactory. Strictly speaking, L and K_{IC} are material constants, whereas σ_0 directly comes from these two. The same concepts are applicable to the fatigue critical distance. σ_0 is called “inherent strength” and its value coincides with σ_u only for materials (e.g. ceramics) in which plasticity is not involved in the fracture process. When materials exhibit localized plasticity before fracture (e.g. ductile metals): $\frac{\sigma_0}{\sigma_u} > 1$. This is linked to the fact that, actually, σ_0 has no physical meaning and, for this reason, it is often used as a calibrating constant. By acting on σ_0 , critical distance value is tuned to find the best experimental data fit (Figure 22).

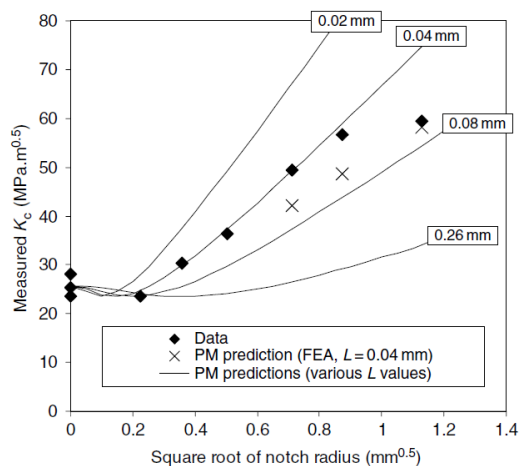


Figure 22 - Fracture toughness - Experimental correlation (9)

In Figure 22 several PM predictions differing in σ_0 are reported. The value of the inherent strength which predicts fracture toughness with the lowest error is $\frac{\sigma_0}{\sigma_u} = 2.7$.

Proposed methods for critical distance estimation usually are based on the assumption that L is a material constant and that it is not affected by the geometry of the component used for its measurement (17; 18; 8; 19; 20; 21). This sounds reasonable in light of the claimed generality of TCD. The author of this work strongly sustains the idea that a general theory should be able to predict the effect of geometry without being affected by that. Critical distance can be estimated from linear elastic stress-distance curves of notched components (Figure 23).

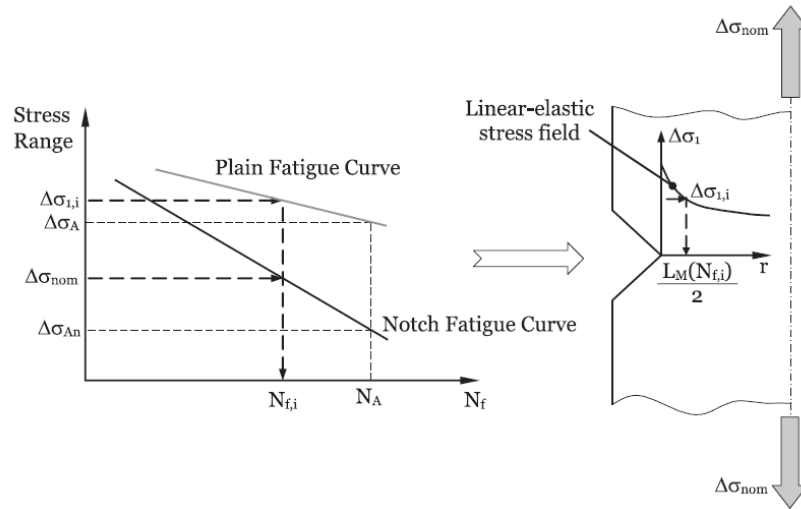


Figure 23 - Critical Distance Estimation (17)

Firstly, it must be said that critical distance evaluation can be made for any number of cycles to failure. From the plain fatigue curve, the critical stress of the plain specimen is extracted. If this stress is supposed to be coincident with the inherent strength, PM predicts incipient failure when the stress-distance curve reaches that value for $r = \frac{L}{2}$. From the notch fatigue curve, it is obtained the value of the stress amplitude $\Delta\sigma_{nom}$ necessary for the failure of the notched component. A FEM model is built and the linear elastic stress curve is extracted on the notch bisector. The coordinate r for which stress equals inherent strength is, according to PM, the approximation of $\frac{L}{2}$ (Figure 23).

Clearly, by using different geometries (e.g. blunt and sharp notches) a possible geometry effect seems to emerge as stress-distance curves present different gradients. However, the two curves can be used to find a value of the inherent strength σ_0 that makes the two estimations agree (Figure 24). This remarks the intrinsic nature of inherent strength and its usability as tuning parameter.

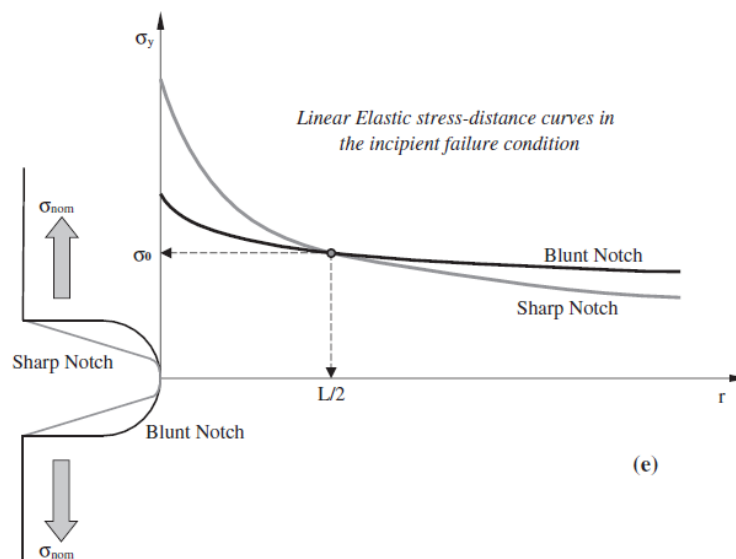


Figure 24 - Critical Distance Estimation for sharp and blunt notches (8)

In any case, it must be noticed that when a blunt notch is adopted, small errors on stresses bring to large error in critical distance estimation. On the contrary, when sharp notches are studied, small errors on critical distance result in large errors on the reference stress. Also for this reason, the use of sharp notches has to be preferred for critical distance estimation. Santus et al. (18; 21) performed sensitivity analyses regarding the problem of critical distance estimation. In those papers, more refined methodologies (inverse search methods) are proposed.

Other research activities are devoted to the study of the size effect in critical distance estimation. Yang et al. (22) found non-constant critical distances in DS Superalloy for which the constancy of the quantity $L' = K_t L$ emerged. Wang et al. (23) supported this modified TCD method considering critical distance size effect in their analyses.

However, according to the author's opinion some considerations on this argument must be made. Firstly, it is clear that K_t acts in this discussion as a parameter designated for the geometry description. When a sample specimen is loaded in controlled tension, K_t definition is straightforward and unambiguous but, if external multi-axiality is introduced, K_t evaluation becomes inexorably linked to the experimenter's hypotheses or reference regulations. Furthermore, the load type (tension, torsion, tension-torsion) would actually affect K_t and, therefore, L . For this reason, the author thinks that the modified TCD can doubtless show good accuracy when adopted for sample specimen, but what for actual industrial applications?

In the case of ICE, loads magnitude and multi-axiality grade continuously vary along time and this could make modified TCD inapplicable since this would require, for instance in a fatigue analysis, a continuous variation of the critical distance value. It may be asserted that a constant and approximated value of K_t could be used, but this approximation makes no sense, because K_t was introduced to properly consider L variability. Here it must be noticed that K_t evaluation may require the use of an equivalence stress criterion to consider multi-axiality. As it will be later explained, some fatigue algorithms cannot work with equivalence criteria, as critical plane criteria are needed. These types of criteria represent two opposite extremes when fatigue is modelled. Using both an equivalence criterion for L estimation and a critical plane criterion for fatigue life assessment may be a theoretical inconsistency.

Finally, as it was stated before, TCD should be able to predict geometric effect, but this would not be possible if TCD were influenced by the geometry effect itself. To the author's opinion, this sounds like using different discretization techniques (e.g. FEM, finite difference) to extract stresses from different geometries, because FEM alone does not work for both. As FEM is built on the general elastic theory, this event does not occur. By using K_t , the mentioned and supported generality of TCD is unavoidably lost. Nevertheless, engineering world is full of examples in which theoretical constraints are relaxed in order to describe actual physical phenomena.

Critical distance may be computed for different number of cycles to failure, N_f . Taylor and Susmel (24) proposed the following power law to express this variability:

$$L = AN_f^B \quad (36)$$

where A, B are material constants that can be used as tuning parameters for fatigue analyses. B is negative. The hypothesis on which Eq. (36) is based is reported in the following. When N_f is small (LCF), the applied stress is high and the size of the process zone (to which critical distance can be related) is large. On the contrary, a small process zone corresponds to the HCF case. In this way, the cyclic plastic behaviour may be modelled by the change in the process zone size (Eq. (36)), whereas stress is extracted through linear elastic laws (Linear Elastic FEA). This hypothesis is applicable for $N_f > 10^3$. Below this limit, Elastoplastic TCD (25; 26) is necessary. Elastoplastic TCD is not treated in this work since it is not employed. In any case, as usually occurs in very low cycle fatigue, stress-based models are replaced by strain-based models. Therefore, all the stress parameters used in classical TCD are replaced, in Elastoplastic TCD, by strain parameters (Figure 28).

2.6 Effect of the error on critical distance

The effect of the error on L is studied through an analytical model coming from the link between LEFM and TCD (Eq. (27)). The study was carried out considering the stress state for a subsequent fatigue analysis. Hence, safety factor is expressed in the form of FRF (Fatigue Reserve Factor) nevertheless, since in the analysed case FRF is a ratio between allowable and applied stress, its meaning remains valid also in a static case. By using Eq. (27) and PM, reference stress can be computed as:

$$\sigma_{PM} = \sigma \sqrt{\frac{\bar{a}}{L}} \quad (37)$$

An error on L is supposed ($E_L = \frac{\Delta L}{L}$) and the resulting error on σ_{PM} is computed:

$$E_\sigma = \frac{\Delta \sigma_{PM}}{\sigma_{PM}} = \sqrt{\frac{1}{1 + E_L}} - 1 \quad (38)$$

the error on Safety Factor is expressed as:

$$E_{FRF} = \frac{\Delta FRF}{FRF} = \frac{\sigma_{PM,correct} - \sigma_{PM,calculated}}{\sigma_{PM,calculated}} = -E_{\sigma} \sqrt{1 + E_L} = \sqrt{1 + E_L} - 1 \quad (39)$$

Figure 25 shows a chart expressing the relation of Eq. (39). The curve slope can be studied:

$$\frac{dE_{FRF}}{dE_L} = \frac{1}{2\sqrt{1 + E_L}} \quad (40)$$

From Eq. (40) it emerges that FRF is very sensitive to negative errors on L , since relevant parts of the stress-distance curve are neglected when L is underestimated.

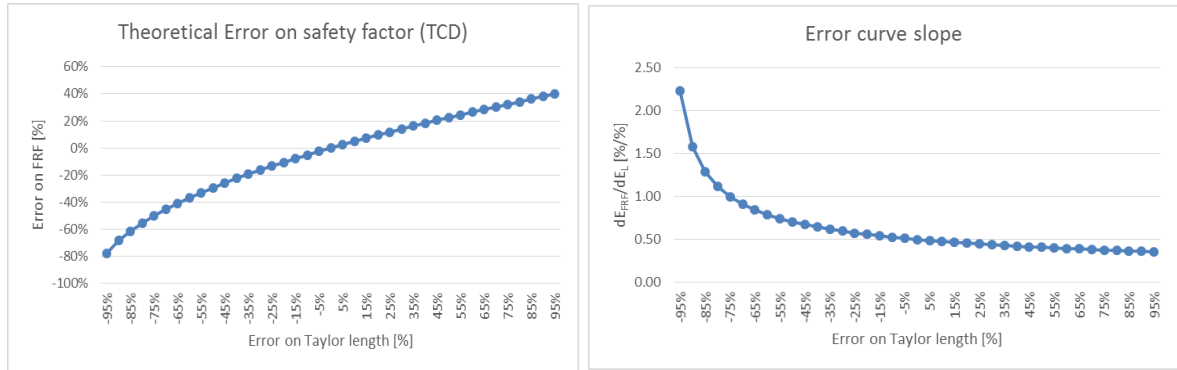


Figure 25 - Error on FRF (left) and curve slope (right)

2.7 TCD: some applications

Industrial applications of TCD are found in Engine Durability Analyses. Bishop (27) analysed the cylinder head and cylinder block through a critical distance/plane method. Namely, for a HCF analysis, a FEM model is set up and the nodal stresses history along time are extracted. The main hypothesis in this work is that, for defect-rich materials, fatigue crack initiation is Mode I dominated. Therefore, normal stress is assumed as damage parameter. This differs from the usual assumption based of fatigue crack initiation mechanism (shear stress and slip planes 1.4). Starting from the maximum normal stress, N_{max} , and the minimum normal stress N_{min} , the mean and the alternate normal stress are computed. Goodman's Mean Stress Correction (MSC) is applied and Safety Factor is computed on Haigh Diagram. The plane with the lowest Safety Factor is recognized as

critical plane of crack initiation. These computations are performed on a circle with a given radius (critical distance) searching for minimum Safety Factor (TCD). Some subjects of this analysis can be starting points for further discussions:

- Stress history is not decomposed into various cycles (each one with specific stress amplitude and mean stresses) but only the maximum and the minimum normal stresses are considered. In this way, the worst cycle alone is considered responsible of fatigue crack initiation. This may be reasonable when crack propagation is not expected and consequently not studied. However, it is certain that by neglecting smaller cycles effect, an approximation is introduced. Experimental validation is the only element that can give information on the weight of this approximation.
- Results obtained by using the normal stress as damage parameter may differ from shear-stress based models. Jang et al. (28; 29) studied the problem of fatigue crack initiation and growth in porous Cast 319-T7, taking into account that fatigue cracking mechanism is dominated by shear planes.
- Critical plane criteria, whose meaning will be later explained in depth, are based on the physical assumption that there is a special plane located where the chosen damage parameter (e.g. shear stress) experiences the maximum variability (stress amplitude). **The plane of minimum safety factor is not necessarily coincident with the plane of the mentioned assumption.** Moreover, when the stress signal contains more than one cycle and consequently more than one stress amplitude level, the research of this plane is not trivial.
- On the basis of the TCD description made up to this point, no other remarks are necessary to express critical distance meaning.

In the field of Academic research, Susmel and Taylor (24) applied the Modified Wöhler Curve Method (MWCM) (30) to predict fatigue lives of notched specimens in the medium/high cycles regime under biaxial loads. MWCM is a critical plane approach. The

normal mean stress $\sigma_{n,m}$, the amplitude of the normal stress $\sigma_{n,a}$ and the shear stress amplitude τ_a , taken on the maximum shear amplitude plane, define the stress ratio ρ_{eff} .

$$\rho_{eff} = \frac{m\sigma_{n,m} + \sigma_{n,a}}{\tau_a} \quad (41)$$

By using Mohr's circles (Figure 7) it is simple to demonstrate that ρ_{eff} may vary between 0 (in fully reversed torsion) and 1 (in fully reversed tension). m is the mean stress sensitivity of the material and it is obtained experimentally. MWCM is essentially based on modifications of the fully reversed torsion Wöhler curve. The curve slope k_τ and fatigue limit $\tau_{A,ref}$ are therefore expressed as linear functions of the stress ratio.

$$k_\tau(\rho_{eff}) = (k - k_0)\rho_{eff} + k_0 \text{ for } \rho_{eff} \leq \rho_{lim} \quad (42)$$

$$k_\tau(\rho_{eff}) = (k - k_0)\rho_{lim} + k_0 \text{ for } \rho_{eff} > \rho_{lim} \quad (43)$$

$$\tau_{A,ref}(\rho_{eff}) = \left(\frac{\sigma_A}{2} - \tau_A\right)\rho_{eff} + \tau_A \text{ for } \rho_{eff} \leq \rho_{lim} \quad (44)$$

$$\tau_{A,ref}(\rho_{eff}) = \left(\frac{\sigma_A}{2} - \tau_A\right)\rho_{lim} + \tau_A \text{ for } \rho_{eff} > \rho_{lim} \quad (45)$$

ρ_{lim} is a limit value imposed to take into account that, when micro/meso cracks are fully open, normal stress increment does not affect fatigue damage (24). k_0 and k represent Wöhler curves slope respectively in torsion and tension. σ_A and τ_A are the fatigue limits respectively in tension and torsion.

From the Modified Curve, the number of cycles to failure is obtained as:

$$N_f = N_A \left[\frac{\tau_{A,ref}(\rho_{eff})}{\tau_a} \right]^{k_\tau(\rho_{eff})} \quad (46)$$

To apply these concepts from a TCD point of view means that the dependence of L from N_f must be considered too (Eq. (36)). For this reason, both N_f and the stress τ_a are unknown and an iterative procedure is necessary (Figure 26). According to the PM, the point for which is searched along the focus path:

$$r = \frac{L}{2} = \frac{AN_f^B}{2} \quad (47)$$

In the case of Variable Amplitude (VA) loadings it is not possible to identify a single τ_a therefore a cycle counting method must be adopted (e.g. Rainflow). Each of the extracted cycles has its own stress amplitude level: how shall the critical plane be searched in this case?

Also this point will be later discussed. However, several method can be adopted to measure shear stress variability on a specific plane. Among them, the Maximum Variance Method (MVM) (31) is considered of primary importance. The variance of the stress signal is indeed supposed to be a measurement of its variability. It is worth underlining at this point that, as MVM, all the criteria available for the critical plane research are based on the stress/stain signal and none of them uses Safety Factor for assessing the position of the critical plane. This actually makes sense if we think that the Safety Factor is something that comes after the fatigue model has been applied, whereas stress signal exists *a priori*. Anyway, most of the actual industrial applications, together with commercial fatigue post-processors (32; 33), assign to the lowest Safety Factor plane the name of “Critical Plane”.

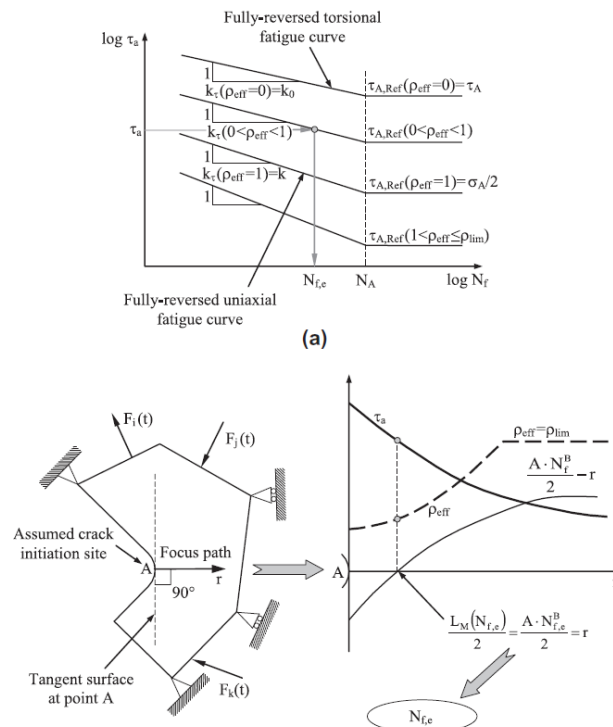


Figure 26 - MWCM and TCD (24)

The calculated Safety Factor will actually be the lowest identifiable. However, one of the author's doubts lies in the fact that this lowest Safety Factor plane is the actual plane of crack initiation. For VA loads, the resolved shear stress on the identified plane is indicated as τ_{MV} . Along the period T , are defined:

$$\tau_m = \frac{1}{T} \int_0^T \tau_{MV}(t) dt \quad (48)$$

$$Var[\tau_{MV}(t)] = \frac{1}{T} \int_0^T (\tau_{MV}(t) - \tau_m)^2 dt \quad (49)$$

$$\tau_a = \sqrt{2Var[\tau_{MV}(t)]} \quad (50)$$

$$\sigma_{n,a} = \sqrt{2Var[\sigma_n(t)]} \quad (51)$$

$$\sigma_{n,m} = \frac{1}{T} \int_0^T \sigma_n(t) dt \quad (52)$$

ρ_{eff} is computed using Eq. (41). From the Modified Wöhler Curve, the number of cycles to failure, $N_{f,i}$, is computed for each cycle i . If n_i is the number of cycles experienced for a certain stress level $\tau_{a,i}$, the cumulative damage D_{tot} is:

$$D_{tot} = \sum \frac{n_i}{N_{f,i}} \quad (53)$$

According to Miner's rule (Eq. (53)), fatigue failure occurs when the critical cumulative damage D_{cr} is reached. As a first approximation, this D_{cr} can be assumed unitary. However, Susmel and Taylor (24) suggest linear relationships relating D_{cr} to ρ_{eff} throughout material calibrating constants. The equivalent number of cycles to failure $N_{f,eq}$ can be expressed as:

$$N_{f,eq} = \frac{D_{cr}(\rho_{eff})n_{tot}}{D_{tot}} \quad (54)$$

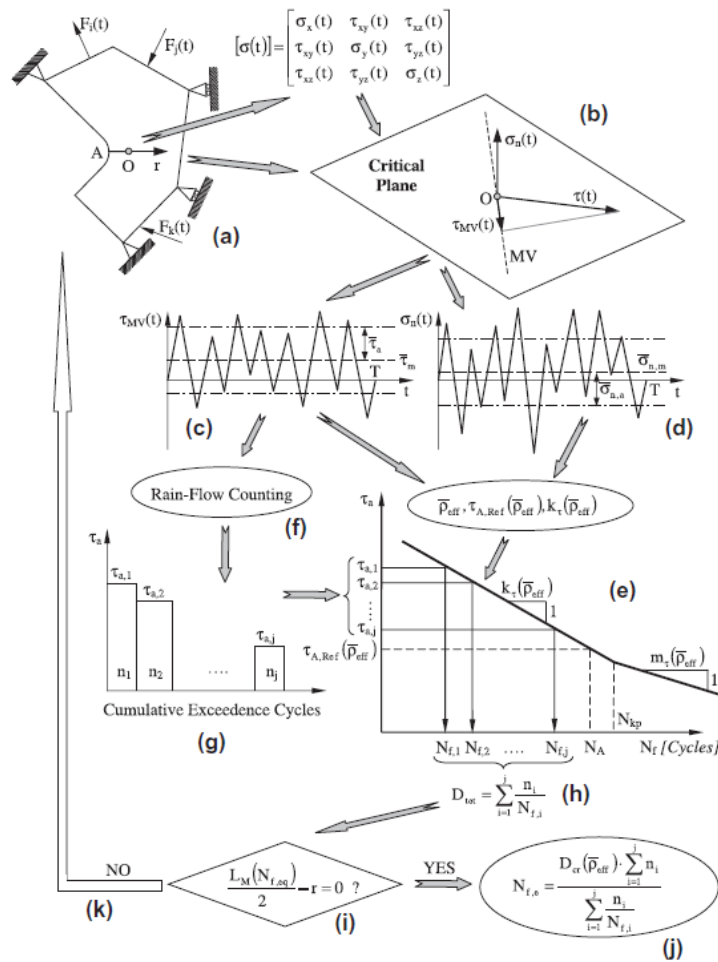


Figure 27 - MWCM and TCD - VA loads (24)

Also in this case, by taking advantage of PM argument, the point for which $r - \frac{AN_{f,eq}^B}{2} = 0$ is searched.

For sake of completeness, a chart showing a similar procedure in Elasto-plastic TCD is reported (Figure 28).

Applications of MWCM are found in the study of the fretting fatigue. Kouanga et al. (17) applied critical distance concepts studying damage mechanics of contacting mechanical surfaces. In ICE's fretting fatigue is detectable, for instance, at the interface between cylinder block and cylinder head. An interesting aspect is that damage mechanism in fretting fatigue failure is similar to the one observed in notched structure.

This is the so-called *notch analogue* that encouraged some researchers to attempt an application of the same fatigue concepts adopted for notched components (TCD) to the fretting fatigue (17; 34).

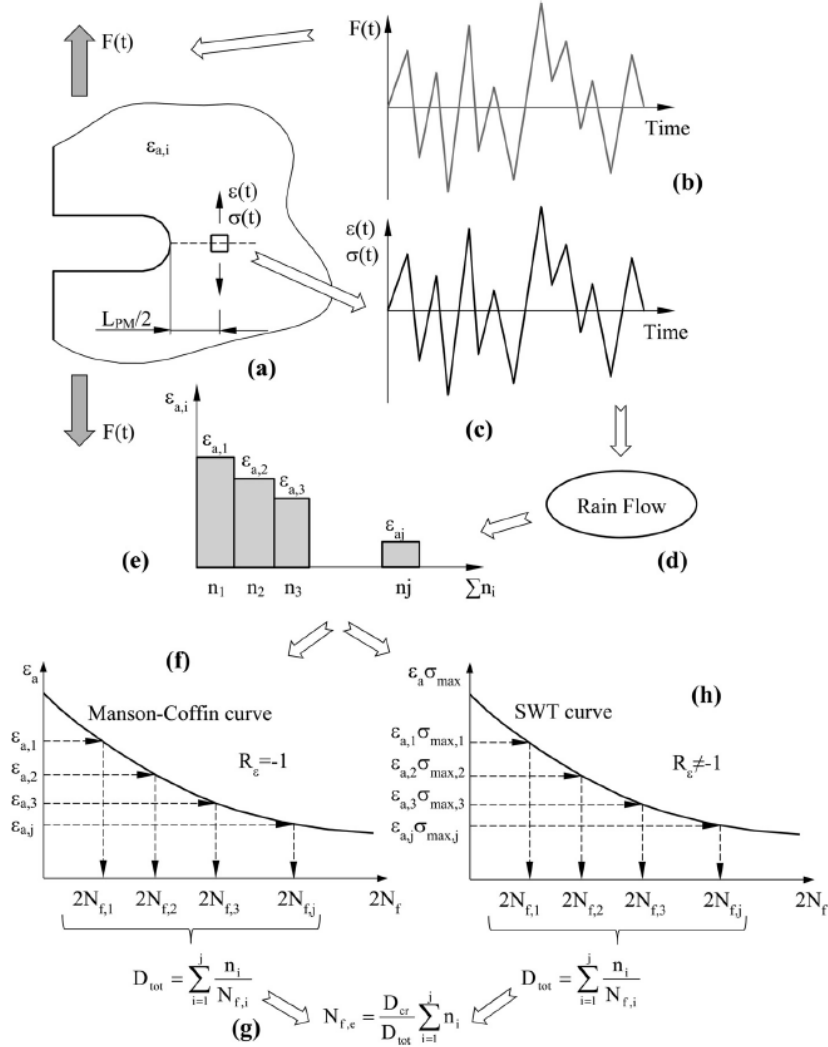


Figure 28 - Elasto-plastic TCD (26)

3 Multiaxial Fatigue: design and endurance criteria

Threaded bores are designed to support uniaxial loads; however, fatigue cracks always originate in the notch zone where the stress state is multiaxial due to the notch effect. For this reason, the use of multiaxial fatigue criteria becomes of primary importance, since even uniaxial loads may lead to bi-axial and three-axial stress states. The term “inherent multiaxiality” refers to the multiaxial stress state resulting from stress concentration features and geometry, rather than from external loads.

As anticipated, the problem of assessing the fatigue life of threaded bores in ICE’s is not resolvable in a closed form that, given some inputs, returns failure assessment as an output.

Reasons of these difficulties are explained into the introduction to this work, where the importance of dividing the problem into smaller and solvable ones, as usually occurs in common engineering practice, definitely stands out.

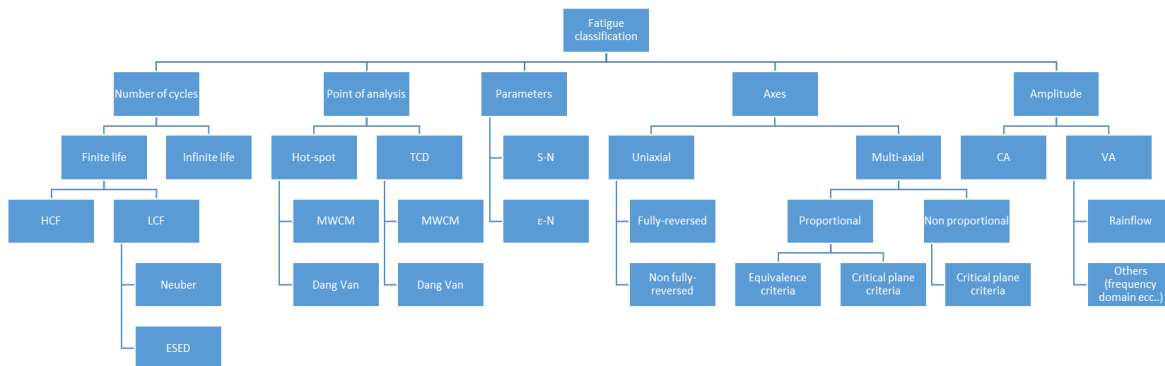


Figure 29 - Fatigue classification

If the problem of fatigue is considered as stand-alone, the understanding of the kind of fatigue to consider already requires simplified hypotheses.

The studied problem may be classified according to the number of cycles to failure. HCF methods clearly differ from LCF ones. When dealing with LCF, plasticity is certainly involved and FEA should take it into account. Non-linearities introduced by plasticity slow down the computation process and increase the analyses' cost. For this reason, the Neuber's rule (35; 36) and the Equivalent Strain Energy Density (ESED) are used in order to correct results coming from elastic FEA by considering plasticity. The great advantage of these methods is that they are applicable after that elastic analyses results are obtained. Usually stress based methods ($S - N$) are adopted in HCF, whereas strain based methods ($\epsilon - N$) are employed in LCF study.

Next, it was shown that both local and non-local approaches may be used regardless of the chosen criterion. Another recurrent misunderstanding in fatigue analyses regards the distinction between Constant Amplitude (CA) and Variable Amplitude (VA) loadings. It often happens that from stress signals mean stress and stress amplitude are extracted looking at the maximum and the minimum stress. Strictly speaking, stress amplitude and mean stress are two terms that have meaning when a sinusoidal stress history is taken into account but if random signals are considered, then, things may be different.

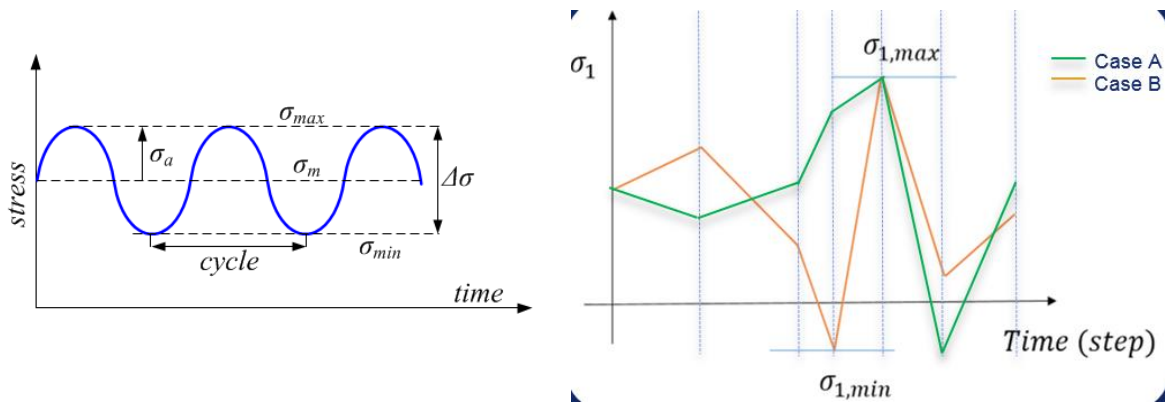


Figure 30 – Sinusoidal stress history (on the left). Different random stress histories (on the right)

As it is shown in Figure 30, two completely different stress histories may result in the same mean stress and stress amplitude, if the above-mentioned approximation is performed. It is

for this reason that several extraction techniques have been developed working both in time and in frequency domain, in order to make random stress histories equivalent to a series of cycles, each or them characterized by its own stress amplitude and mean stress. Among them, the Rainflow (37) method is the most used (Figure 31). If it were possible to perform fatigue assessment directly in time domain, the use of mean stress and stress amplitude would be unnecessary. This is hard to believe as engineers' minds automatically associate these quantities to fatigue analyses since Wöhler and Goodman published their works.

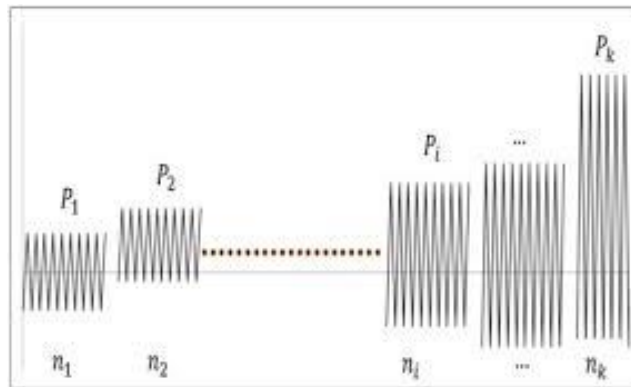


Figure 31 - Stress history after Rainflow application

Only the Dang Van Criterion, that will be later introduced, shows this ability.

As it was shown in MWCM, CA and VA loads require different algorithms. Fatigue and material properties are usually referred to as uniaxial tests. Consequently, uniaxial loadings do not need equivalence criteria. Conversely, multiaxial loadings need a kind of transformation to compare them with uniaxial loading. This constantly occurs in static yielding criteria, when the Tresca or the Von Mises hypothesis is employed. Regarding fatigue, this cannot always be applied since loads do not differ only in direction, but also in their phasing in the time domain.

The problem analysed in this thesis regards the threaded bores of the engine block. The engaged bolts connect the engine block to the engine head and the engine block to the main caps. Since in these regions the stress history depends on the engine operation point, it is not possible to assess the actual fatigue cycle because different engines experience different loads in their life. It is clear that statistical quantities and Power Spectral Density

(PSD) methods may accomplish to this task. However, being in a first approximation analysis, these complexities are not included. Instead, the hypothesis that the full load engine cycle is the stress provider for the whole engine life is carried on, seeming the most conservative one. However, the risk of being too conservative is obvious, as no engine will constantly work in full load conditions. Aluminium components are expected to overcome 10^7 cycles: HCF is therefore considered. Due to the multiaxiality of the stress state at the notch root, non-local approaches (TCD) and the Multiaxial Fatigue are used herein.

3.1 Proportionality of loads

Multiaxial fatigue implies loads variability along time. When loads act in phase, principal stress moduli vary in time but principal stress directions are fixed. These are proportional loadings. In this case, stress tensor $\boldsymbol{\sigma}(t)$ may be expressed through the stress amplitude tensor $\boldsymbol{\sigma}_a$ and the mean stress tensor $\boldsymbol{\sigma}_m$:

$$\boldsymbol{\sigma}(t) = \boldsymbol{\sigma}_a f(t) + \boldsymbol{\sigma}_m \quad (55)$$

Given the normal vector to a specific plane \mathbf{n} , normal stress and shear stresses can be expressed as:

$$\sigma_N(t) = (\mathbf{n} \cdot \boldsymbol{\sigma}(t) \cdot \mathbf{n}) \cdot \mathbf{n} \quad (56)$$

$$\tau(t) = (\boldsymbol{\sigma}(t) \cdot \mathbf{n} - (\mathbf{n} \cdot \boldsymbol{\sigma}(t) \cdot \mathbf{n}) \cdot \mathbf{n}) \quad (57)$$

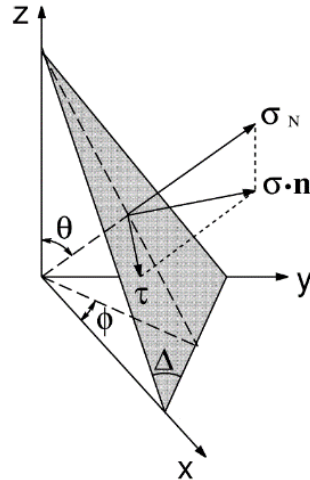


Figure 32 - Normal Stress and Shear Stress vectors (38)

If $\sigma_m = k\sigma_a$:

$$\tau(t) = \|\sigma_a \cdot \mathbf{n} - (\mathbf{n} \cdot \sigma_a \cdot \mathbf{n}) \cdot \mathbf{n}\|(f(t) + k) \quad (58)$$

the shear stress amplitude and mean shear stress are:

$$\tau_a = \|\sigma_a \cdot \mathbf{n} - (\mathbf{n} \cdot \sigma_a \cdot \mathbf{n}) \cdot \mathbf{n}\| \quad (59)$$

$$\tau_m = k\|\sigma_a \cdot \mathbf{n} - (\mathbf{n} \cdot \sigma_a \cdot \mathbf{n}) \cdot \mathbf{n}\| \quad (60)$$

In this case, the shear stress vector does not change direction and the path Ψ , described by the vector $\tau(t)$, collapses into a straight line (38): at this point, dealing with vector moduli or vectors is the same matter.

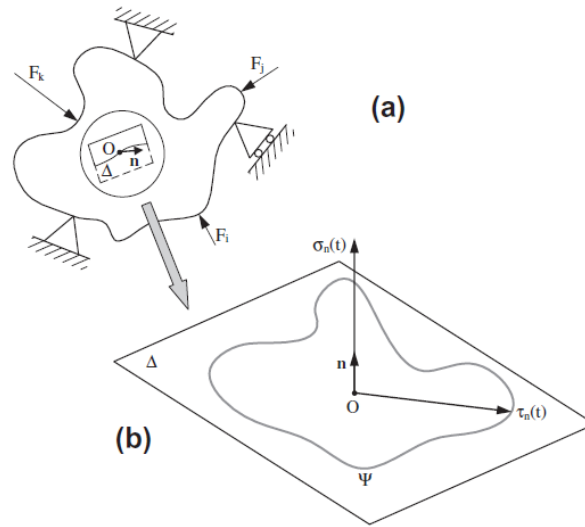


Figure 33 - Body subjected to external forces (a). Shear stress vector path (b) (31)

Moreover, it is even clearer that, when it is not possible to write Eq. (59) and Eq. (60), defining a shear stress amplitude is no longer straightforward and it must be defined through a particular measure of the stress path Ψ (38). In the case of out of phase loadings, principal stress directions vary along time. The consequences of this fact are not negligible.

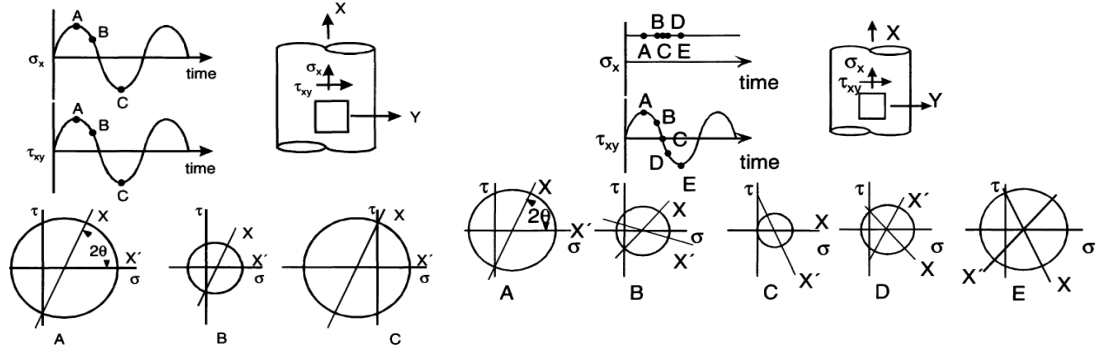


Figure 34 - Load Proportionality. Proportional loads on the left. Non-Proportional loads on the right. (2)

3.2 Equivalence and critical plane criteria

As highlighted, when principal stress directions remain constant, the meanings of vector and moduli overlap. The Principal stress ranges $\Delta\sigma_{1,2,3}$ may be combined, making algebra, in order to obtain equivalent stress ranges to compare with uniaxial fatigue properties. These are **equivalence criteria**. One of them is the octahedral shear stress criterion (Von Mises):

$$\Delta\sigma_{eq} = \frac{1}{\sqrt{2}} [(\Delta\sigma_1 - \Delta\sigma_2)^2 + (\Delta\sigma_2 - \Delta\sigma_3)^2 + (\Delta\sigma_3 - \Delta\sigma_1)^2]^{\frac{1}{2}} \quad (61)$$

If loadings are non-proportional (that is the most general case): $\Delta\sigma_1 - \Delta\sigma_3 \neq \Delta(\sigma_1 - \sigma_3)$. In such a case the equivalence criteria make no sense.

Critical plane criteria solve this inconsistency. The basic idea is that the directionality of the problem must be taken into account; among all the possible directions, the plane of fatigue crack initiation plays a prominent role. Generally, some parameters are extracted from a rotated stress tensor. These parameters are combined to form the so-called **damage parameter $P(\theta)$** , that is in its turn a function of the selected plane. The plane on which $P(\theta)$ is maximised is the critical plane. $P(\theta)$ is then related to a material model which expresses fatigue strength.

Generally:

$$P(\theta)_{max} = f(N_f)_{elastic} + f(N_f)_{plastic} \quad (62)$$

Since the critical plane is expected to be related to the plane of crack initiation, $P(\theta)$ is often linked to physical quantities involved in the fracture process. Among them: shear stress/strain, normal stress/strain or combinations of these are the most used. If shear stress acts for crack initiation, then, normal stress controls crack propagation and the final fracture process.

$$P(\theta) = \tau_a \quad (63)$$

$$P(\theta) = \sigma_{n,a} \quad (64)$$

$$P(\theta) = \tau_a + \alpha \sigma_{n,a} \quad \alpha \text{ constant} \quad (65)$$

As these quantities are studied along precise directions, the discussed problem regarding equivalence criteria is not encountered.

Findley (39) was the first one to propose this type of criterion basing on experimental data. According to this criterion, fatigue failures starts from the plane on which the term on the left side of Eq. (66) is maximised. The right-end side is a material property.

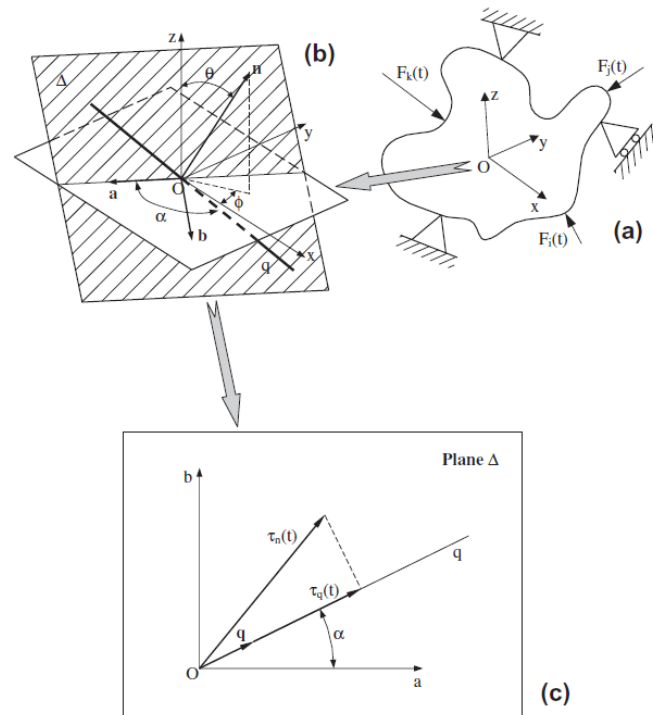


Figure 35 - From system of forces (a) to resolved shear stress (c) (31)

$$\left(\frac{\Delta\tau}{2} + k\sigma_n\right)_{max} = f \quad (66)$$

Critical plane research is one of the thorniest argument in multiaxial fatigue dissertation. Let suppose to take shear stress as damage parameter. It was demonstrate that, according to the shape of the stress path Ψ , defining a stress amplitude may become ambiguous. Different methods were proposed to solve this problem. Among them, the **longest chord method**, the **longest projection methods** and the **minimum circumscribed circle method** (38) are the most used. **MVM** (31) showed to be one of the most efficient algorithms for critical plane identification, as the computational time does not depend on the length of the stress history.

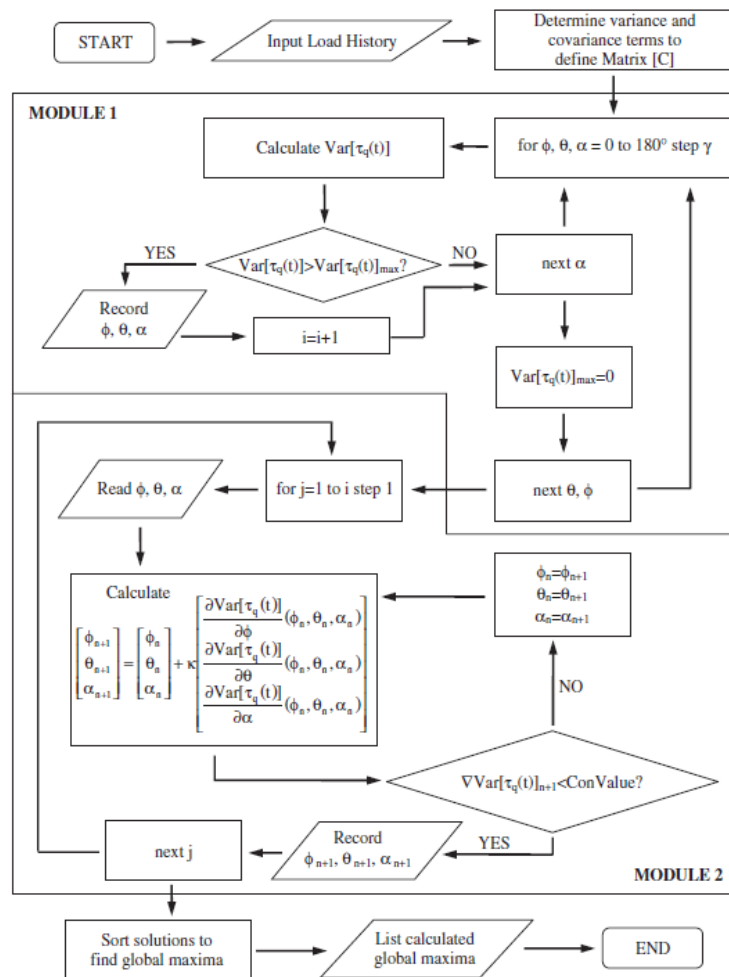


Figure 36 - Maximum Variance Method (31)

Figure 36 shows a flow chart describing the algorithm proposed by Susmel. In the first module, the time history of the variance of the resolved shear stress is computed in a roughly discretized space defined by angles ϕ, α, θ . The possible local maxima are stored and used as starting point for the application of the Gradient Ascent method in the second module. Finally, Maximum Variance Plane is identified.

3.3 Fatigue life criteria

As reported in Eq. (62), a common structure for different fatigue life models can be found. They are so defined:

- ϵ'_f Fatigue ductility coefficient
- c Fatigue ductility exponent
- σ'_f Fatigue strength coefficient
- τ'_f Fatigue strength torsional coefficient
- b Fatigue strength exponent

The first critical plane stress-based model was proposed by Findley (Eq. (66)) and it can be used both for a Safety Factor evaluation and for a number of cycles to failure computation. In the latter, a Basquin curve is defined:

$$\frac{\Delta\tau}{2} + k\sigma_n = \tau_f^* (N_f)^b \quad (67)$$

τ_f^* is strictly related to τ'_f . All the critical plane stress-based criteria work in a similar way (e.g. McDiarmid). On the contrary, static yield criteria are based on the assumption that an equivalent uniaxial stress can be found starting from a multiaxial stress.

Maximum normal stress, maximum shear stress and von Mises criterion work in this direction. In the case of maximum shear stress:

$$\Delta\sigma_{eq} = \frac{\Delta\sigma_1 - \Delta\sigma_3}{2} \quad (68)$$

Problems related to these criteria when non-proportional or VA loads are applied have been already discussed.

Strain-based models were introduced in 1950s when Coffin and Manson demonstrated a power law relationship between plastic strain and fatigue life in LCF (2):

$$\frac{\Delta\epsilon}{2} = \frac{\Delta\epsilon_{elastic}}{2} + \frac{\Delta\epsilon_{plastic}}{2} = \frac{\sigma'_f}{E} (2N_f)^b + \epsilon'_f (2N_f)^c \quad (69)$$

When multiaxiality is involved, it is possible to introduce equivalence strain criteria as well as stress-based models. Maximum normal strain, maximum shear strain and octahedral shear strain may be therefore used as equivalence strains.

Almost twenty years after the works of Coffin and Manson, it was found that equivalent strain criteria did not correlate tension and torsion test. In light of the treated subjects, reasons for this event to occur should be clear to the reader. Critical plane criteria were therefore introduced also in the case of LCF.

Brown and Miller proposed a Findley-like model considering that, dealing with LCF, cyclic shear and normal strain acting on the maximum shear plane should be considered. The damage parameter is defined as:

$$P_{BM} = \frac{\Delta\gamma_{max}}{2} + S\Delta\epsilon_n \quad (70)$$

where S is the normal strain coefficient and it is a material constant.

A fatigue life model similar to Manson-Coffin curve can be expressed in this way:

$$P_{BM} = \frac{A\sigma'_f}{E} (2N_f)^b + B\epsilon'_f (2N_f)^c \quad (71)$$

with $A = 1.3 + 0.7S$ and $B = 1.5 + 0.5S$. Fatemi and Socie suggested that normal strain should be replaced by normal stress in Eq. (77) and modified Brown-Miller model.

The mentioned criteria assume that crack nucleation is shear-dominated and this is physically consistent. Nevertheless, in some materials (e.g. cast iron) cracks nucleate in shear but their early growth is controlled by normal stress (2). In this context, Smith, Watson and Topper developed the so-called SWT parameter on the principal strain range plane as:

$$P_{SWT} = \frac{\sigma_{n,max}\Delta\epsilon_1}{2} = \frac{\sigma'^2_f}{E} (2N_f)^{2b} + \sigma'_f\epsilon'_f (2N_f)^{b+c} \quad (72)$$

It is common to find SWT parameter expressed also as $P_{SWT} = \sqrt{\sigma_{n,max} \Delta \epsilon_1 / 2}$

In this way, the mean stress effect is also taken into account. For this reason, SWT is also used as a Mean Stress Correction (MSC) form even in uniaxial cases.

Morrow MSC, instead, is to be intended as a modification of the Manson-Coffin curve.

$$\frac{\Delta \epsilon}{2} = \frac{\Delta \epsilon_{elastic}}{2} + \frac{\Delta \epsilon_{plastic}}{2} = \frac{\sigma'_f - \sigma_m}{E} (2N_f)^b + \epsilon'_f (2N_f)^c \quad (73)$$

3.4 Dang Van Criterion

Literature refers to DVC (40) as one of the most used multiaxial fatigue criterion in the automotive design, but examples of its application are available in many fields. As demonstrated, the great problem of multiaxial fatigue lies in the fact that FEA delivers full component stress tensor (41), but material properties are referred to uniaxial tests. The concepts of alternate, mean and equivalent stress are introduced to formulate some hypotheses that relate multiaxial time histories to uniaxial parameters. Critical plane criteria solve this issue by considering only some components of a rotated tensor. In any case, time history needs to be transformed in order to separately take into account the effect of alternate and mean stresses. What if we could directly compare stress tensor time history with uniaxial fatigue properties?

Certainly, cycle-counting methods were not necessary, but the problem of transforming a stress tensor into a scalar (keeping the information on multiaxiality) remains evident. DVC performs this task as long as it is used for crack initiation assessment, though it is based on a multi-scale approach.

DVC was firstly used in France, in the field of automotive industry. It is based on the assumption that, when dealing with HCF, stress at macroscopic scale remains elastic, whereas at microscopic scale, the metals are neither isotropic nor homogeneous, since crystals are random oriented (42). Indeed, in some favourable oriented grains, local stress may exceed yield strength. According to DVC, if the stabilized response in these grains is not elastic shakedown, micro-cracks nucleate. Macroscopically, this corresponds to the

stress conditions close to the fatigue limit. At least as far as its first appearance, DVC capability in fatigue assessment cannot overcome the phase of crack nucleation in predictions. With **elastic shakedown** state it is meant the state of a material exhibiting a total elastic stabilized response when it is cyclically stressed. In this context, the hardening model acquires significant importance (Figure 37).

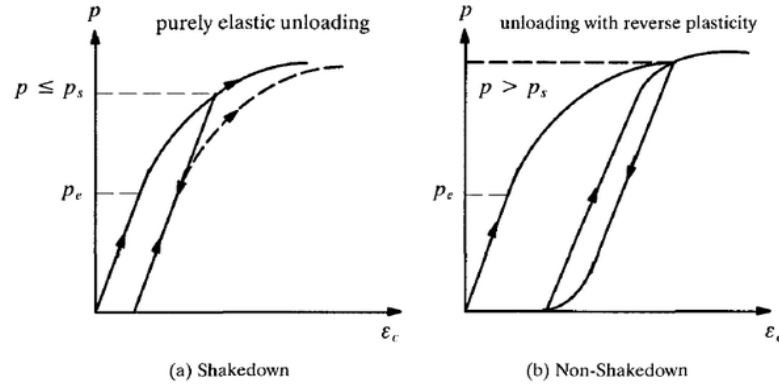


Figure 37 - Elastic Shakedown

When a certain function of the microscopic stabilized stress exceed a threshold value, crack initiation is therefore predicted to occur. Since this condition may be verified at any time, it is clear that this criterion can directly work in the time domain. Indeed, for crack nucleation it is sufficient that the threshold is reached even for a single instant. To the author's opinion, transposing these concepts in the finite-life regime may be unsafe since a single instant, in which the stress equals a defined threshold, could be not sufficient to assess failure for a defined number of cycles. However, Wang et al. adopted a modified DVC in which the constants parameters of the method are modified by using Wöhler curves, in order to predict the number of cycles to failure in the exhaust system (43).

Microscopic shear stress τ_{ms} is supposed to be responsible of fatigue crack initiation, whereas the hydrostatic pressure acts for crack opening. The failure criterion can be therefore expressed as:

$$\tau_{ms}(t) + \alpha p(t) = \beta \quad (74)$$

where α, β are material constants directly obtainable from torsion and tension fatigue properties. Eq. (74) may be graphically as in Figure 38.

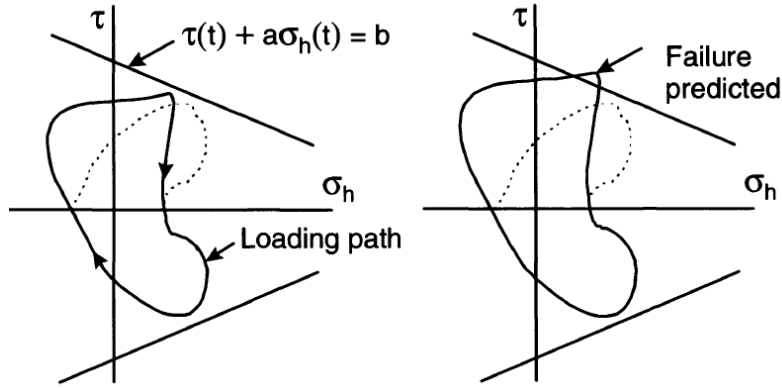


Figure 38 - Dang Van Plot

Transposing DVC into the finite life regime means: $\alpha = \alpha(N_f)$ and $\beta = \beta(N_f)$. Since $\tau_{ms}(t)$ can be computed on different planes, the critical plane approach is adopted to take into account multiaxiality. In its original formulation, Eq. (74) was:

$$\max_n \left\{ \max_t [|\tau_{ms}(n, t)| + \alpha p(t)] \right\} = \beta \quad (75)$$

where n defines the normal to the examined plane. It was later modified making approximations on the critical plane shear stress:

$$\tau_{ms}(t) = (\sigma_{1,ms}(t) - \sigma_{2,ms}(t))/2 \quad (76)$$

The *microscopic stress tensor* is computed by introducing the *microscopic residual stress tensor* ρ :

$$\sigma_{ms} = \sigma + \rho \quad (77)$$

The computation of the residual stress tensor ρ involves the use of yield surfaces. Essentially, the stress tensor time history can be represented in a six-dimension space. The centre of the smallest hypersphere in which the macroscopic loading path is included is strictly related to the residual stress tensor. Further details on the macroscopic-microscopic scale transition are reported in (44). Ciavarella et al. apply this algorithm in the study of rolling contact fatigue (45). Several applications of DVC are found.

- Ferjani et al. (46) applied DVC to predict the number of cycles to failure of threaded connections in the oil-gas industry field.
- Bolts fatigue is analysed by Fares et al. (47).
- Einolghozati et al. (48) studied the behaviour of wind turbine hubs subjected to multiaxial non-proportional VA loadings and solved an optimization problem.
- Savu et al. (49) proposed a revised DVC in which the role of hydrostatic pressure is played by mesoscopic normal stress.
- In the early use in the automotive field, Henry et al. (50) applied DVC to crankshafts and proposed crank-web design modifications on the basis of the HCF Dang Van analysis.
- Ouakka and Langa (51) optimized automotive coil springs.
- DVC is applied along TCD in the study of fretting fatigue by Araujo et al. (34). In this study, a comparison between DVC and MWCM is carried out both from a local and TCD standpoint. The highest accuracy is obtained by applying TCD along with the MWCM. Hot-spot approaches overestimated fatigue damage.
- Cerullo (52) simulated rolling contact in wind turbine roller bearings.
- Hoffman et al. (53) applied DVC by considering microstructure.

By using DVC concepts, the Safety Factor can be expressed as:

$$SF = \frac{\beta}{\max(\tau_{ms}(t) + \alpha p(t))} \quad (78)$$

Many authors (43) suppose that neglecting differences between macroscopic and microscopic stress tensors is an acceptable engineering hypothesis.

3.5 Durability analysis in commercial fatigue post-processors

Commercial fatigue post-processors implement some of the presented concepts. Stress histories may be delivered by Elastic FEA (which require the use of HCF algorithms or Neuber's rule for plasticity correction) or by Elastic-plastic FEA. In uniaxial cases (rarely occurring), stress-based models are based on the Basquin curve:

$$\frac{\Delta\sigma}{2} = S_a = \sigma_f' (2N_f)^b \quad (79)$$

This model may be modified in order to take into account the presence of mean stresses. Goodman's MSC is based on the Goodman's diagram (Figure 39).

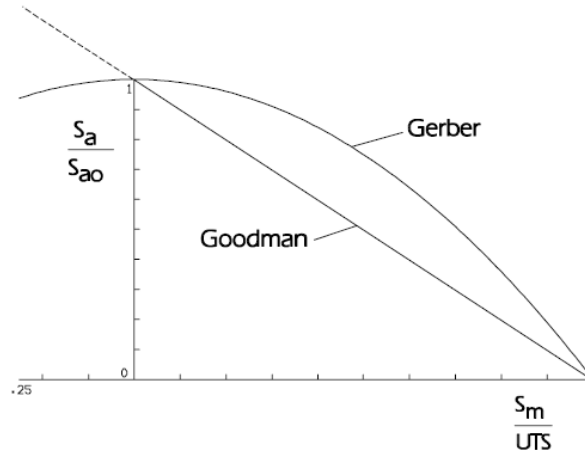


Figure 39 - Goodman and Gerber MSC (14)

If no mean stress S_m were present, the Stress amplitude S_{a0} would act on the component. S_{a0} can be computed from both Goodman relation:

$$\frac{S_a}{S_{a0}} + \frac{S_m}{UTS} = 1 \quad (80)$$

and Gerber hyperbola

$$\frac{S_a}{S_{a0}} + \left(\frac{S_m}{UTS}\right)^2 = 1 \quad (81)$$

This is another point of view from which Goodman Diagram can be seen since it is usually employed to decrease endurance properties (fatigue limit), rather than increase the value of the applied stress S_a . However, this is the only approach that can be adopted if a MSC is to be applied in a Basquin-like model as no endurance limit comes into view in Eq. (79).

VA Stress histories are processed through the Rainflow and the Miner's Rule. Critical cumulative damage is imposed to be unitary in some post-processors (32), whereas its value can be varied in others (33). As emphasized in 2.7, making use of this parameter as a calibrating constant is what allows numerical-experimental correlation to be established.

Durability analyses can pursue the goal of computing the Safety Factor for fatigue failure or the fatigue life. In these software, the Safety Factors calculated may be the Fatigue Reserve Factor (FRF) or Factor of Strength (FOS).

FRF is computed as the ratio (radial, vertical or horizontal) between segment A and segment B, referred to the worst cycle (Figure 40).

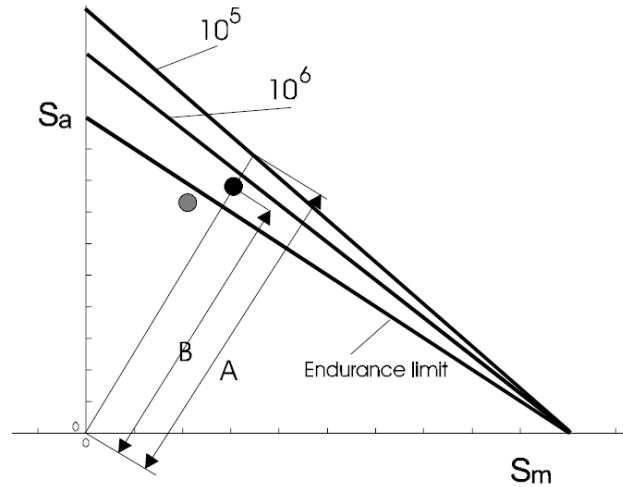


Figure 40 - FRF calculation (14)

If a complex VA load history is taken into account, smaller cycles (grey in Figure 40) may be many and the worst cycle (black in Figure 40) alone may overestimate Safety Factor Calculation. For this reason, FRF analysis may be unsafe. Since FRF algorithms do not involve computations of the number of cycles to failure, they are usually defined as *Infinite Life Analysis*. In this case, the target life is user-defined and has not to be confused with the Wöhler Curve “knee” as, at least theoretically, these quantities may be different.

On the contrary, FOS has to be intended as a multiplicative constant of the stress state leading to a user-defined target life. Being an iterative procedure, FOS computation is more time-consuming than FRF, but all cycles contained in the stress signal are taken into account. This analysis needs the number of cycles to failure to be computed for each iteration: for this reason it is usually defined as *Finite Life Analysis*.

Multiaxial fatigue is often treated by means of critical plane analysis. In these post-processors, fatigue lives are calculated on different planes. From the stress signal, cycles are extracted and corrected for mean stress (e.g. Goodman, Gerber, Walker, Morrow, Smith-Watson-Topper, User-defined, no mean stress correction), the fatigue model is selected (normal stress, normal strain, shear strain, Brown-Miller,...) and the fatigue life is computed. The plane showing the lowest calculated life is designated as critical plane. It is clear that this kind of analysis does not take into account the problems emphasized in 3.1 and 3.2 regarding the critical plane analysis.

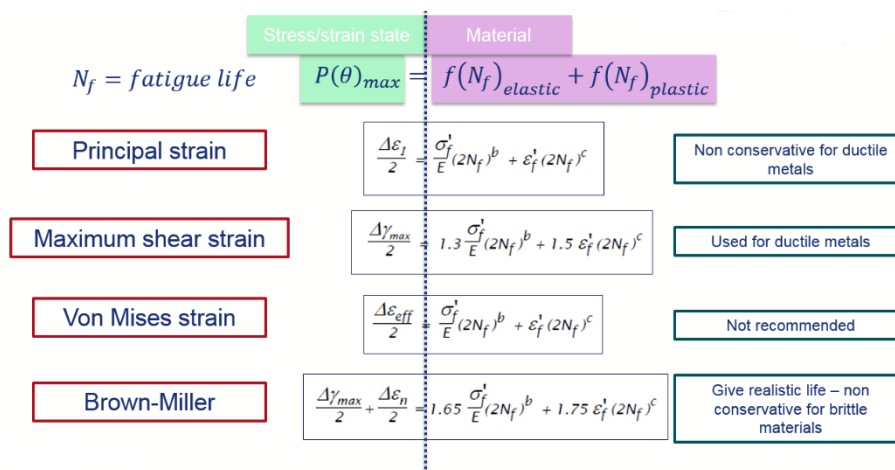


Figure 41 - Examples of critical plane algorithms

At this point, critical plane analysis performed by lowest Safety Factor research clearly appears questionable. By definition, no plane can show lower Safety Factor (highest cumulative damage) than the calculated plane. This fact may be misleading since, from a numerical point of view, the user thinks to work in most conservative situation but is this conservative analysis also realistic? Surely, if the calculated plane were the plane of crack initiation, it would be. However, it must be noticed that physical phenomena occurring behind fatigue fracture processes are not Safety Factor-dominated. This parameter is only a simplification imposed by engineers, in order to assemble all phenomena that they are not taking into account in their mathematical models. The proof of this lies in the fact that it is

not directly measurable in a component. Conversely, stresses and strains actually permeate stressed materials and directly affect fatigue crack initiation. In any case, those planes, seeming theoretically so distant, may sometimes coincide. Based on this, an analysis is carried out (Figure 42).

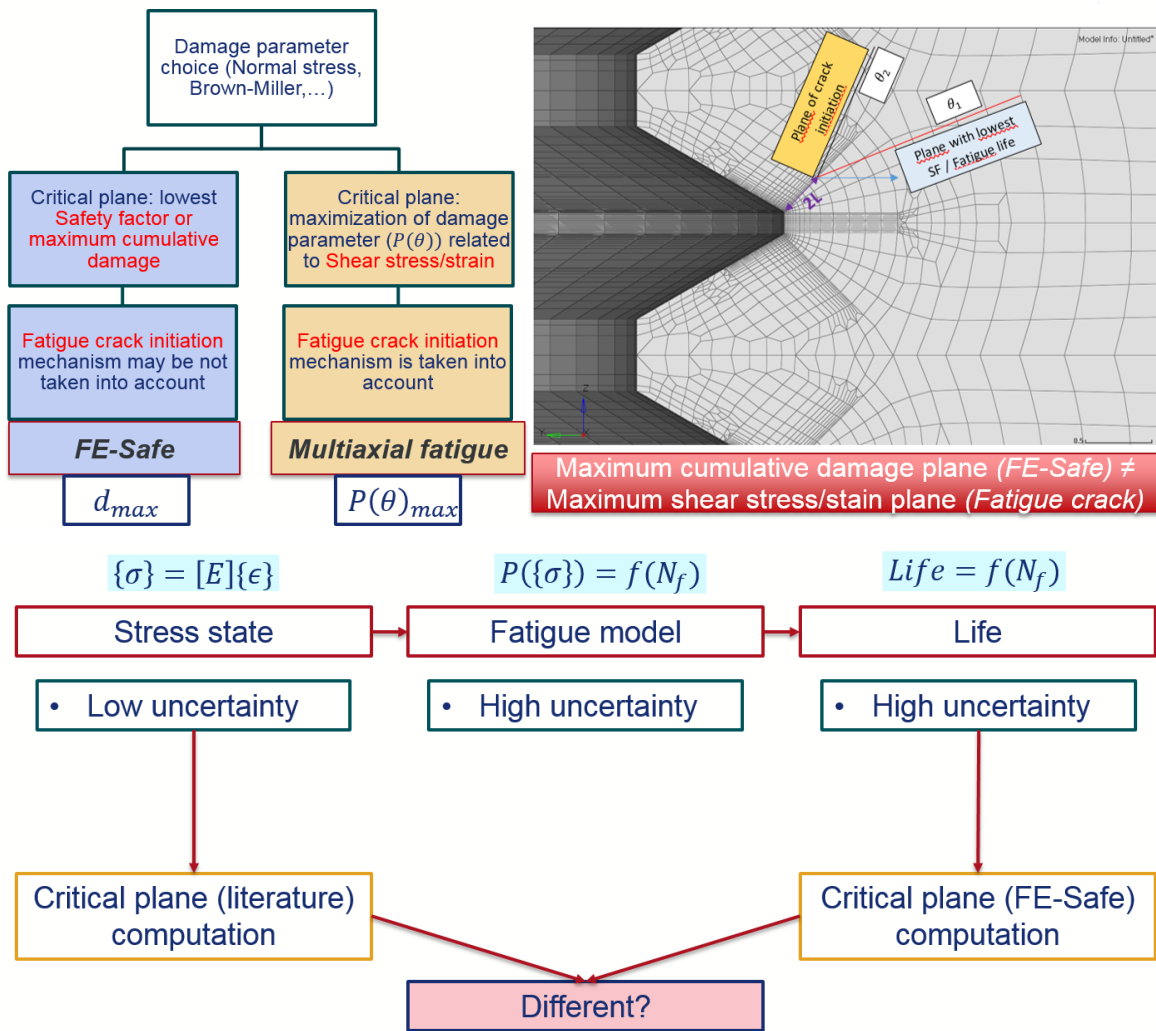


Figure 42 - Critical Plane observations

Is the maximum cumulative damage plane able to model fatigue crack initiation plane?
 For the aluminium AA 2014-T6 (54), a VA load history is supposed in order to produce a realistic calculated life (Figure 43, Figure 44). Normal Stress Algorithm and Goodman MSC (Figure 45) are adopted for fatigue life computations on different planes. A Matlab code is used.

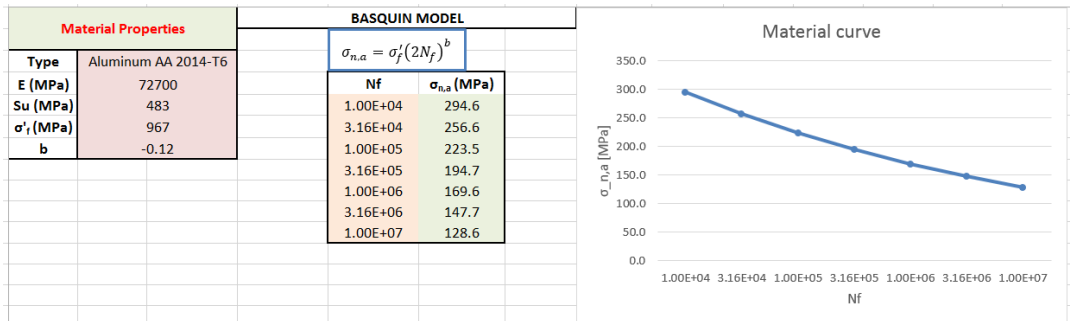


Figure 43 - Material Curve AA 2014-T6

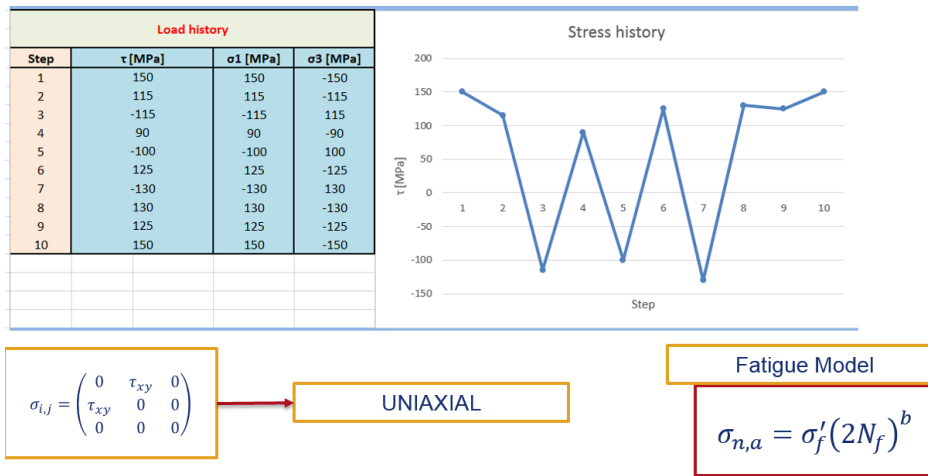


Figure 44 - VA Stress History

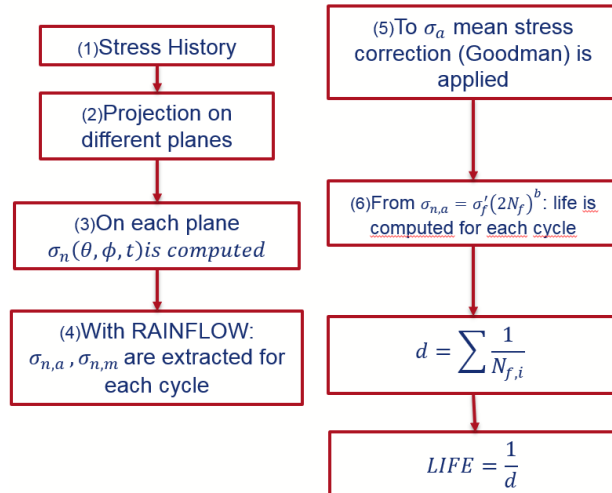


Figure 45 - Normal Stress Algorithm

Normal Stress is then projected on different planes (Figure 46).

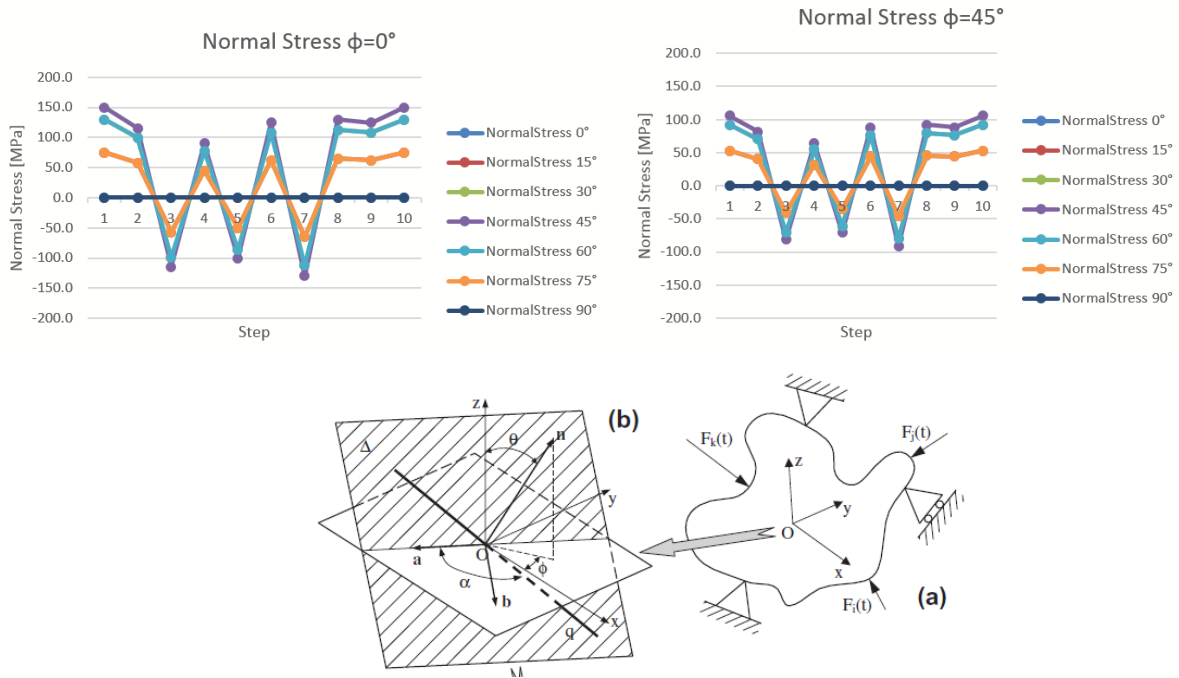
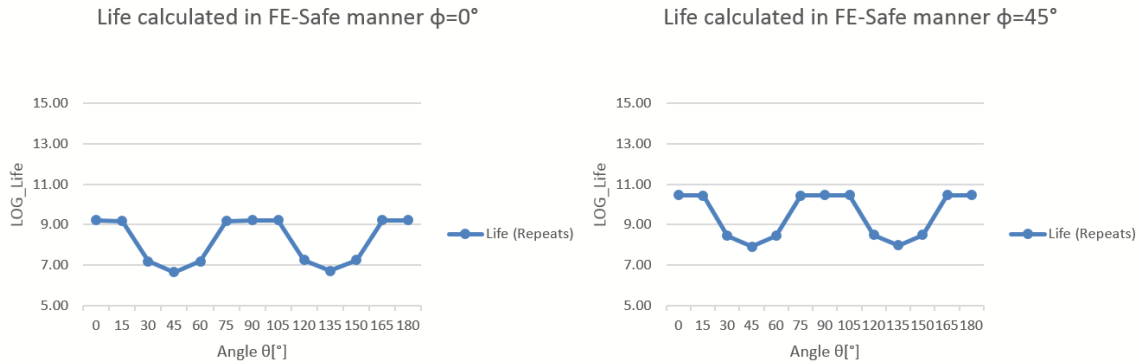


Figure 46 - Normal Stress Projection

Then fatigue life is calculated. As expected, critical plane is 45° inclined (Figure 47). Indeed, uniaxial torsional loadings maximise normal stress on the 45° plane and this is true also in static conditions (Mohr’s circle). Among critical plane research method, MVM is chosen to compare minimum Safety Factor plane with stress/strain based critical plane. In this case, since no multiaxiality is introduced, the two planes coincide. A multiaxial case is then supposed.



RESULTS	FE-Safe algorithm	NO FE-Safe but with approximations (Maximum Variance Sigma)
PREDICTED LIFE	4.49E+06	4.49E+06
CRITICAL PLANE theta angle	45	45
CRITICAL PLANE phi angle	0	0

Figure 47 - Fatigue lives on different planes

The multiaxial load history is supposed to be composed by non-proportional loading (Figure 48).



Figure 48 - Multiaxial non-proportional load history

Normal Stress is projected on different planes (Figure 49).

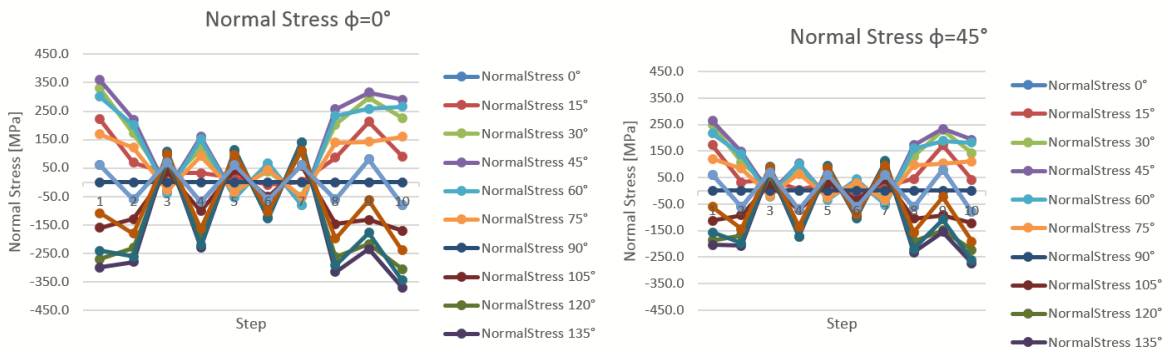


Figure 49 - Normal Stress projection - Non-proportional loads

From the fatigue model, life is calculated (Figure 50):

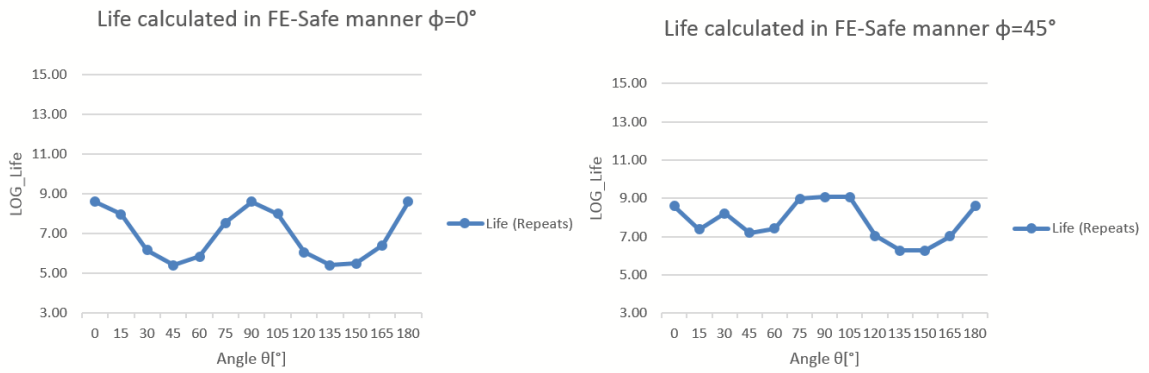


Figure 50 - Fatigue lives non-proportional loadings

Also in this case, MVM critical planes coincides with lowest SF plane (Figure 51).

RESULTS	FE-Safe algorithm	NO FE-Safe but with approximations (Maximum Variance Sigma)
PREDICTED LIFE	2.62E+05	2.62E+05
CRITICAL PLANE theta angle	45	135
CRITICAL PLANE phi angle	0	0

Figure 51 - Fatigue lives comparison non-proportional loads

The same computations are made by Brown-Miller Algorithm with no MSC (Figure 52).

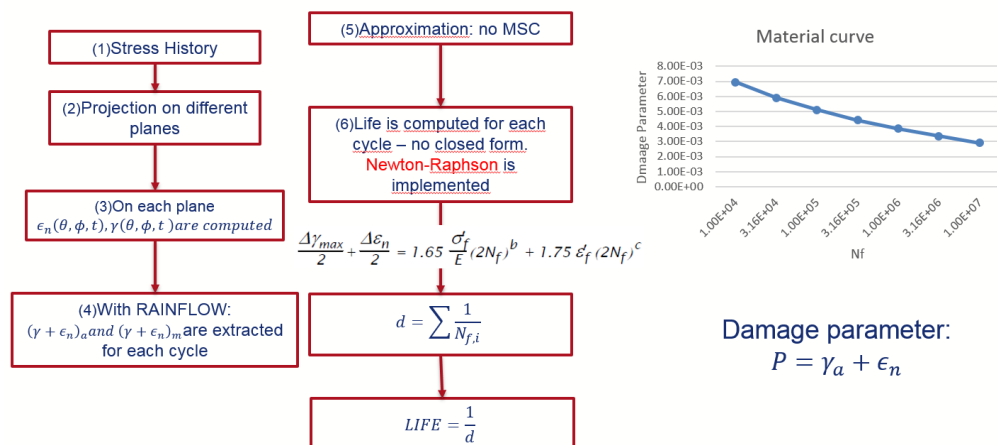


Figure 52 - Brown-Miller Algorithm

Life is calculated on different planes (Figure 53). Since fatigue curves are meaningful in the range $10^4 - 10^7$ cycles, a calculated life greater than 10^7 should be trimmed to 10^7 . However, this is not done in order to catch the trend of the extracted curves.

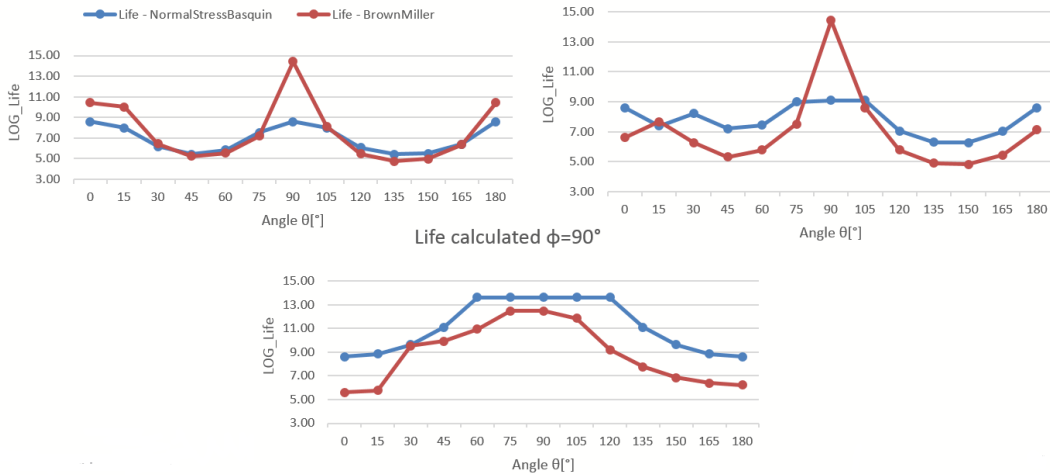


Figure 53 - Fatigue lives Normal Stress and Brown-Miller

In this case, substantial differences are found. The fatigue life computed on the maximum cumulative damage plane (FE-Safe algorithm) differs from the fatigue life computed on the maximum shear strain variance plane. On the maximum shear stress plane, fatigue life differs from both (Figure 54).

RESULTS	FE-Safe algorithm	NO FE-Safe but with approximations (MaximumVarianceGamma)	NO FE-Safe but with approximations (MaximumVarianceTau)
PREDICTED LIFE	5.63E+04	4.13E+05	2.66E+10
CRITICAL PLANE theta angle	135	0	0
CRITICAL PLANE phi angle	0	90	0

Figure 54 - Fatigue lives comparison

As reported in Figure 55, the critical plane choice may strongly affect the fatigue assessment.

LOG_LIFE	Plane	FE-Safe Plane	MaxVarGamma Plane	MaxVarTau Plane	MaxVarSigmaN Plane
Algorithm					
Normal Stress		5.4			5.4
BM - NoMsc		4.8	5.6	10.4	

ANGLE θ [°]	Plane	FE-Safe Plane	MaxVarGamma Plane	MaxVarTau Plane	MaxVarSigmaN Plane
Algorithm					
Normal Stress		45			135
BM - NoMsc		135	0	0	

ANGLE ϕ [°]	Plane	FE-Safe Plane	MaxVarGamma Plane	MaxVarTau Plane	MaxVarSigmaN Plane
Algorithm					
Normal Stress		0			0
BM - NoMsc		0	90	0	

Figure 55 - Critical Plane research comparison

At this point it can be argued that the calculated maximum cumulative plane (Matlab Code) is different from the plane that FE-Safe would locate for the supposed stress history. This has been verified by means of an analysis contained in the Appendix.

Coming back to stress post-processing by commercial codes, some comments may be done on the use of TCD. When dealing with the FRF, the number of cycles to failure is not really computed, since an estimation of how distant is the component from failure is performed on the basis of the stress/strain state. Because of the external imposition on N_f , a fixed critical distance may be used. If N_f is requested as output, TCD must be used in the form of Eq. (36). In this case, the change in size of the process zone with N_f is modelled within the TCD by means of a variable L . Since the reference stress is a function of L , an iterative process is needed. Generally, commercial fatigue post-processors do not implement this iterative process and do not allow TCD-based algorithms to work in the finite life regime (FOS). However, the TCD can be definitely applied in the high cycle regime as well as in the medium one (24). DVC is generally available and suggested for infinite life analyses.

3.6 Fatigue damage in threaded joints

In the case of threaded connections, multiaxial fatigue criteria find a wide range of applications. Taylor and Pan (55) estimated location and direction of fatigue cracks in threaded fasteners. Moreover, by using LCF Brown-Miller approach, they estimated fatigue life. A FEM model is built for which the following points hold:

- First Engaged Thread (FET) may be affected by the load application therefore, several unengaged threads are modelled.
- Helical geometry is not simulated since it has a relatively small effect on results.
- Axisymmetric elements are used.

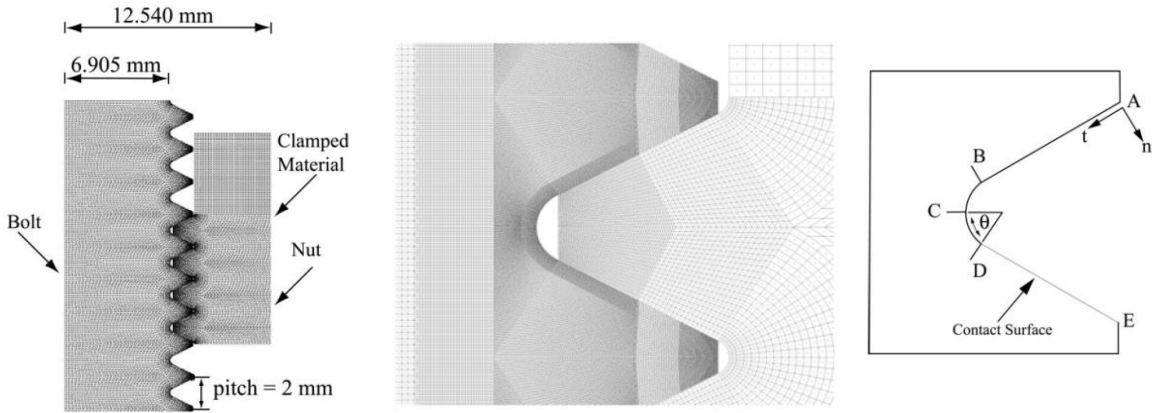


Figure 56 - FEM model and submodel (55)

On the maximum shear strain amplitude plane, the Brown-Miller parameter:

$$P_{BM} = \gamma_a + K(\epsilon_n)_a \quad (82)$$

is used to compute the number of cycles to failure through Manson-Coffin Curve:

$$P_{BM} = \frac{\sigma'_f}{E}(2N_f)^b + \epsilon'_f(2N_f)^c \quad (83)$$

Residual stresses coming from rolling process and mean stress effect are neglected. When the temperature is not taken into account, failure usually occurs in the FET. In the presented case, the crack initiation is predicted for $\theta = 18^\circ$ and the critical plane is 45° inclined.

Kuribara et al. (56) studied internal threads in motorcycles engines.

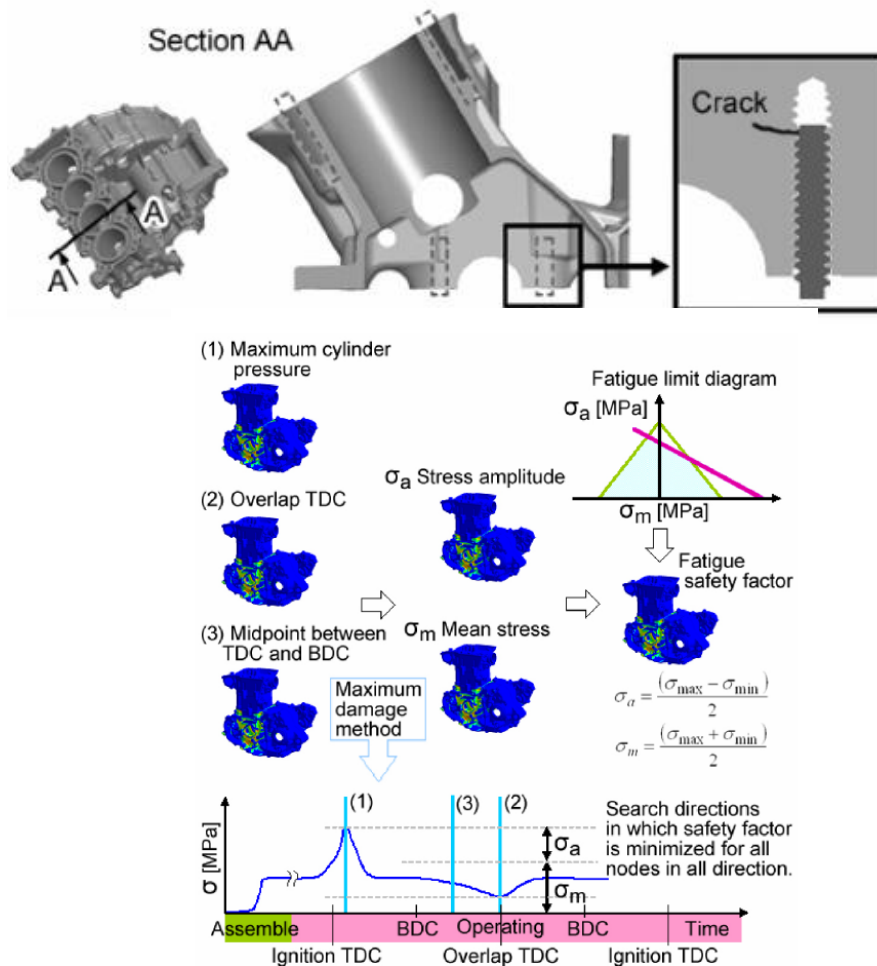


Figure 57 - Internal thread in cylinder head and Safety Factor evaluation

Firstly, numerical correlation of FEM strains is verified in the fastening area in order to validate the model. A constant engine speed durability test is simulated and stresses are extracted for fatigue post-processing. The worst-cycle approach is adopted (Figure 57). Thermal expansion phenomena are taken into account by FEM analysis. Main strains are generated by residual strains of casting, assembly process, firings and engine working cycle, uneven expansion (thermal) and oscillations. In Figure 58 the trend of mean stress and stress amplitude along threads engagement is represented.

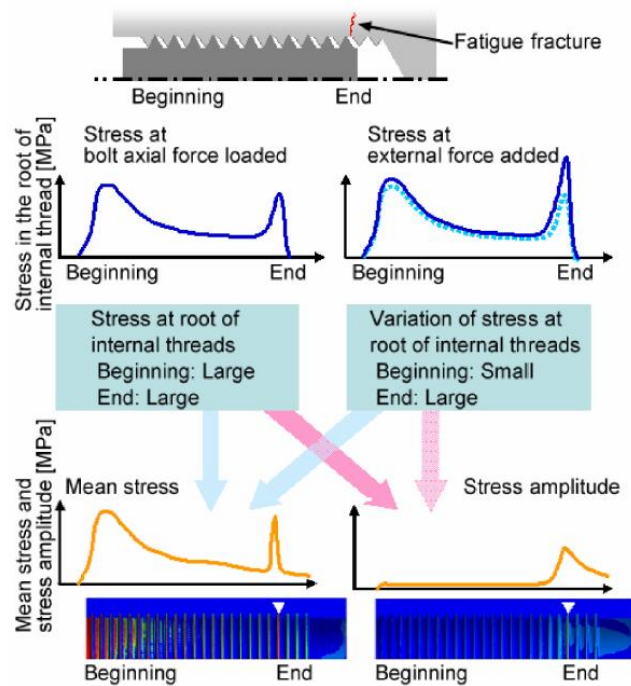


Figure 58 - Mean stress and stress amplitude along threads (56)

The mean stress is high both at the beginning and at the end of the engagement, whereas the stress amplitude has large values at the end. The mean stress is expected to be high at the beginning as it is well-known that most of the bolt load is absorbed by first six-seven threads. However, because of the abrupt change in rigidity (56) and stress concentration, mean stress increases also at the end. If these concepts are reported in a Haigh diagram (Figure 59), it is possible to notice that at the beginning, high mean stress plastically deforms material but this is not sufficient for fatigue failure. On the other hand, failure occurs where both mean stress and stress amplitude (Last Engaged Threads - LET) have high values.

Knez et al. (57) devoted research activities to fatigue assessment in hydraulic piston rod threaded end. Strain amplitude related to normal stress is supposed to be predominant and no multi-axiality is considered. The Manson-Coffin model is adopted.

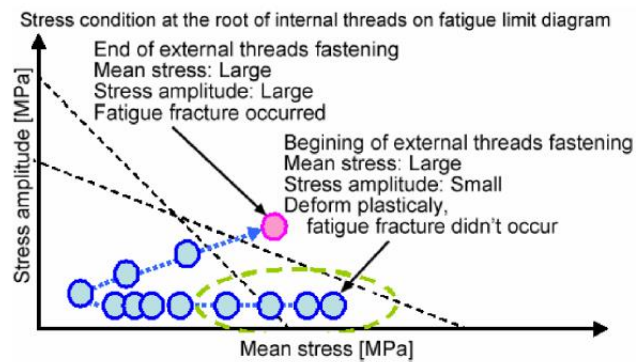


Figure 59 - Haigh Diagram (56)

Another important phenomenon occurring in ICE threaded fasteners is related to the **bolt load loss**. This is linked to relaxation and creep and takes place already in the first working cycles. DeJack et al. (58) implemented creep models in FEA to predict bolt relaxation. In this study, a creep model (59) is calibrated by correlating numerical predictions on bolt load loss with oven tests. Then, firing condition load cases are simulated in order to extract equivalent stress amplitude and mean stresses at each node based on a normal stress critical plane criterion. Haigh Diagram and Goodman's criterion allow for Safety Factor estimation. Haigh Diagram is modified through a scale factor based on empirical considerations in order to take into account residual stresses in cast aluminium. Clearly, by supposing uniformly scaled strength due to roll forming process, strong approximations are introduced. The surprising outcome is that Safety Factors calculated taking into account creep phenomena do not show significant differences with results obtained by neglecting creep. Although the mean stress is relaxed by creep, stress amplitude increases in the LET. Safety Factors variability is therefore negligible. Nothing is possible to say when different fatigue criteria are employed.

The thread forming process introduces plastic deformations and residual compressive stresses in the notch root. Improvement of surface quality and increase of the surface hardness contribute to fatigue strength betterment (60). Blaha et al. (60) performed fractographic investigations on specimens coming from the bulkhead region of the engine

block. In this work it is demonstrated that the rolling process introduces residual stresses that retard crack growth but do not inhibit crack initiation.

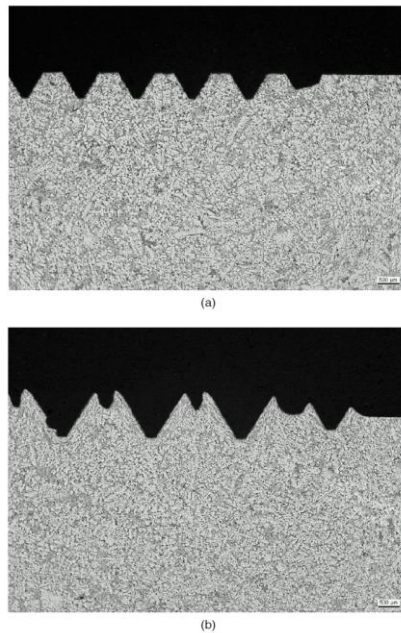


Figure 60 - Cylinder Block - (a) cut thread (b) rolled thread (60)

Residual stresses estimation is actually one of the most complex task in fatigue assessment of rolled threads. Available methods for residual stress estimation may be contained in three macro-categories reported in Figure 61.

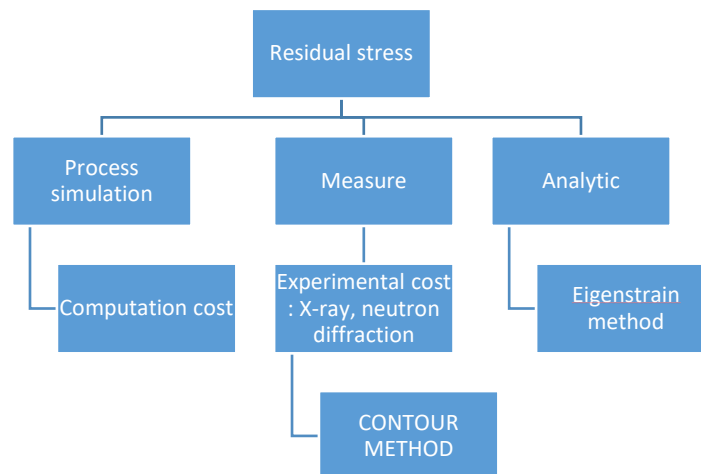


Figure 61 - Residual stress evaluation

The simulation of the forming process is one of the possibilities but its computational cost is heavy and it would increase the process of the complete fatigue analysis. Mathurin et al. (61) simulated the process through an infinitely rigid forming screw. FEA results were used, in this case, to study the effect of hole's dimension on the screwing torque.

Residual stress direct measurement may be costly from an experimental point of view, since X-ray or neutron diffraction are needed. Contour and eigenstrain (62; 63; 64; 65) methods take advantage of Finite Element Models. They have neither the experimental costs of X-ray nor computational cost of process simulations. The main hypothesis is that the incompatible strain field generated in continuously processed bodies is geometry-independent. Applications of these methods are found in cold expansion processes (63) of threaded fasteners, welds modelling (64) and laser shock processing (66).

4 Application to a case study: a fatigue assessment in Diesel Engine threaded bores

Critical distance and critical plane concepts are applied to assess fatigue endurance of threaded bores placed in the engine block. In this case, the engaged bolts connect engine block to the main caps, but this kind of analysis can be also applied to the connections between engine head and engine block. As demonstrated, the variables coming into play are many, and even if fatigue were considered independently from other factors (residual stresses, creep, bolt relaxation, contact nonlinearities, etc.), the applicable fatigue criteria would be many. At this stage, it is clear that applying simplifying hypotheses, as long as these are linked to physical reasons, is the only way in which the problem can be solved. The more the problem is simplified, the more its solution is quickly accessible. However, the more the solution is simplified, the more it is difficult to correlate predictions to experimental evidence. Many times, in the engineering field, we are concerned with including as many parameter as possible in our analyses, ignoring that our problem may be insensitive to some of them. At the same time, we simplify as much as possible our models, leaving out of consideration many influent factors. As trivial as it seems, in this issue lies the key for engineering solutions that may be certainly not perfectly designed, not fully deterministic but they work well as they represent a trade-off.

4.1 Analysis Procedure

These are the main features of the procedure applied herein:

- The engine is supposed to work in full-load conditions at constant speed. This is the most conservative hypothesis. This considerably simplifies models, as acting loads surely change along the engine working cycle but this remain constant in time.
- Steel bolt and cast aluminium block contacts are taken into account by FEA. The same occurs for thermal expansion.
- Cut threaded bores are analysed in order to neglect the effect of residual stresses.
- The damage parameter for fatigue crack initiation is supposed to be the normal stress (Mode I crack). Of course, this is the most debatable hypothesis as, even if for some materials the first crack stages may be normal stress-controlled, the fatigue damage always initiates on shear stress planes (2). Nevertheless, normal stress criteria are often used for fatigue assessment in brittle materials. On the contrary, the static failure for brittle materials is usually normal stress-controlled.

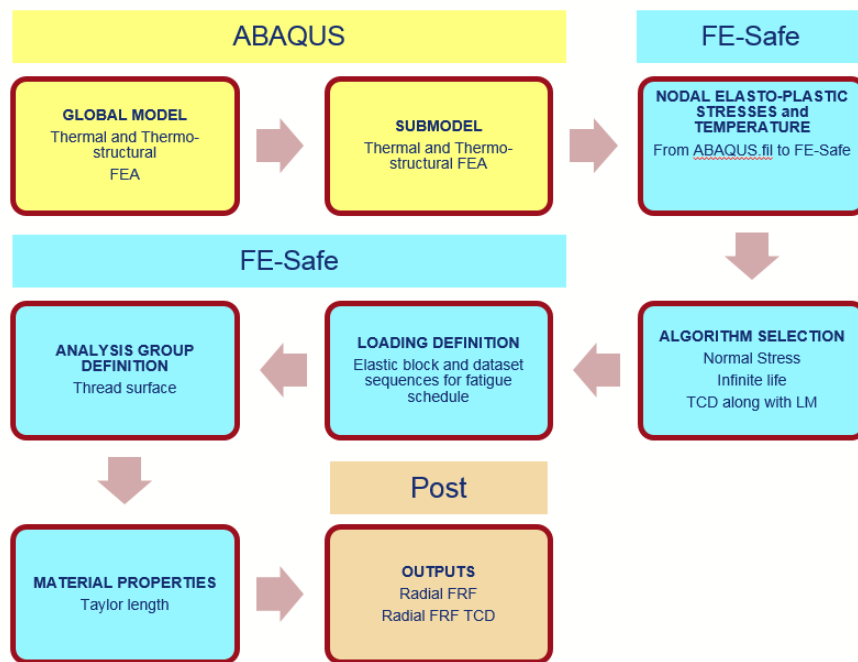


Figure 62 – Durability Analysis set-up

The analysis set-up is reported in Figure 62.

- The available FEM model of the engine structure is employed for a Thermal-structural analysis. Hypermesh and ABAQUS are used to arrange the model and the analysis. Firstly, a steady state Heat Transfer analysis is run to simulate full load working conditions, by taking into account water jacket boiling and Heat Transfer Coefficient coming from CFD results.
- Nodal temperatures, resulting from the previous step, enter the thermal-mechanical analysis of the global engine model. In this model, threads geometry is modelled through cylindrical contact surfaces between bolt and bore. A multistep analysis is performed simulating the assembly process and cylinder firings. Bolts pretension and a heuristic model of the bolt load loss is considered.
- In the threaded bore submodel, a dense mesh is employed. Nodal temperatures of the global heat transfer analysis are used as boundary conditions in the heat transfer analysis of the bore submodel.
- The thermal-structural submodel is run using as boundary conditions nodal temperatures coming from heat transfer submodel and the nodal displacements coming from thermal-structural global model. Helix angle is not neglected (but results do not change ignoring this angle) and FEM model is three-dimensional. Boundary conditions are not axisymmetric. Finally, nodal stresses on the thread surfaces are extracted for the durability post-processing.
- Since no Neuber's rule is employed, elasto-plastic analyses are run. Moreover, components are expected to be subjected to HCF and plasticity should be not expected. However, stress concentration features, contact nonlinearities and temperature effect may modify this condition.
- Nodal stresses and temperatures are post-processed through the commercial code FE-Safe.
- Fatigue material properties are considered in the -3σ range of their scatter band (conservative hypothesis, with σ standard deviation).

- The normal stress algorithm is chosen and a critical plane/distance analysis is carried out. The problems concerning critical plane analysis in these kind of softwares have been discussed yet. Heavy stress concentration features are present due to notch effect. For this reason, TCD analysis is performed. Since finite life analysis is not allowed when using TCD, only Safety Factor in the form of FRF can be computed. Target life is imposed to be 10^7 cycles. User-defined MSC is adopted for negative mean stresses. Positive mean stresses are corrected by using Goodman MSC.

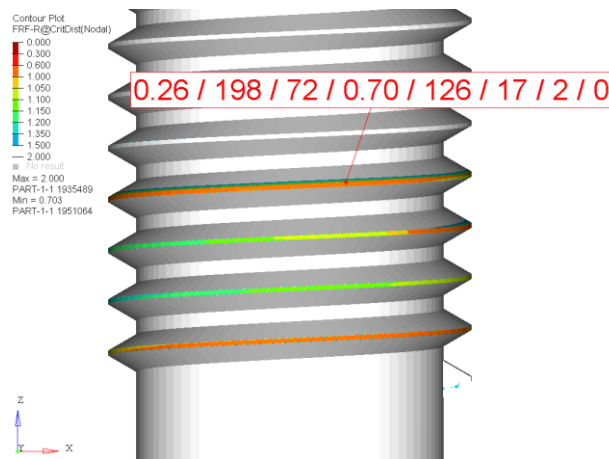


Figure 63 - FRF Threaded Bore

4.2 Results discussion

Results are reported in Figure 63. The values are given in the following order: FRF on the surface, Mean Stress on the surface, Stress amplitude on the surface, FRF computed with LM stresses, Mean Stress computed through LM, Stress Amplitude computed through LM. All stresses are in MPa. Obviously, as said in Chapter 3, these values make sense only if the worst cycle of a VA stress history is considered. The remaining two values are diagnostic codes. Clearly, the use of critical distance values widens the limits of acceptability since stresses values far from surface are lower than “skin” ones. Nevertheless, it should be obvious to the reader that according to what said in Chapter 2, considering TCD exclusively as a way to expand acceptability limits is completely meaningless. In the case of the

performed analysis, if $FRF = 1$ is taken as critical value, the component has to be considered unsafe.

Nevertheless, it is worth noticing that Safety Factor is not a coefficient referred to what we know. On the contrary, it has to be intended as an indication of what we do not know: the higher is the number of uncertainties and simplification in our analysis, the larger our safety margin must be. In light of this fact, it is clear that by equating the condition $FRF = 1$ to failure, we are saying that our capability in assessing a certain problem is excellent.

Fatigue is a strongly non-deterministic phenomenon in which the number of uncertainties is very high. For this reason, it is very common to use a Safety Factor $SF = 3$ to assess failure, that is: because of the high uncertainty, it is sufficient that reference stress is a third of the material limit stress for failure to occur. Nevertheless, in the specific case material properties were already degraded by considering the -3σ interval.

Moreover, by using FRF, only the worst cycle is considered. According to some opinions, the worst cycle is sufficient when dealing with crack initiation only. Other opinions, including the author's one, consider this as an approximation.

Another problem linked to the use FRF is presented in the following. Once a threshold FRF is defined, failure is predicted for analyses that result below the threshold value. Let us suppose that the component predicted to be safe ($FRF > FRF_{threshold}$) fails. We know that our model did not work but how can we quantify the error made? Was our error very huge or very small? Was it due to an ill-correlated model or to model uncertainties? By using FRF, these assessments become really complicated tasks, since in a failed component it is not possible to measure FRF. This problem does not occur if the number of cycles to failure is used in place of FRF.

The critical distance value is defined as a material property and is estimated as described in Figure 23. Being a material property, a possible dependence from temperature could be studied, since in these models temperature may vary in space and time.

4.3 Critical distance: sensitivity analysis

From this model, it is not possible to assess the effect of the critical distance variability. For this reason, durability analyses are re-run to assess the sensitivity of the method to L .

Varying the value of the *Taylor length* L ($\pm 10\%$) in the case of the threaded bore (A 319-T7):

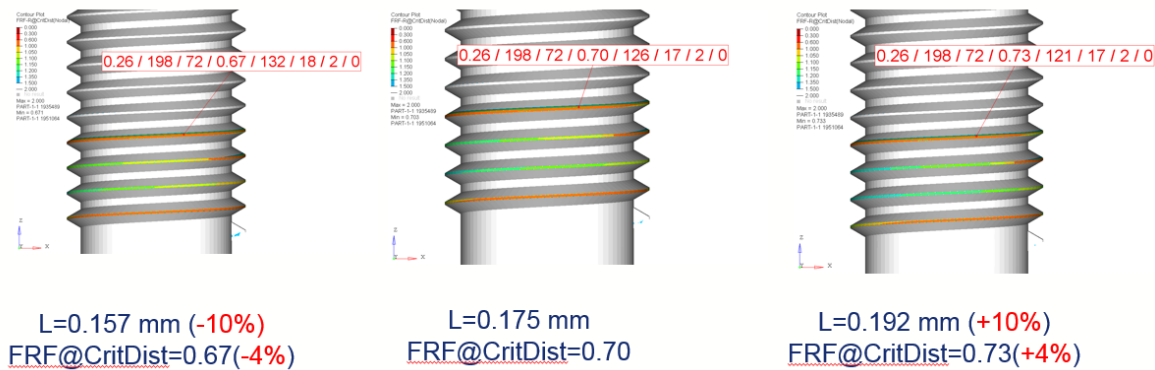


Figure 64 - Sensitivity analysis

First of all, it is worth noticing that results are compatible with TCD as averaging stress fields in a wider range (far from hot-spot) inevitably lead to a lower calculated stress (Safety Factor increases - Figure 64). By varying critical distance of $\pm 10\%$, FRF varies of $\pm 4\%$. This variability is definitely negligible if compared with the errors that are made by using FEM. However, by recalling the analytical model of Eq. (39) and Figure 25, it is clear that critical distance variability effect on FRF depends on the range the error E_L . In some ranges, FRF may be subjected to huge variations. From Figure 64 this cannot be assessed since the found variability is valid only in the range of study. An interesting outcome is that the analytical model proposed in Eq. (39) is able to predict FRF variability of Figure 64. This is showed in Figure 65.

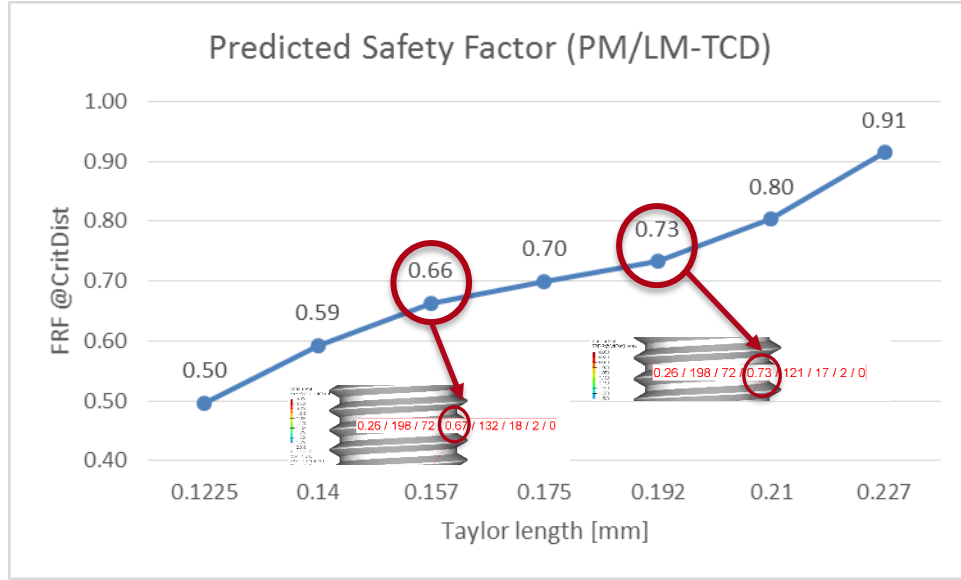


Figure 65 - Model of Safety Factor sensitivity

Analyses are re-run by using several algorithms (Maximum Shear Strain, Brown-Miller, Dang Van, Von Mises) with different MSC's (Morrow, SWT, Goodman, etc.) trying to compute FOS, FRF and N_f . Since an experimental data on threaded bores failure were not present, it was not possible to judge results reliability that, for this reasons, are not reported. However, experimental data are available for a notched plate of the same material. Therefore, durability analyses and different criteria and MSC's are applied to that case in Chapter 5 searching for the best-correlated fatigue criterion.

4.4 Dang Van criterion applied to threaded bores

By using the post-processor nCode Design Life, Dang Van durability analyses are carried out relying on the same FEA results. Dang Van constants of Eq. (74) are expressed as:

$$TAFE \text{ (Type A Fatigue Endurance)} = \beta = \tau_f \quad (84)$$

$$HSS \text{ (Hydrostatic Stress Sensitivity)} = \alpha = \frac{3\tau_f}{\sigma_f} - \frac{3}{2} \quad (85)$$

τ_f and σ_f are, respectively, the torsional and the tensile fatigue limits. Data on torsional fatigue properties of the material adopted were not present; therefore, two different sensitivity analyses are performed. In the first (Figure 67), Safety Factor variability is studied varying the ratio σ_f/τ_f at fixed σ_f . In the second (Figure 66), Safety Factor is studied with a fixed ratio σ_f/τ_f but varying τ_f . Material properties are not explicitly provided for obvious reasons.

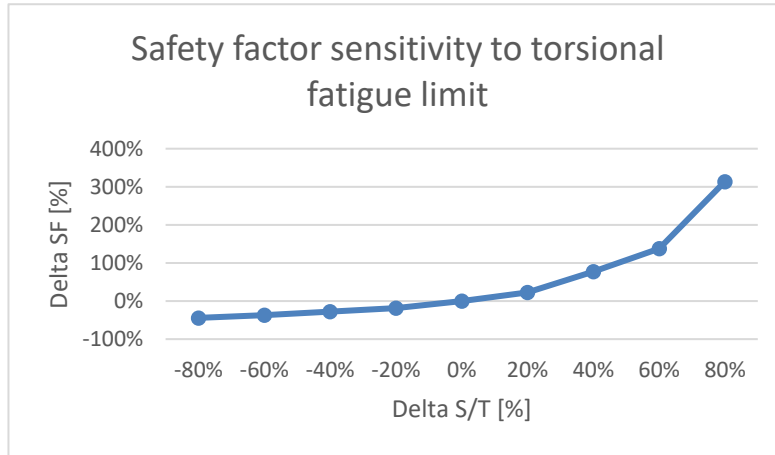


Figure 67 - Fixed fatigue limit - SF variability

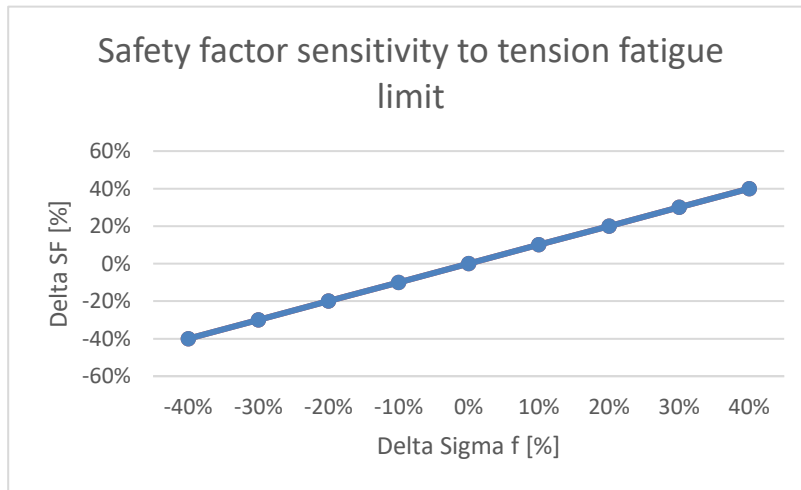


Figure 66 - Fixed σ_f/τ_f - SF variability

If Safety Factor is computed as expressed in Eq. (78), the linear variability of Figure 66 is easily explainable. Significant variations are perceptible in Figure 67. This highlights the importance of torsional material properties in Dang Van analyses.

Results coming from non-TCD Dang Van analysis (nCode Design Life) are compared with results coming from non-TCD analysis performed in 4.1 (Figure 68).

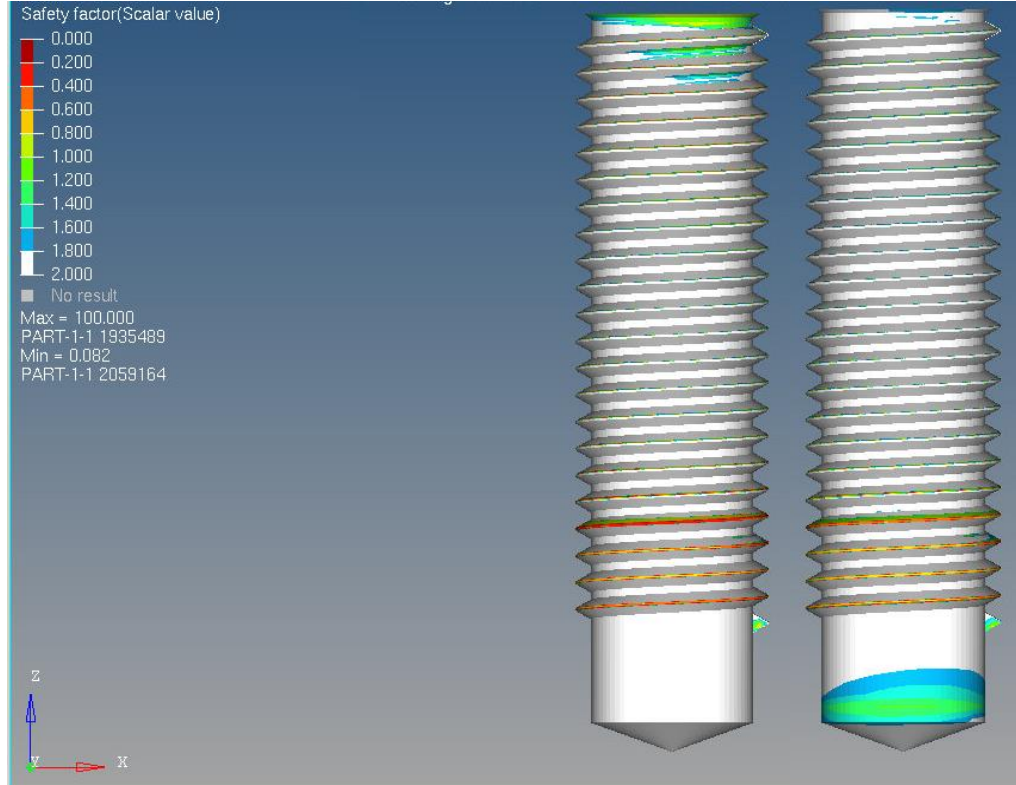


Figure 68 - non-TCD Safety Factor HCF evaluation - Dang Van on the left. Normal Stress/Goodman on the right

In this case, both algorithms predict component failure:

$$\text{non - TCD SF NormalStress} = 0.26 \quad (86)$$

$$\text{non - TCD SF Dang Van} = 0.15 \quad (87)$$

Even if in relative terms the two SF are quite different, from an engineering point of view 0.1 variations are definitely negligible in Safety Factor estimation.

5 Numerical-Experimental correlation: Durability Analyses in aluminium notched plate

Experimental data coming from fatigue tests on notched specimens (Figure 69), extracted from the block (bulkhead) region, are compared with fatigue life predictions resulting from different algorithms. Specimens are tested at 150°C with a load ratio $R = \frac{\sigma_{min}}{\sigma_{max}} = 0.5$.

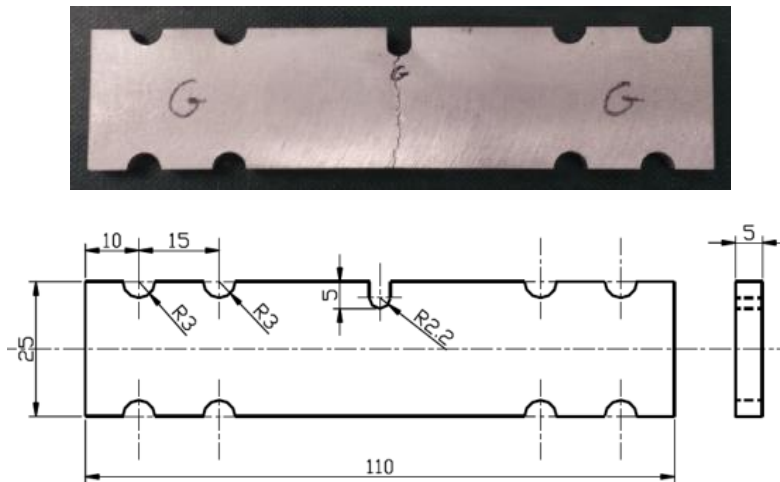


Figure 69 - Notched Specimens

Six load cases out of ten coming from stair-case tests are considered. From failure stresses, loads are computed by simple algebra (Figure 70).

U-Notched	
Thickness [mm]	5
R notch [mm]	2.2
L length [mm]	60
Notch depth [mm]	5

$$\Delta F = \Delta \sigma_{net} A_{net}$$

$$F_{mix} = \frac{\Delta F}{1 - R}$$

$$R = \frac{\sigma_{min}}{\sigma_{max}} = 0.5$$

$$LogLife = \log_{10} N_f$$

Figure 70 - Notched plate - Geometry and formulas

5.1 FEM modelling

A FEM model of the structure was built by means of Hypermesh and Abaqus (Figure 72). The Geometry was modelled through a 2D mesh made of 4-node and 3-node reduced integration shell elements (S4RT, S3RT) are employed for *Coupled Temperature-displacement* analysis.

Originally, the process of warm up from 25°C to 150°C wanted to be simulated (Figure 71).

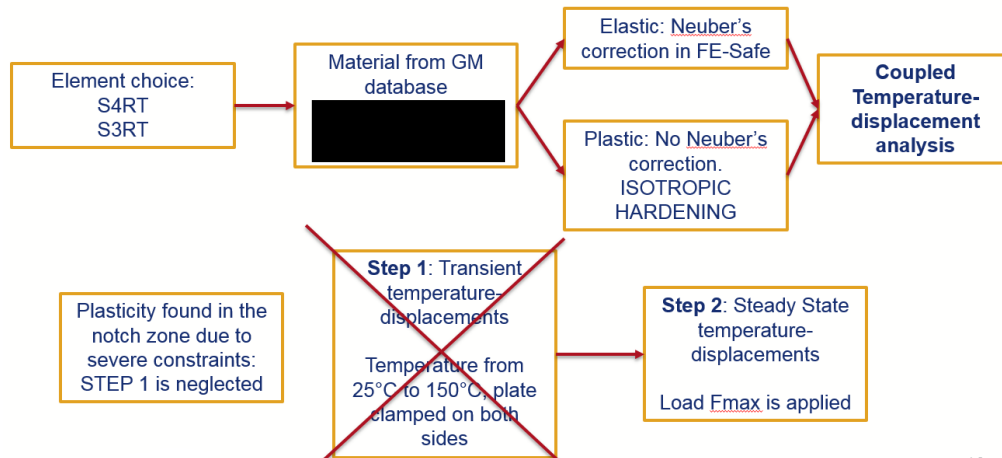


Figure 71 - Input File scheme – Notched Plate

Finally, the first step that modelled the transient state was neglected, since residual stress state coming from Step 1 was too much severe and probably non-representative of the actual test. For the warm up stage there was no experimental correlation, therefore Step 1 was neglected. *Some data reported in this chapter are hidden, in the public version of this work, according to the modalities requested by the company. Nevertheless, for the most practiced and careful reader, this fact is naturally superfluous. A qualitative assessment is what can be shown in this context in order to make engineering evaluations.*

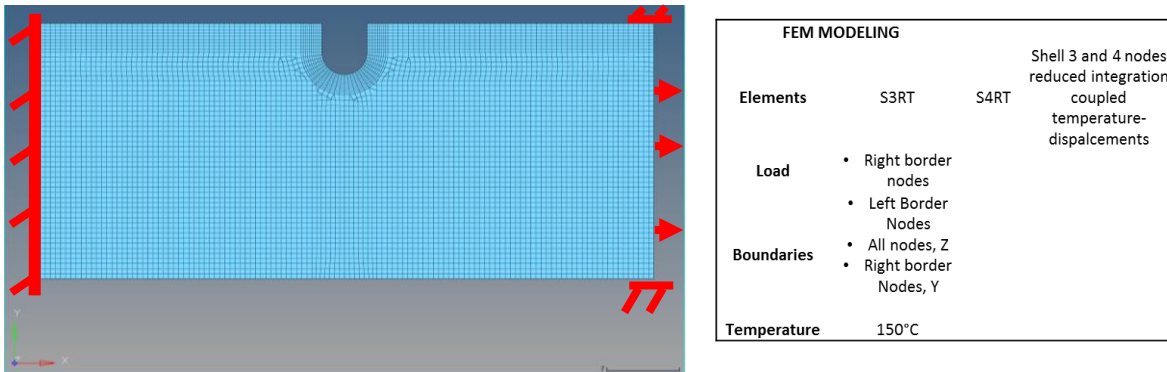


Figure 72 - FEM model, loads and constraints

Load F_{max} is applied by distributing it on the right-side nodes. Rigid elements (e.g. RBE3) are not used since, differently from S4R and S3R, temperature degree of freedom (S4RT, S3RT) could have not be applied for a transient coupled temperature-displacement analysis.

This inevitably affects the stress distribution. Component stiffness is variable along the Y axis because of the presence of the notch, however the load is equally distributed along the Y axis. Stress distribution along the Y axis is therefore expected to be different from the theoretical notched-component one. Nevertheless, this may be irrelevant for the fatigue assessment on the surface, even if it is significant for static stresses. Results are reported in Figure 74.

5.2 Fatigue assessment

FEA results coming from elastic-plastic analyses are transferred in FE-Safe environment for a CA fatigue analysis without Neuber's correction. Different algorithms and MSC's are used (Figure 73).

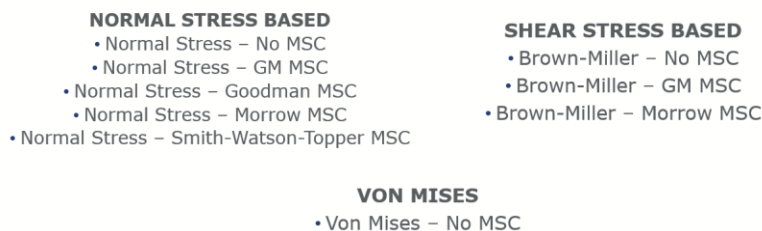


Figure 73 - Fatigue algorithms and MSC's

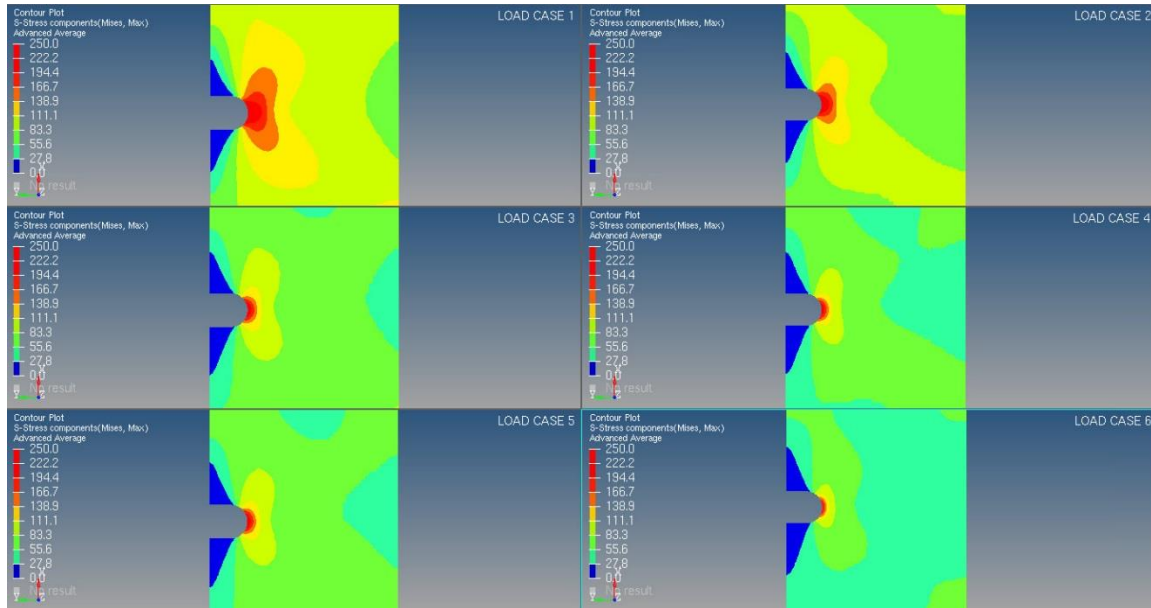


Figure 74 - FEA results for different load cases

Almost 60 numerical tests are performed. FOS and fatigue lives are computed. FRF is not calculated in that, for the reasons already explained, it is not possible to compute at the same time FRF (infinite life) and number of cycles to failure (finite life).

In order to evaluate the FOS ability to predict failures, the *FOS-LIFE* diagram is introduced.

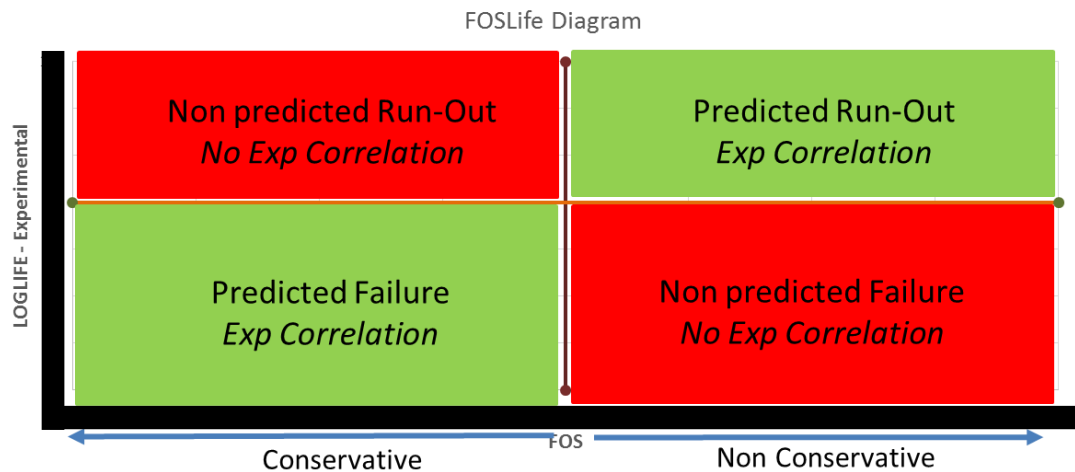


Figure 75 - FOS-LIFE diagram

FOS is reported on the abscissa axis, whereas Experimental life is reported on vertical axis. Run-out specimens are considered to trespass 10^7 cycles. Critical FOS (FOS_{th}) is supposed to be unitary, being aware that this correspond to the hypothesis that our capability in solving the fatigue problem is total. If $FOS > FOS_{th}$ our model is predicting a run-out, hence our analysis is correct if experimental life overcomes 10^7 cycles. Conversely, if $FOS < FOS_{th}$ we are predicting a failure. Our model correctly works if experimental life is beneath 10^7 cycles. These situations may be represented in four quadrants of the FOS-LIFE diagram. By using Normal Stress algorithms, FOS are computed at the notch root (Figure 76).

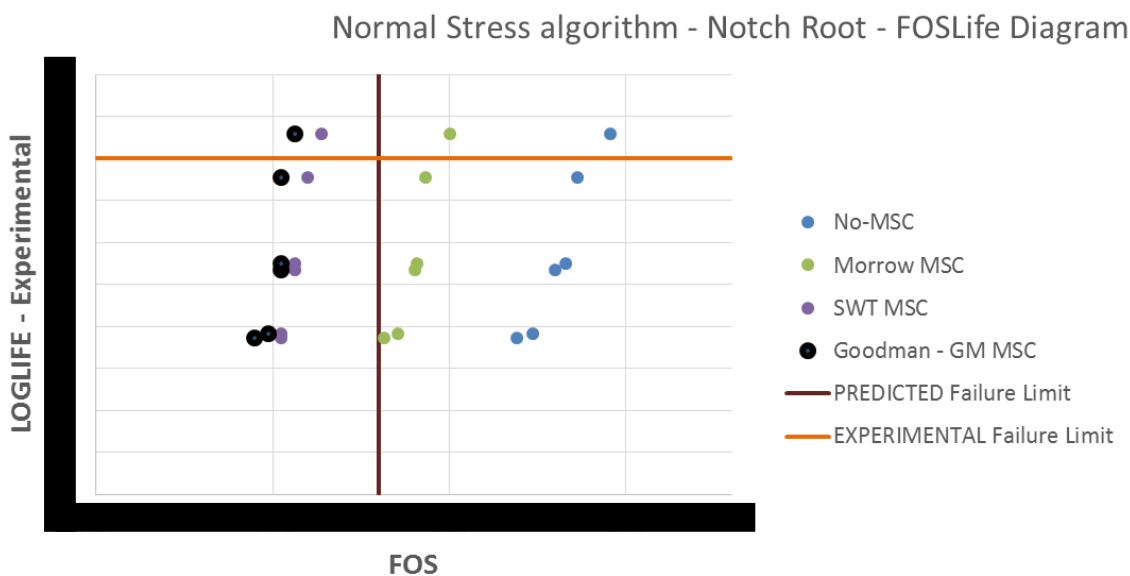


Figure 76 - Normal Stress - FOSLife diagram

Some observations may be done:

- No-MSC and Morrow MSC are able to predict run-out conditions but not failures if threshold FOS is imposed to be unitary ($FOS_{th} = 1$).
- On the contrary, SWT and Goodman MSC's predicts component failure but not run-outs.
- Goodman MSC results to be the most conservative.
- No-MSC (as expected) is the least conservative.

- By moving FOS_{th} value, the exposed judgements clearly change.
- It is not possible to assess which is the best MSC, since we know that the model fails in the second and in the fourth quadrant of the FOS-LIFE diagram, though we cannot quantify the error.

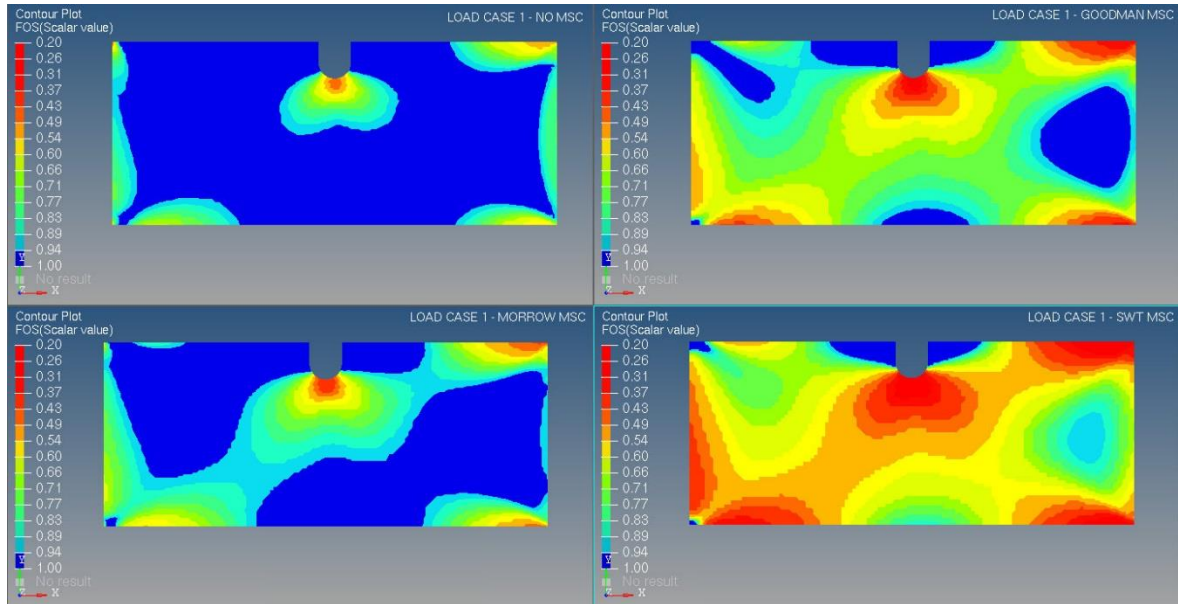


Figure 77 - FOS - Normal Stress with different MSC's

For sake of completeness, FOS contour plots are reported (Figure 77). However, far from the notch tip, stress distributions are affected by boundaries conditions and load application. Stress-based Brown-Miller and Von Mises FOS are reported in Figure 79

Completely different considerations can be made if the predicted number of cycles to failure is compared with the experimental ones.

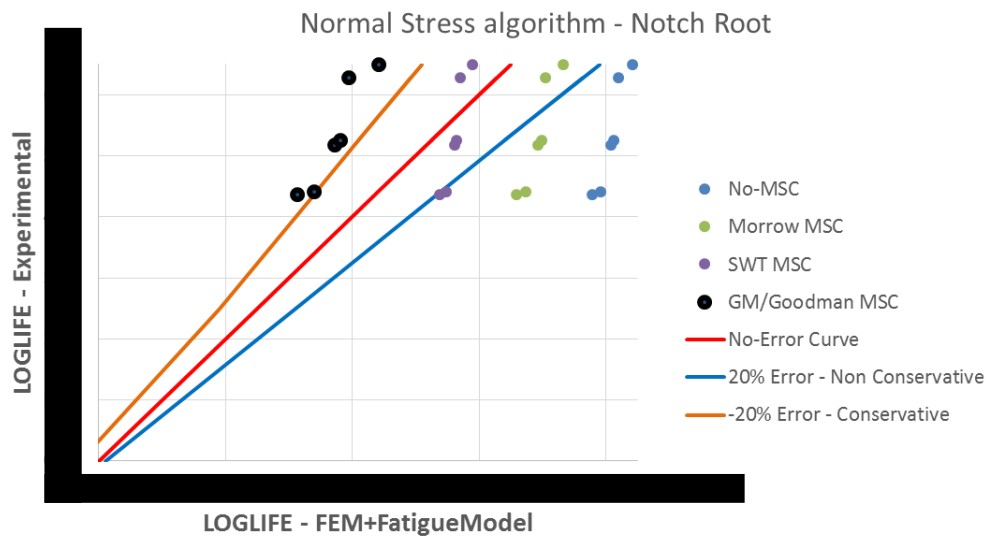


Figure 78 - Normal Stress Algorithm - life-to-life diagram

Figure 78 shows a comparison between fatigue life predictions and experimental fatigue lives. *LIFE-TO-LIFE* diagram is useful for the error estimation.

The red line is the quadrant bisector. When points lie on this line, predictions are perfectly correlated with experiment data. Above the red line, predictions are conservative, whereas below the red line they are non-conservative, since the model predicts a higher number of cycles to failure than the experimental ones. In addition, in this case some observation must be done:

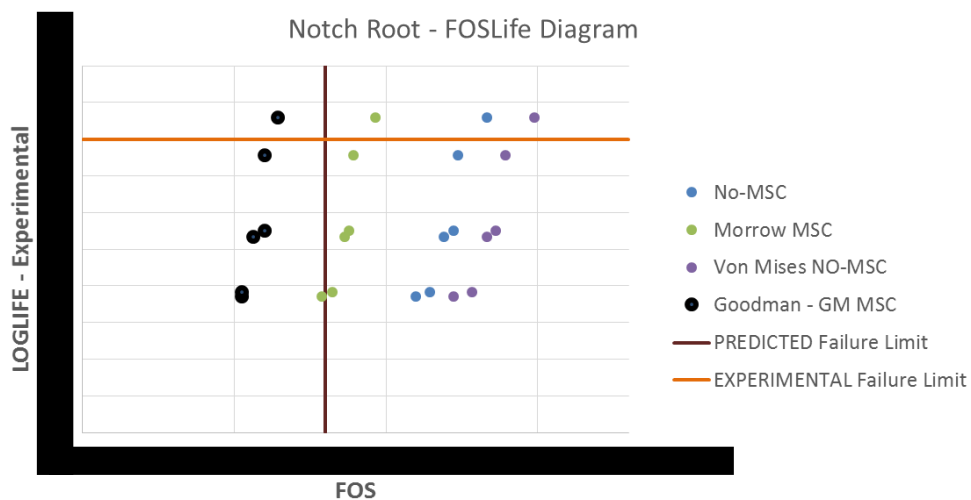


Figure 79 - Brown-Miller and Von Mises - FOSLife diagram

- Goodman MSC results, also from this analysis, the most conservative correction. However, in this case it is possible to quantify how much it is conservative: more than 20% on logarithmic lives. This error, as expressed in logarithmic coordinates, is huge. From the FOS-LIFE analysis, it is impossible to perform this kind of estimation.
- All other MSC's result to be non-conservative. SWT MSC can predict failure always within +/-20% error.

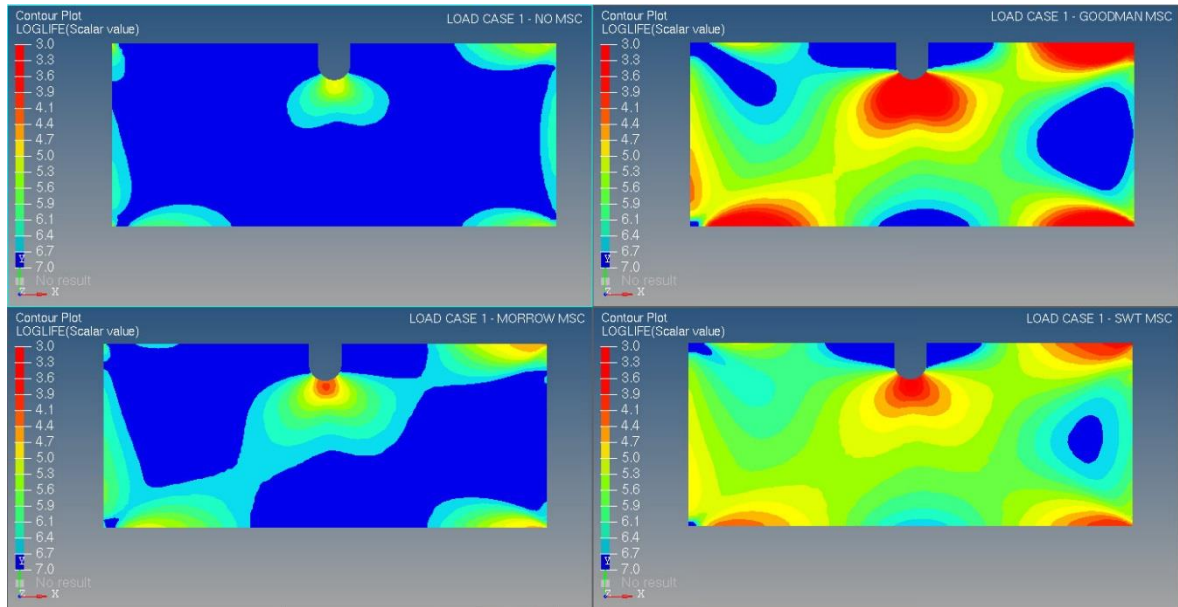


Figure 80 - LOGLIFE - Normal Stress with different MSC's

Stress-based Brown-Miller is adopted with different MSC's (Figure 81).

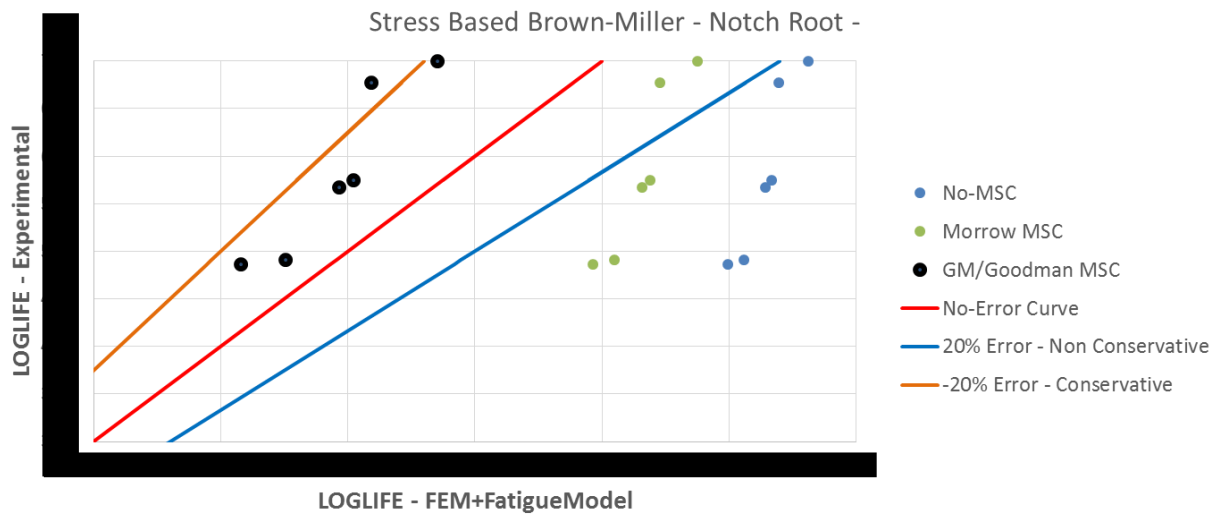


Figure 81 - Stress-based Brown-Miller life-to-life diagram

In Figure 82 different algorithms and MSC's are reported in the form of life-to-life diagram.

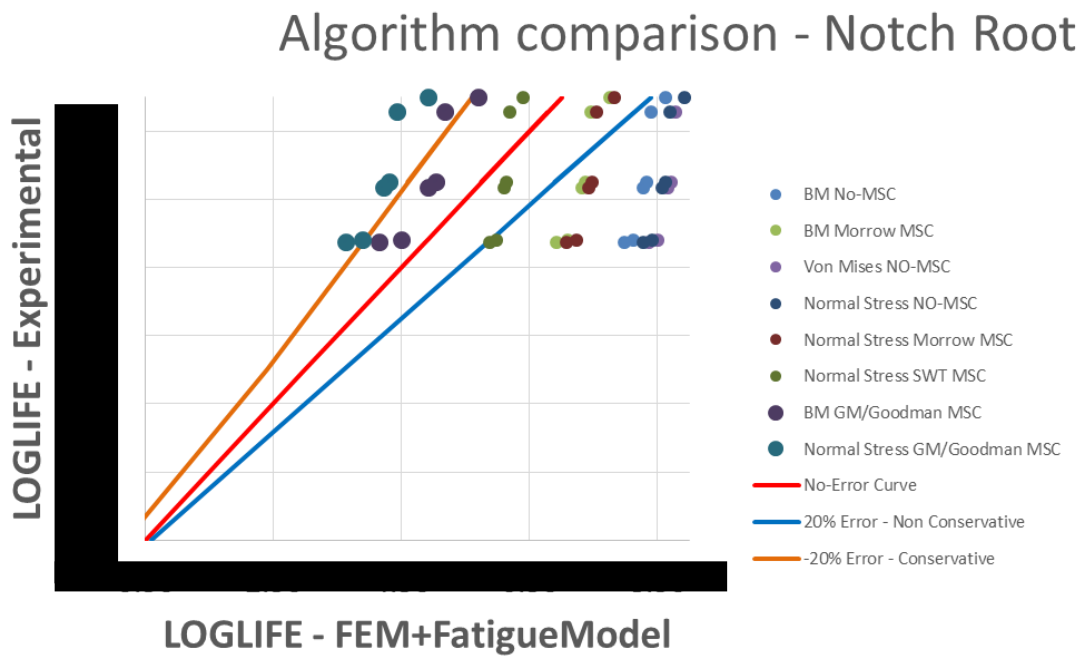


Figure 82 - Algorithm comparison life-to-life diagram

Normal Stress algorithm with SWT MSC and Brown-Miller algorithm with Goodman MSC appeared to be the most correlated ones.

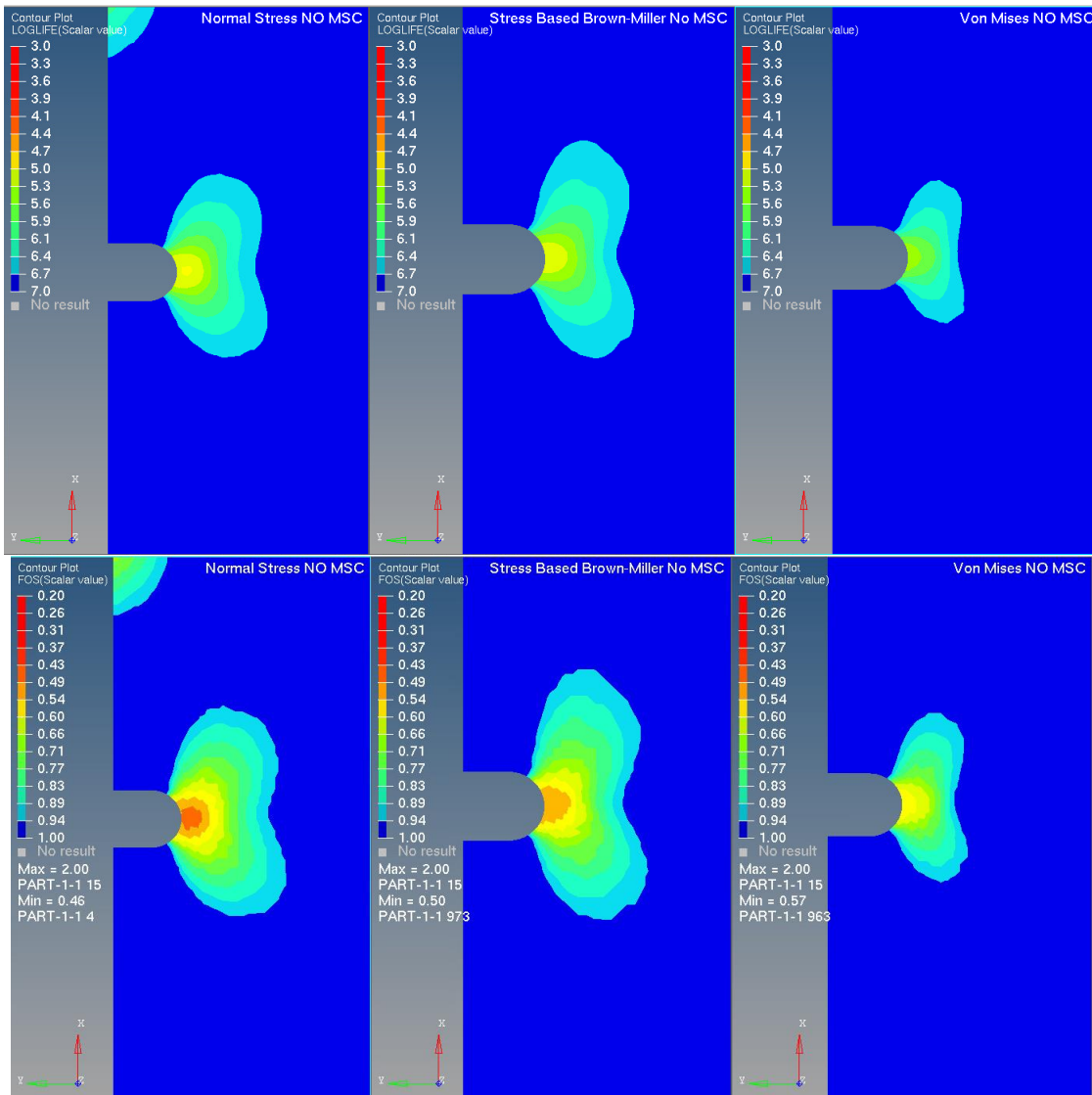


Figure 83 - LOGLIFE calculated with no MSC on top. FOS calculated with no MSC on bottom

All algorithms and all MSC show a narrow range of predicted lives, whereas experimental fatigue lives ranges are wider. Namely, in life-to-life diagram, points are placed quite vertically. The cause of the model **insensitivity** to the applied loads is researched.

5.3 Fatigue Model insensitivity

Two types of possible errors are supposed:

- Error in FEM modelling used for stress extraction (before fatigue model –TYPE 1).
- Error in fatigue algorithms for life estimation (after fatigue model –TYPE 2).

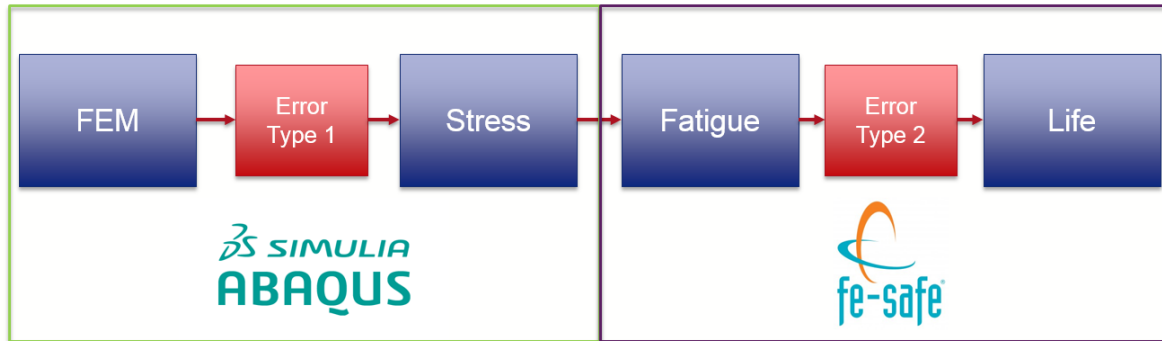


Figure 84 - Error types

FEM error is expected due to the way in which loads are applied. Another model is built by applying loads with rigid elements (force is applied in one point connected to border nodes through rigid elements).

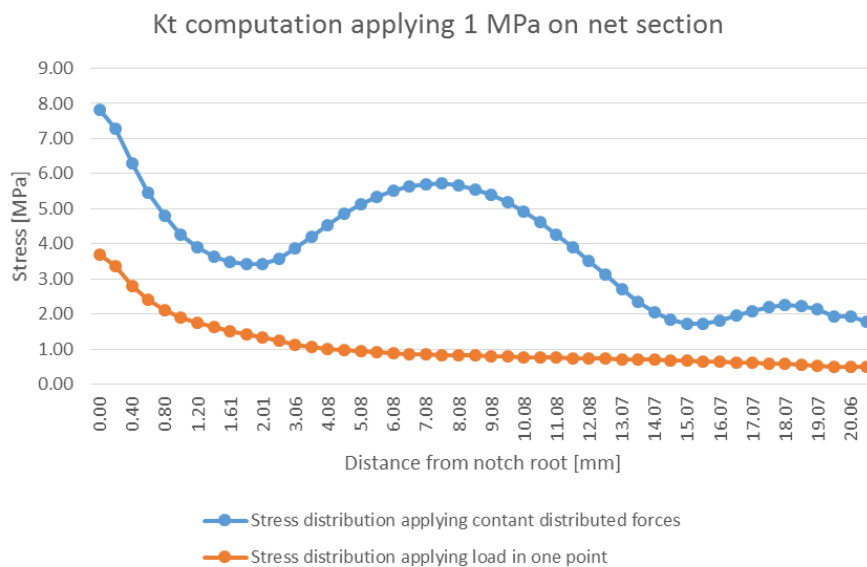


Figure 85 - Stress-distance curve from the notch tip

The notch concentration factor K_t is computed in both cases. The orange curve retraces theoretical stress distribution and theoretical K_t . Actually, TYPE 1 error is present, since the blue curve differs from the orange one. However, TYPE 1 error should overestimate stresses and, consequently, underestimate fatigue lives. Contrary to this, errors on fatigue lives are both positive and negative and do not have a constant (always negative) bias. Number of cycles to failure predicted to be higher than the experimental ones are not explainable through TYPE 1 error.

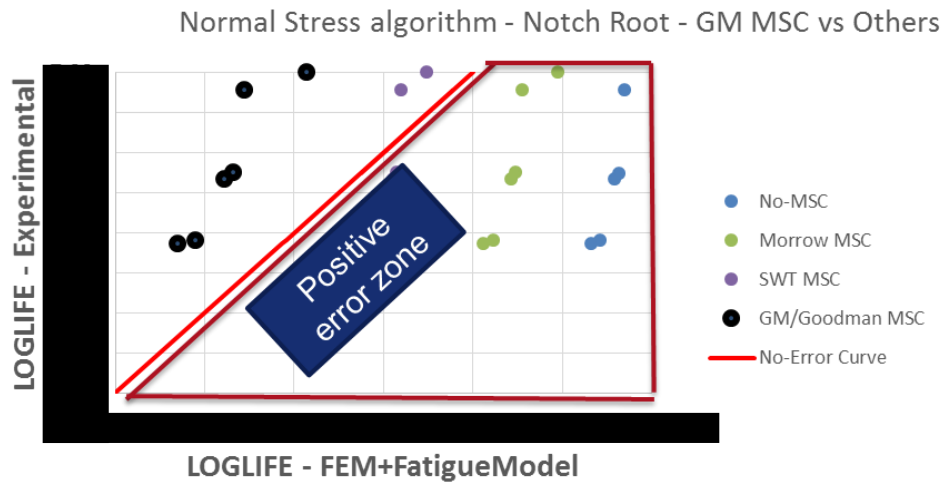


Figure 86 - Positive error zone

Durability analyses are re-run by using FEA results coming from one-point-load models. For the two experimental life extrema, calculated fatigue lives do not change significantly. This means that, even by cancelling TYPE 1 error, fatigue model predictions do not change (Figure 87). TYPE 2 error is the only explanation for the found results. It is linked to the algorithm inability to describe the fracture process in some cycle regimes, for the specified material. Moreover, it is well-known that stress-based criteria are not able to correlate data in the LCF regime.

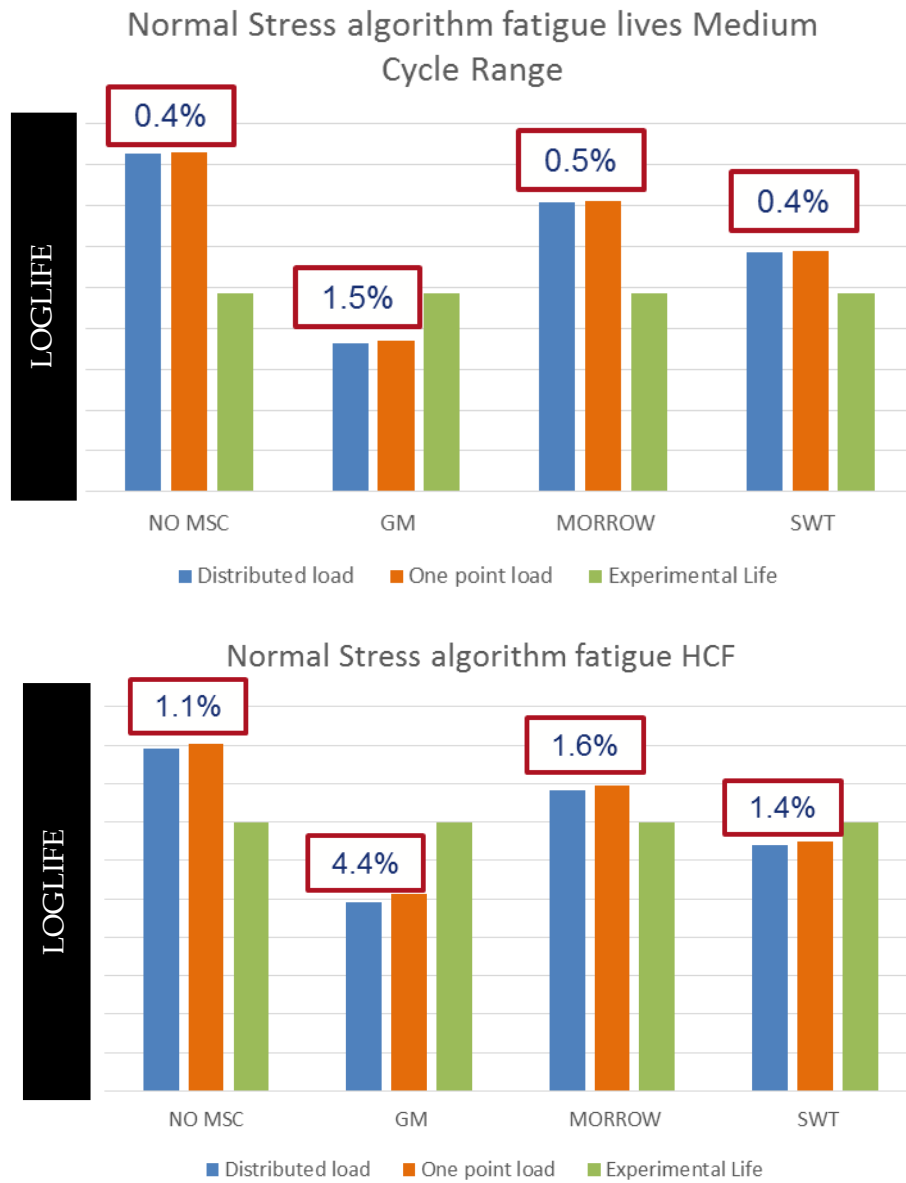


Figure 87 - Fatigue lives - Models Comparison

6 Conclusions

The original purpose of this work was to study the methodologies adoptable in the fatigue assessment of ICE's threaded bores. The first interesting outcome of this work is surely related to the meaninglessness that may have introducing many parameters without being conscious of their relevance. Several non-linearities mix-up in the fatigue assessment of ICE's component and taking into account them all in a single assessment is not straightforward. For this reason, great part of this work was devoted to the study of components presenting features similar to those of the threaded joints. Fatigue behaviour of notched structures becomes relevant in this context and TCD emerges as a powerful tool. From a wide bibliographic research on this topic, its relevant role as general fracture theory stands out. Surely, this theory can be neither considered as a "far-from-surface" assessment to enlarge components acceptability limits, nor as a theory linked only to crack propagation. Indeed, many HCF fatigue criteria are applicable for crack initiation assessment from a TCD perspective. However, close connections with LFM can be identified.

The presence of notches involves multi-axiality and critical plane analysis. Exploring in depth these subjects has emphasized the leading role played by critical plane research methods, as they may strongly affect FEA fatigue post-processing. Applications of both stress-based and strain-based methods are present in ICE's fatigue assessments and threaded joints analyses. Although linked by a common structure, results given by different methods are obviously different, and only experimental evidence can help choose the most suitable one for the studied case. Especially when many factors are involved, it is not possible to evaluate the best choice, since the identified method inevitably fails when some hypothesis are modified. It is clear that robust methods has to be researched in place of perfectly correlated ones. DVC arises as one of the possibilities since time history does not need

transformations (Rainflow, Mean Stress Correction, stress amplitudes evaluation, etc.) in order to be compared with material strength. This is remarkable if we think that, as it occurs for energy in thermodynamics, the higher the number of steps that information goes through, the longer the part of it is inevitably lost.

The analysis of a case study showed the applicability of TCD arguments and the effect of simplifying hypotheses. Safety Factor-based and fatigue life-based models were compared with experimental data. From this analysis, many problems related to the choice of Safety Factor as parameter for experimental correlation came out. The most important one is that the Safety Factor is not directly measurable in a component, therefore the error quantification is not allowed. Actually, this feature is needed when best algorithms are researched even in HCF and when materials exhibit fatigue limits. Namely, since in these cases failures are clearly expected to occur before the infinite life N_f , the ability of the chosen model to predict N_f must be tested. The number of cycles to failure is therefore analysed to compare experimental data with predictions. Many aspects, not verifiable by using Safety Factor, are emphasized.

7 Appendix

Chapter 3 shows a comparison between calculated lives on different critical planes. One of these (maximum cumulative damage/minimum safety factor plane) is found by using a Matlab code. The life calculated on this plane is compared with results coming from FE-Safe software, as they are supposed to be the same. A FEM model of a clamped beam is built and it is loaded in such a way that a specific node experiences the supposed multiaxial load history (Figure 88, Figure 89).

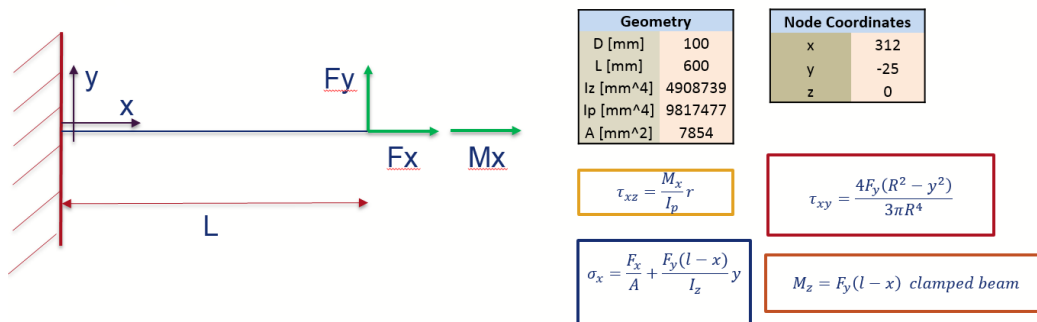


Figure 88 - Clamped Beam - closed form solution

From analytical formula, forces and moments to apply in order to obtain the supposed stress history in the selected node are computed. Hypermesh/Abaqus (67) are employed for a multistep elastic FEA (Figure 90).

FEA stresses are compared with theoretical stresses (Figure 91).

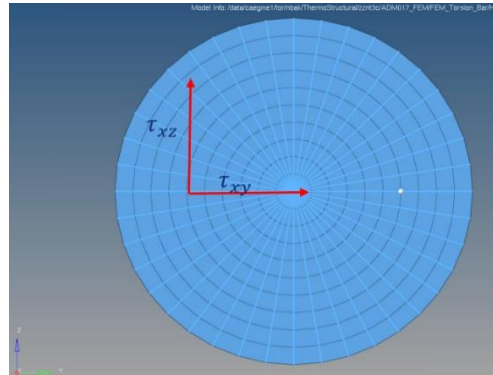


Figure 89 - Selected node

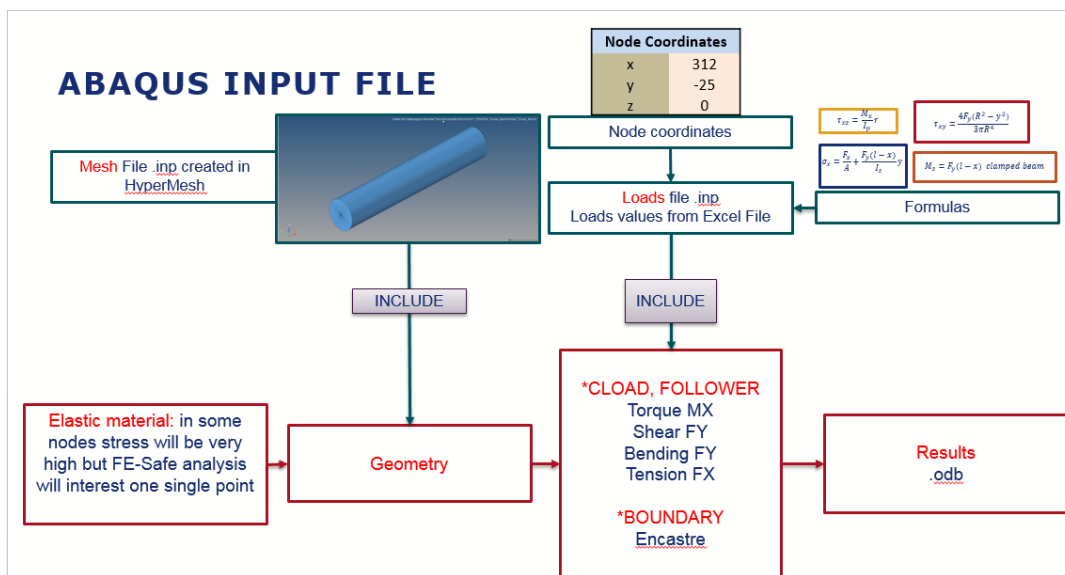


Figure 90 - Abaqus input file - clamped beam

The FE-Safe life is calculated and compared with Matlab code results (Figure 92). Differences of the 10% order are found. These are acceptable since FEM model is already affected by 15% errors. Then, an explanation of a such high FEM error (Figure 91) in normal stress is found.

Hypotheses on FEM error are advanced:

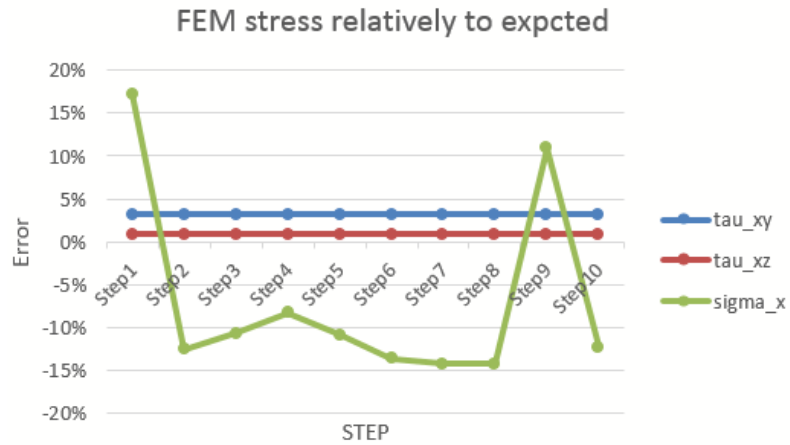


Figure 91 - FEM error

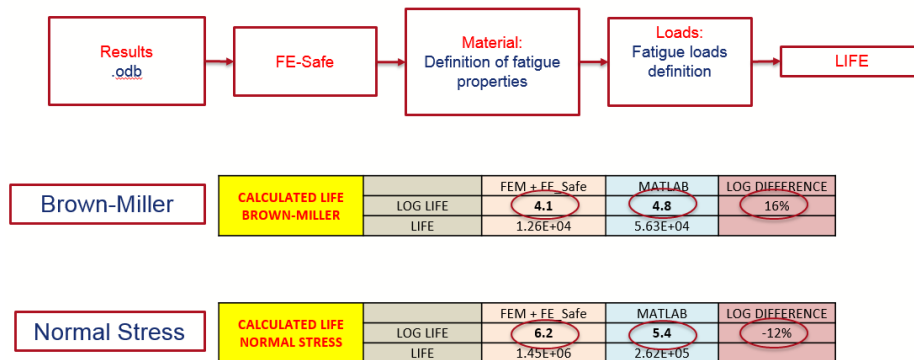


Figure 92 - Fatigue lives

- Locking: element inability to represent stress field in a bending case. This is unlikely to occur since reduced integration is already applied.
- Euler’s model (analytical formula) not applicable to the geometry
- Section deformation due to torsion
- Central elements (C3D6R) affect behaviour of other elements (C3D8R) since loads are applied in the centre.

Error trend is studied along three different sections of the beam (Figure 93).

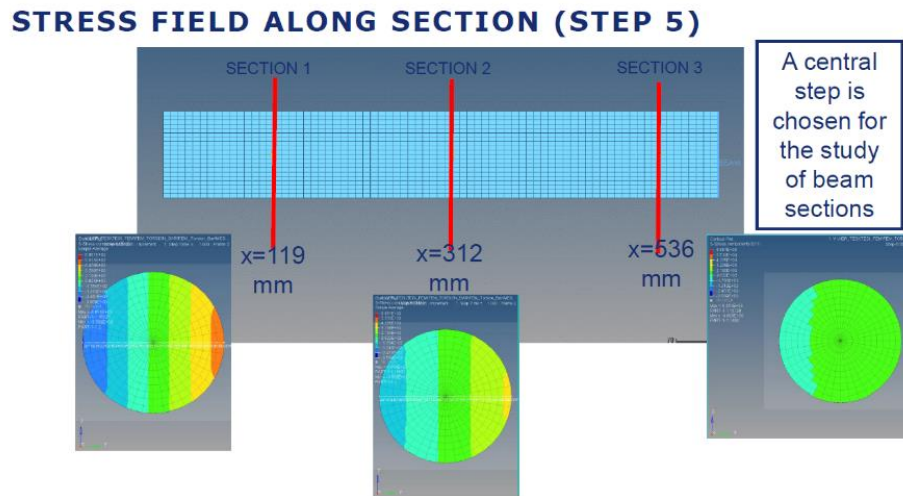
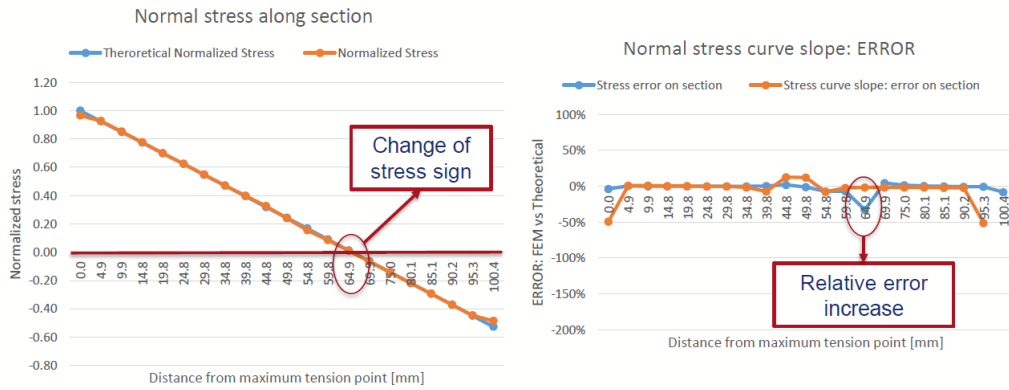


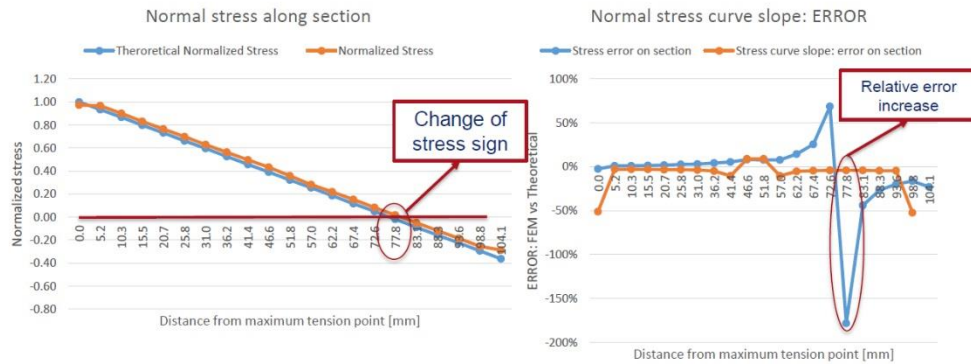
Figure 93 - Stress Field along section

Relative error suddenly increases when stress changes in sign (Figure 94).

SECTION 1



SECTION 2



SECTION 3



Figure 94 - Error on section

Due to the arbitrary stress history, stresses may be very high in some regions since they may exceed elastic limits. This results in very high stress gradients.

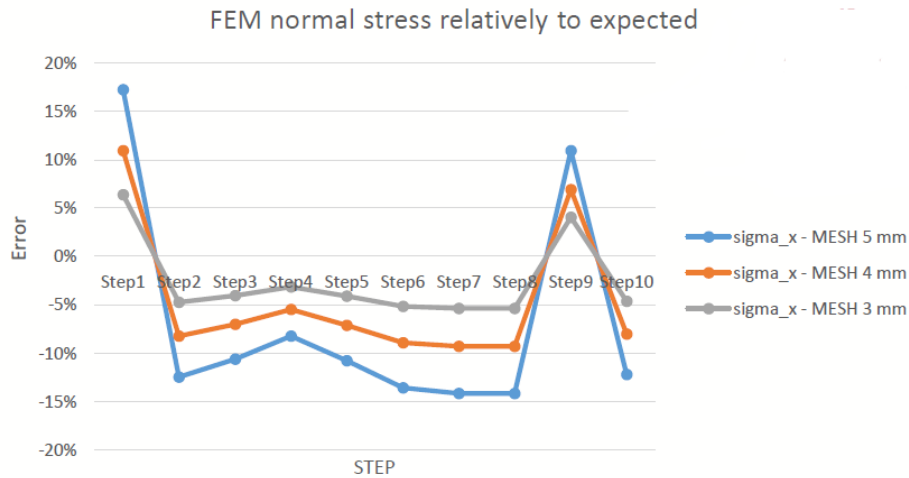
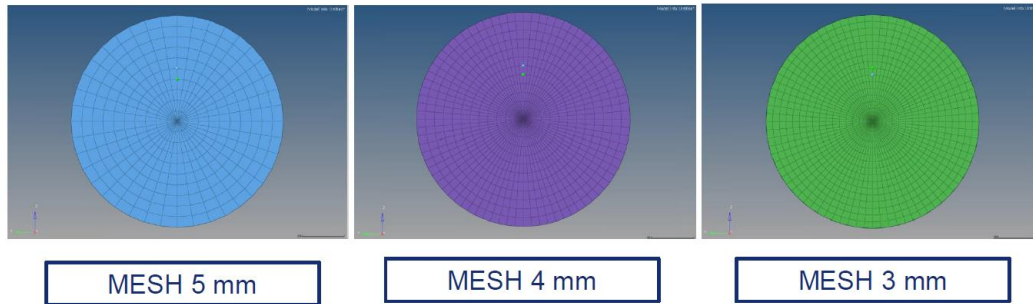


Figure 95 - Mesh refinement

In order to correctly represent the bending stress state, a mesh refinement is necessary especially in the zones close to stress sign change. The mesh should be able to represent the stress variability along the section.

It is concluded that the mesh size strongly affects the relative errors in the zones where the stress changes in sign. High stress gradients resulting from an arbitrary defined stress history cause this dependence.

STRESS GRADIENT	Section1	Section2	Section3
Theoretical slope [Mpa/mm]	-77.0	-46.1	-10.2

Figure 96 - Stress gradients

- Globally: FEM error is compatible with the error made on normal stress that is, in its turn, compatible with the error made on other stress components.
- Locally: FEM error on normal stress may be very high. The point of analysis for fatigue algorithms implementation is one of these.

Moreover, central elements and torsion loads do not affect these stresses. The study is repeated by changing the central elements order. Results remain unchanged. The same occurs removing torsion loads (Figure 97).

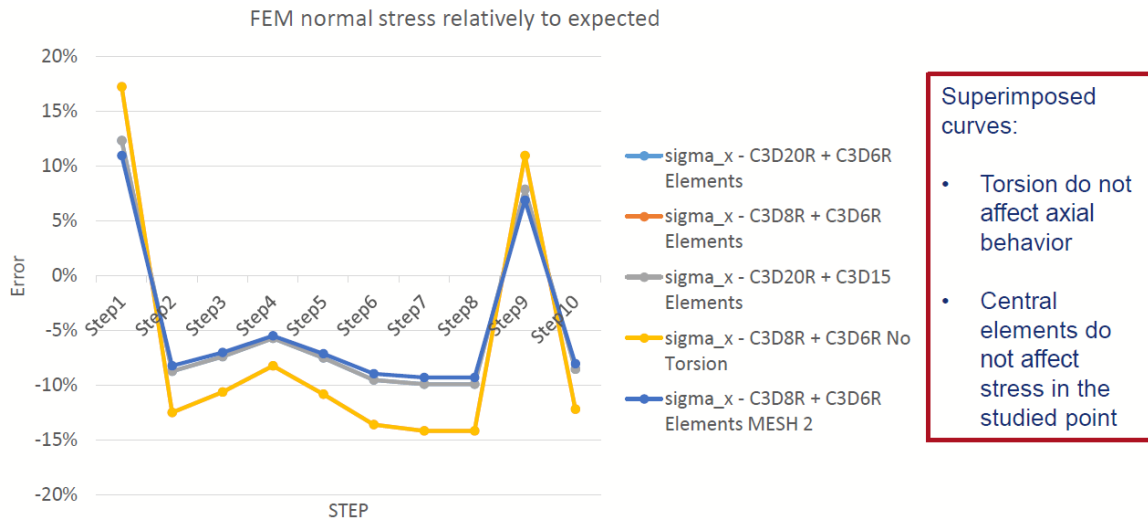


Figure 97 - Effect of torsion and central elements

7.1 Torsion Bar – Input File

```

*HEADING
Torsional Bar analysis with Tension-Torsion-Shear Loading
*****

**SETTINGS
*****

**PARAMETERS
*****

*INCLUDE, INPUT=LOAD_VALUE
*****

**MESH FILE
*INCLUDE, INPUT=MESH_Torsion_Bar.inp
*****

**PROPERTIES
*****

*MATERIAL, NAME=ALUMINUM
*ELASTIC, TYPE=ISOTROPIC
72700, 0.33
**

*SOLIDSECTION, ELSET=Bar, MATERIAL=ALUMINUM
*****

**HISTORY DATA
*****

*STEP
Step01
**

*STATIC
**
    
```

```
*BOUNDARY
BC_NODES, ENCASTRE
N_LOAD, 3,3,0
**
*CLOAD, FOLLOWER
N_LOAD, 1, <N1>
N_LOAD, 4, <MX1>
N_LOAD, 2, <T1>
**
*OUTPUT, FIELD, FREQUENCY=1000
*NODE OUTPUT
U
*ELEMENT OUTPUT
S, E
*END STEP
*****
*STEP
Step02
**
*STATIC
**
*CLOAD, FOLLOWER, OP=NEW
N_LOAD, 1, <N2>
N_LOAD, 4, <MX2>
N_LOAD, 2, <T2>
**
*END STEP
**-----
```

```
*STEP
Step03
**
*STATIC
**
*CLOAD, FOLLOWER, OP=NEW
N_LOAD, 1, <N3>
N_LOAD, 4, <MX3>
N_LOAD, 2, <T3>
**
*END STEP
**-----
*STEP
Step04
**
*STATIC
**
*CLOAD, FOLLOWER, OP=NEW
N_LOAD, 1, <N4>
N_LOAD, 4, <MX4>
N_LOAD, 2, <T4>
**
*END STEP
**-----
*STEP
Step05
**
*STATIC
```

```
**  
*CLOAD, FOLLOWER, OP=NEW  
N_LOAD, 1, <N5>  
N_LOAD, 4, <MX5>  
N_LOAD, 2, <T5>  
**  
*END STEP  
**-----  
*STEP  
Step06  
**  
*STATIC  
**  
*CLOAD, FOLLOWER, OP=NEW  
N_LOAD, 1, <N6>  
N_LOAD, 4, <MX6>  
N_LOAD, 2, <T6>  
**  
*END STEP  
**-----  
*STEP  
Step07  
**  
*STATIC  
**  
*CLOAD, FOLLOWER, OP=NEW  
N_LOAD, 1, <N7>  
N_LOAD, 4, <MX7>
```

```
N_LOAD, 2, <T7>
**
*END STEP
**-----
*STEP
Step08
**
*STATIC
**
*CLOAD, FOLLOWER, OP=NEW
N_LOAD, 1, <N8>
N_LOAD, 4, <MX8>
N_LOAD, 2, <T8>
**
*END STEP
**-----
*STEP
Step09
**
*STATIC
**
*CLOAD, FOLLOWER, OP=NEW
N_LOAD, 1, <N9>
N_LOAD, 4, <MX9>
N_LOAD, 2, <T9>
**
*END STEP
**-----
```

*STEP

Step10

**

*STATIC

**

*CLOAD, FOLLOWER, OP=NEW

N_LOAD, 1, <N10>

N_LOAD, 4, <MX10>

N_LOAD, 2, <T10>

**

*END STEP

**-----

7.2 U-Notched Plate: input file (load by rigid elements)

```
*HEADING
U-Notched plate Thermal-stress analysis
**
*PREPRINT,ECHO=NO,HISTORY=NO,MODEL=NO
**
**PARAMETERS
**
*PARAMETER
TC_25=25
TC_150=150
THICK=5
N_NODES=55
LOAD_1=12000
LOAD_2=10000
LOAD_3=8000
LOAD_4=7200
LOAD_5=7600
LOAD_6=6000
*****
**MATERIALS
*****
*INCLUDE, INPUT=Block_Material.inc
**
*SHELL SECTION, ELSET=U-Notched, MATERIAL=MATERIAL_CARD
<THICK>
**
**MESH FILE
```

```
*****
**INCLUDE, INPUT=MESH_U_Notched.inp
**
*****
**HISTORY DATA
*****
**INITIAL CONDITION, TYPE=TEMPERATURE
NALL, <TC_150>
**STEP, AMPLITUDE=RAMP
**Step01 - Temperature increasing
**COUPLED TEMPERATURE-DISPLACEMENT, DELTMX=10
**10, 3600
**
**BOUNDARY
**BC_NODES, ENCASTRE
**BC_NODES_2, ENCASTRE
**NALL, 3, 3, 0
**NALL, 11, 13, <TC_150>
*****
**RESULTS
*****
**END STEP
**
**STEP
Step02 - Load Application TENSILE 1
**STATIC
**
**BOUNDARY, OP=NEW
```

```
BC_NODES, ENCASTRE
**BC_NODES_2, 2, 2, 0
NALL, 3, 3, 0
**NALL, 11, 13, <TC_150>
**
*CLOAD, OP=NEW
N_LOAD, 1, <LOAD_1>
**
*END STEP
```

7.3 U-Notched Plate: input file (uniformly loaded on border nodes)

```

*HEADING
U-Notched plate Thermal-stress analysis
**
*PREPRINT,ECHO=NO,HISTORY=NO,MODEL=NO
**
**PARAMETERS
**
*PARAMETER
TC_25=25
TC_150=150
THICK=5
N_NODES=55
LOAD_1=12000/N_NODES
LOAD_2=10000/N_NODES
LOAD_3=8000/N_NODES
LOAD_4=7200/N_NODES
LOAD_5=7600/N_NODES
LOAD_6=6000/N_NODES
*****
**MATERIALS
*****
*INCLUDE, INPUT=Block_Material.inc
*SHELL SECTION, ELSET=U-Notched, MATERIAL=MATERIAL_CARD
<THICK>
**MESH FILE
*****

```

```
*INCLUDE, INPUT=MESH_U_Notched.inp
*****
**HISTORY DATA
*****
**INITIAL CONDITION, TYPE=TEMPERATURE
**NALL, <TC_25>
**STEP, AMPLITUDE=RAMP
**Step01 - Temperature increasing
**COUPLED TEMPERATURE-DISPLACEMENT, DELTMX=10
**10, 3600
**BOUNDARY
**BC_NODES, ENCASTRE
**BC_NODES_2, ENCASTRE
**NALL, 3, 3, 0
**NALL, 11, 13, <TC_150>
*****
**RESULTS
*****
**END STEP
**
**STEP, AMPLITUDE=RAMP
Step02 - Load Application TENSILE 1
**COUPLED TEMPERATURE-DISPLACEMENT, STEADY STATE
**
**BOUNDARY, OP=NEW
BC_NODES, ENCASTRE
BC_NODES_2, 2, 2, 0
NALL, 3, 3, 0
```

NALL, 11, 13, <TC_150>

**

*CLOAD, OP=NEW

N_LOAD, 1, <LOAD_1>

**

*END STEP

7.4 Engine and Threaded Bore FEM model

The input ABAQUS files referring to the Engine global model and threaded bore submodel cannot be provided being company data. Nevertheless, several thermal and thermal-structural analyses were set-up for these components.

References

1. **González-Velázquez, Jorge Luis.** *Fractography and Failure Analysis*. Cham, Switzerland : Springer, 2018.
2. **Socie, Darell and Marquis, G.** *Multiaxial fatigue*. Warrendale : Society of Automotive Engineers, 2000.
3. **Chung, Kwansoo and Lee, Myoung Gyu.** *Basic of Continuum Plasticity*. Singapore : Springer, 2018.
4. **Richard, Hans Albert and Sander, Manuela.** *Fatigue Crack Growth : Detect-Assess-Avoid*. Switzerland : Springer, 2016.
5. *A path independent integral an the approximate analysis of strain concentration by notches and cracks.* **Rice, J.R.** 1968, Journal of Applied Mechanics, Vol. 35, pp. 379-386.
6. *Prediction of non propagating cracks.* **El Haddad, M.H., Topper, T.H. and Smith, K.N.** 1979, Engineering Fracture Mechanics, pp. 573-584.
7. *Applications of the theory of critical distances in failure analysis.* **Taylor, D.** 2011, Engineering Failure Analysis, Vol. 18, pp. 543-549.
8. *The Theory of Critical Distances to assess failure strength of notched plain concrete under static and dynamic loading.* **Pelekis , I. and Susmel, L.** 2017, Engineering Failure Analysis, pp. 378-389.
9. **Taylor, David.** *The Theory of Critical Distances: A New Perspective in Fracture Mechanics*. Amsterdam : Elsevier, 2007.
10. *The theory of critical distances.* **Taylor, D.** 2008, Engineering Fracture Mechanics, Vol. 75, pp. 1696-1705.
11. *The theory of critical distances: a review of its applications in fatigue.* **Susmel, L.** 2008, Engineering Fracture Mechanics, Vol. 75, pp. 1706-1724.
12. **Neuber, H.** *Theory of notch stresses: principles for exact stress calculation*. s.l. : Univesity Microfilms, 1966.
13. **Pilkey, W.D. and Pilkey, D.F.** *Peterson's Stress Concentration Factors*. Hoboken N.J. : John Wiley, 2008.

14. **Draper, J. and Engineering Integrity Society.** *Modern Metal Fatigue Analysis*. s.l. : EMAS Pub, 2008.
15. *The Fracture Mechanics of finite crack extension.* **Taylor, D., Cornetti, P. and Prugno, N.** 2008, *Engineering Fracture Mechanics* , pp. 1021-1038.
16. *A Mechanistic Approach to Critical-Distance Methods in Notch Fatigue.* **Taylor, D.** 2001, *Fatigue and Fracture of Engineering Material and Structures*, pp. 215-224.
17. *On the estimation of Finite Lifetime Under Fretting Fatigue Loading.* **Kouanga, C.T., et al.** 2018, *International Journal of Fatigue*, Vol. 112, pp. 138-152.
18. *Determination of the Fatigue Critical Distance According to the Line and Point Method with Rounded V-Notched Specimen.* **Santus, C., Taylor, D. and Benedetti , M.** 2018, *International Journal of Fatigue*.
19. *A generalised approach to rapid finite element design of notched materials against static loading using Theory of Critical Distances.* **Louks, R., Askes, H. and Susmel, L.** 2016, *Materials and Design*, pp. 769-779.
20. *An extension research on the theory of critical distances for multiaxial notch fatigue finite life prediction.* **Liu, B. and Yan, X.** 2018, *International Journal of Fatigue*, pp. 217-229.
21. *Experimental determination and sensitivity analysis of the fatigue critical distance obtained with rounded V-notched specimens.* **Santus, C., Taylor, D. and Benedetti, M.** 2018, *International Journal of Fatigue*, pp. 113-125.
22. *High Temperature LCF Life Prediction of Notched Ds Ni-Based Superalloy Using Critical Distance Concept.* **Yang, X., Wang, J. and Liu, J.** 2011, *International Journal of Fatigue*, pp. 1470-1476.
23. *HCF strength estimation of notched Ti-6Al-4V specimens considering the critical distance size effect.* **Wang, J. and Yang, X.** 2012, *International Journal of Fatigue*, pp. 97-104.
24. *A critical distance/plane method to estimate finite life of notched components under variable amplitude uniaxial/multiaxial fatigue loading.* **Susmel, Luca and Taylor, David.** 2012, *International Journal of Fatigue*, Vol. 38, pp. 7-24.
25. *An Elasto-Plastic Reformulation of the Theory of Critical Distances to Estimate Lifetime of Notched Components Failing in the Low/Medium-Cycle Fatigue Regime.* **Susmel, L. and Taylor, D.** 2, 2010, *Journal of Engineering Materials and Technology*, Vol. 132.

26. *Estimating Lifetime of Notched Components Subjected to Variable Amplitude Fatigue Loading According to the Elastoplastic Theory of Critical Distances.* **Susmel, L. and Taylor, D.** 1, 2015, *Journal of Engineering Materials and Technology*, Vol. 137.
27. *Implementation of Non-Local Critical-Plane Fatigue Analysis Program with Applications to Cylinder Heads.* **Bishop, J.** 2004, SAE Technical Paper.
28. *Fatigue Crack Initiation Mechanism for Cast 319-T7 Aluminium Alloy.* **Jang, Y., et al.** 7, 2009, *Metallurgical and Materials Transactions a: Physical Metallurgy and Material Science*, Vol. 40, pp. 1579-1587.
29. *Fatigue Life Prediction for Porosity-Containing Cast 319-T7 Aluminum Alloy.* **Jang, Y., et al.** 5, 2009, *Metallurgical and Materials Transactions A*, Vol. 40, pp. 1090-1099.
30. *The Modified Wöhler Curve Method Applied along with the Theory of Critical Distances to Estimate Finite Life of Notched Components Subjected to Complex Multiaxial Loading Paths.* **Susmel, L. and Taylor, D.** 12, 2008, *Fatigue and Fracture of Engineering Materials and Structures*, Vol. 31, pp. 1047-1064.
31. *A simple and efficient numerical algorithm to determine the orientation of the critical plane in multiaxial fatigue problems.* **Susmel, L.** 2010, *International Journal of Fatigue*, Vol. 32, pp. 1875-1883.
32. *Fe-safe 2017 USER GUIDE.* **Dassault Systems.**
33. *nCode Design Life Theory Guide.* **Ansys.**
34. *On the Prediction of High-Cycle Fretting Fatigue Strength: Theory of Critical Distances VS. Hot-Spot Approach.* **Araujo, J.A., et al.** 7, 2008, *Engineering Fracture Mechanics*, Vol. 75, pp. 1763-1778.
35. *Deviatoric Neuber method for stress and strain analysis at notches under multiaxial loadings.* **Ince, A. and Dongjun, B.** 2017, *International Journal of Fatigue*, Vol. 102, pp. 229-240.
36. *A Generalization of Neuber's Rule for Numerical Applications.* **Kujawski, D. and Joshua, LK T.** 2017, *Procedia Structural Integrity*, Vol. 5, pp. 883-888.
37. *Rainflow Counting Based Block Cycle Development for Fatigue Analysis Using Nonlinear Stress Approach.* **Zhang, W., Guo, M. and Srikantan, S.** 2, 2013, *Sae International Journal of Materials and Manufacturing*, Vol. 6, pp. 330-338.

38. *Efficiency of algorithms for shear stress amplitude calculation in critical plane fatigue criteria.* **Bernasconi, A. and Papadopoulos, I.V.** 2005, Computational Material Science, Vol. 34, pp. 355-368.
39. *A theory for the effect of mean stress on fatigue of metals under combined torsion and axial load or bending.* **Findley, W.N.** 4, 1959, Journal of Engineering for Industry, Vol. 81, pp. 301-305.
40. *Sur la résistance à la fatigue des métaux.* **Dang Van, K.** 1973, Sciences et Techniques de l'Armement, Vol. 3, pp. 647-722.
41. *Fatigue Modeling for Automotive Applications.* **Thomas, J.J. and PSA Peugeot Citroen.** 2002, SAE Technical Paper.
42. *High Cycle Fatigue and a Finite Element Analysis.* **Ballard, P., et al.** 3, 1995, Fatigue and Fracture of Engineering Materials and Structures, Vol. 18, pp. 397-411.
43. *Modified Dang Van Approach for Fatigue Estimation of Exhaust System.* **Wang, Z., et al.** 3, 2009, Atz Worldwide, Vol. 113, pp. 34-37.
44. *On a new multiaxial fatigue limit criterion: theory and applications.* **Dang Van, K., Griveau, B. and Message, O.** 1989, Biaxial and Multiaxial Fatigue, pp. 479-496.
45. *On the Dang Van fatigue limit in rolling contact fatigue.* **Ciavarella, M., Monno, F. and Demelio, G.** 2006, International Journal of Fatigue, Vol. 28.
46. *A computational approach for the fatigue design of threaded connections.* **Ferjani, M., Averbuch, D. and Constantinescu, A.** 2011, International Journal of Fatigue, Vol. 33, pp. 610-623.
47. *Determining the life cycle of bolts using a local approach and the Dang Van criterion.* **Fares, Y., et al.** 8, 2006, Fatigue & Fracture of Engineering Materials & Structures, Vol. 29, pp. 588-596.
48. *A Novel Approach for Numerical Calculation and Optimization of High-Cycle Fatigue Life under Multi-Axial Loads.* **Einolghozati, M., et al.** 2014, SAE Technical Paper.
49. *A Mesoscopic-Stress Based Fatigue Limit Theory - A revised Dang Van's Model.* **Savu, V., et al.** 2014, SAE Technical Paper.
50. *Crankshaft Durability Prediction - A New 3-D Approach.* **Henry, J., et al.** 1992, SAE Technical Paper.

51. *Fatigue Design of Automotive Suspension Coil Springs*. **Ouakka, A. and Langa, M.** 2002, SAE Technical Paper.
52. *Application of Dang Van criterion to rolling contact fatigue in wind turbine roller bearings Under Elastohydrodynamic Conditions*. **Cerullo, M.** 12, 2014, Proceedings of the Institution of Mechanical Engineers, Part C: Journal of Mechanical Engineering Science, Vol. 228.
53. *Numerical Exploration of the Dang Van High Cycle Fatigue Criterion: Application to Gradient Effects*. **Hofmann, F., et al.** 2, 2009, Journal of Mechanics of Materials and Structures, Vol. 4, pp. 293-308.
54. *eFatigue Material Properties Finder*. **Altair.**
55. *Fatigue Crack Initiation in Threaded Fasteners Using the Critical Plane Approach*. **Taylor, D. and Pan, J.** 2003, SAE Technical Paper.
56. *Establishment of Prediction Technology of Fatigue Strength in Roots of Internal Thread for Crankcase Assembly and Clarification of Cracking Mechanism in Roots of Internal Thread*. **Kuribara, H., et al.** 2010, SAE Technical Paper.
57. *Fatigue assessment of piston rod threaded end*. **Knez, M., Glodez, S. and Kramberger, J.** 2009, Engineering Failure Analysis, Vol. 16, pp. 1977-1982.
58. *Bolt Load Relaxation and Fatigue Prediction in Threads with Consideration of Creep Behavior for Die Cast Aluminum*. **DeJack, M., Ma, Y. and Craig, R.** 2010, SAE Technical Paper.
59. *Theory of creep deformation with kinematic hardening for materials with different properties in tension and compression*. **Zolochovsky, A. and Voyiadjis, G.** 2005, International Journal of Plasticity, Vol. 21, pp. 435-462.
60. *Fatigue Strength Effect on Thread Forming Process in Cast Aluminum*. **Blaha, J., et al.** SAE Technical Paper.
61. *3D Finite Element Modeling of an Assembly Process with Thread Forming Screw*. **Mathurin, F., et al.** 4, 2009, Journal of Manufacturing Science and Engineering, Transactions of the Asme, Vol. 131.
62. *Multi-Axial Contour Method for Mapping Residual Stresses in Continuously Processed Bodies*. **Dewald, A.T. and Hill, M.R.** 2006, Proceedings of the Society for Experimental Mechanics.

63. *Residual Stress from Cold Expansion for Fastener Holes: Measurement, Eigenstrain and Process Finite Element Modeling.* **Ribeiro, R.L. and Hill, M.R.** 4, 2017, Journal of Engineering Materials and Technology, Transactions of the Asme, Vol. 139.
64. *Modeling the effects of residual stresses on defects in welds of steel frame connections.* **Matos, C.G. and Dodds Jr, R.H.** 2000, Engineering Structures, Vol. 22.
65. *A New Measuring Method of Residual Stresses with the Aid of Finite Element Method and Reliability of Estimated Values.* **Ueda, Y., et al.** 2, 1975, Transactions of JWRI, Vol. 4, pp. 123-131.
66. *Eigenstrain simulation of residual stresses induced by laser shock processing in a Ti6Al4V hip replacement.* **Correa, C., et al.** 2015, Materials and Design, Vol. 79, pp. 106-114.
67. *Abaqus 6.13 Documentation.* **Dassault Systems.**
68. *Cumulative Fatigue Damage in the Diesel Engines Application.* **Barboza, W., et al.** 2005, Sae Technical Paper.
69. *Comparative study on the fatigue criteria for the prediction of failure in engine structure.* **Saeidi Googarchin, H., et al.** 2017, Engineering Failure Analysis, Vol. 79, pp. 714-725.